NASA TECHNICAL REPORT

NASA TR R-351

NASA TR R-351

THE SOLAR CONSTANT AND THE SOLAR SPECTRUM MEASURED FROM A RESEARCH AIRCRAFT

Edited by Matthew P. Thekaekara

Goddard Space Flight Center

Greenbelt, Md. 20771

NATIONAL AERONAUTICS AND SPACE ADMINISTRATION • WASHINGTON, D. C. • OCTOBER 1970

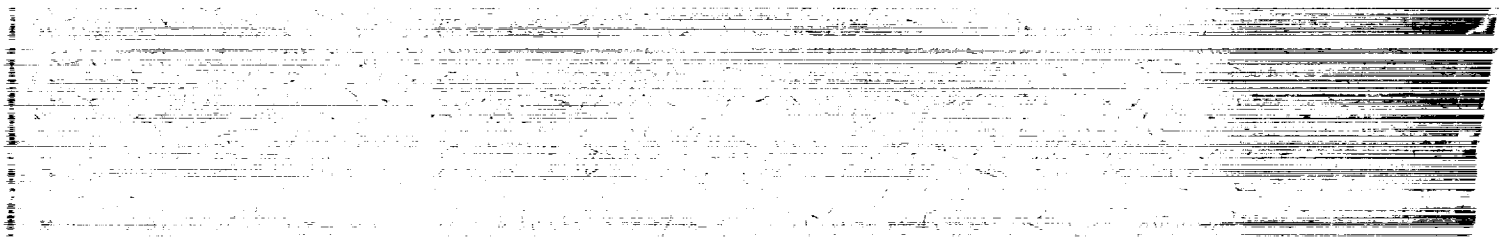

TECHNICAL REPORT STANDARD TITLE PAGE

1. Report No.	2. Government Accession No.	3. Recipient's Catalog No.
NASA TR R-351		

4. Title and Subtitle	5. Report Date
The Solar Constant and the Solar Spectrum Measured From a Research Aircraft	October 1970
	6. Performing Organization Code

7. Author(s)	8. Performing Organization Report No.
Matthew P. Thekaekara	G-991

9. Performing Organization Name and Address	10. Work Unit No.
Goddard Space Flight Center Greenbelt, Maryland 20771	124-09-27-01-51
	11. Contract or Grant No.
	13. Type of Report and Period Covered
12. Sponsoring Agency Name and Address	Technical Report
National Aeronautics and Space Administration Washington, D. C. 20546	14. Sponsoring Agency Code

15. Supplementary Notes

16. Abstract

The solar constant and solar spectrum were measured from a research aircraft flying at 38,000 feet, above the highly variable and absorbing constituents of the atmosphere. A wide range of solar zenith angles was covered during six flights for over 14 hours. Eleven instruments, five for total irradiance and six for spectral irradiance, were employed. The instruments complemented each other in the measuring techniques employed and wavelength range covered, and were calibrated and operated by different experimenters. The combined results of these experiments are presented, and also a proposed standard for the solar constant and zero air mass solar spectral irradiance. The solar constant is found to equal 135.3 mW cm^{-2} or 1.940 cal min^{-1} cm^{-2}.

17. Key Words Suggested by Author	18. Distribution Statement
Solar constant Solar spectral irradiance Research aircraft solar measurements	Unclassified—Unlimited

19. Security Classif. (of this report)	20. Security Classif. (of this page)	21. No. of Pages	22. Price *
Unclassified	Unclassified	85	$3.00

THE RESEARCH TEAM: NASA 711 GALILEO EXPERIMENT, AUGUST 1967

Management and Experimenters Team
Goddard Space Flight Center

Dwight C. Kennard, Jr., Head, Research and Technology Office, Test and Evaluation Division, Project Manager.

Matthew P. Thekaekara, Principal Investigator—Perkin-Elmer, P-4 Interferometer, Data Analysis.

Raymond Kruger, Head, Space Simulation Research Section, Project Coordinator, Acting Project Manager at Ames Research Center—Cone Radiometer, Mounting Fixtures.

Charles H. Duncan, Head, Radiometry Section, Assistant Project Manager—Ångström 7635 Pyrheliometer, Thermophysics Branch Experiments.

John F. Rogers, Assistant Project Manager—P-4 and I-4 Interferometers, Flight Paths, Mounting Fixtures.

Ralph Stair, Consultant—Filter Radiometer, Perkin-Elmer, Data Analysis.

James J. Webb—Electronic Scanning Spectrometer, Ångström 7635 Pyrheliometer, Thermophysics Branch Experiments.

Roy McIntosh—Leiss Monochromator, Thermophysics Branch Experiments.

Patrick Ward—P-4 and I-4 Interferometers.

Antony J. Villasenor—Computer Programs for P-4 and I-4 Interferometers and Perkin-Elmer Monochromator.

Robert J. Maichle—Electronics, Tape Recorder, Time Code Generator, Signal Calibration.

Arthur McNutt—Ångström 6618, Hy-Cal and Eppley Normal Incidence Pyrheliometers.

Arthur R. Winker—Perkin-Elmer Monochromator, Thermodynamics Branch Experiments.

Thomas A. Riley—Ångström 6618, Hy-Cal, and Eppley Normal Incidence Pyrheliometers.

Daniel L. Lester—Filter Radiometer, Thermophysics Branch Mounting Fixtures.

Segun G. Park—Leiss Monochromator, Thermophysics Branch Mounting Fixtures.

Cooperating Team (Cary 14 Monochromator)
Ames Research Center

John C. Arvesen

Roy N. Griffin

Bart T. Kinney

Airborne Sciences Office Personnel

Michael Bader, Chief, Airborne Sciences Office.

Robert M. Cameron, Test Coordinator.

Roy L. Adkins, Pilot.

Jack Kroupa, Navigator.

Glen Stinnet, Co-pilot.

Frank Brasmer, Senior Flight Engineer.

B. B. Gray, Flight Engineer.

Dave Shute, Sun Compass.

Milton Henderson, Sun Compass.

James Cox, Aircraft Maintenance.

CONTENTS

LIST OF ILLUSTRATIONS

THE SOLAR CONSTANT AND THE SOLAR SPECTRUM MEASURED FROM A RESEARCH AIRCRAFT

edited by
Matthew P. Thekaekara
Goddard Space Flight Center

PART I

THE AIRBORNE SOLAR IRRADIANCE OBSERVATORY

M. P. Thekaekara

A. The Flying Observatory Project

Three groups of experimenters of the National Aeronautics and Space Administration undertook, in August 1967, a combined project to measure the solar constant and solar spectral irradiance from a research airplane flying at 38,000 feet. Two of the groups were from Goddard Space Flight Center, Greenbelt, Maryland, which initiated the project, and the third was from Ames Research Center, Moffett Field, California, where the flights originated. The airplane was fitted out as a high-altitude solar irradiance laboratory with 12 instruments—seven for spectral irradiance and five for total irradiance measurements. The instruments represented a wide variety of measuring techniques and incorporated some of the best available features in precision radiometry.

The solar constant is the amount of solar energy of all wavelengths received per unit time per unit area exposed at right angles to the sun's rays at the average distance of the earth in the absence of the earth's atmosphere. The solar spectral irradiance is the distribution of this energy in narrow spectral bands. Our present knowledge of these physical quantities is based mainly on ground-based measurements. Most of the pioneering work was done by the Smithsonian Institution, Washington, D. C., which gathered extensive data over a period of 50 years up to 1955.

These quantities are of considerable significance in satellite technology. The surface degradation due to near ultraviolet (UV) solar energy is an important parameter for the thermal balance of spacecraft. The discrepancy of 40 percent[1] or more between different investigators about the energy in this range is a serious drawback in studies of the degradation of satellite coatings. Solar cells are the major source of power for scientific satellites; precise prediction of their performance requires knowledge of solar spectral irradiance in the near infra-red (IR) range.[2] A vast

amount of effort is now being made in NASA centers and contracting laboratories to build and operate solar simulators. As efforts are made to improve the energy output and spectral matching of lamps which simulate the sun, a parallel effort should be made to determine more accurately what to simulate. These are some of the considerations which motivated the two groups at Goddard Space Flight Center—the Thermodynamics Branch, Test and Evaluation Division, and the Thermal Systems Branch, Spacecraft and Technology Division, which formed a joint team to make the high altitude measurements.

The importance of these two quantities in different physical sciences is discussed at such length in standard text books[3] that only a brief mention need be made here. The production of solar energy depends on processes inside the sun. Energy received at the earth yields information about these processes, and also about the absorption and re-radiation of energy in the intervening space, mainly in the sun's reversing layer. The variation of the solar energy and solar spectrum with sunspot cycles, solar rotation, surface phenomena of the sun, etc., is important in understanding the physics of the sun. Comparison of measurements taken at a very high altitude with those made on the ground leads to better knowledge of the absorptive processes in the atmosphere. Almost all major topics in geophysics and meteorology, many problems like heat balance of the earth, physics of the upper atmosphere, fluctuations in the radiation belts, albedo of the earth, weather forecasting,[4] etc., are closely related to the total amount and spectral distribution of energy received from the sun.

Thus, the objective of the experiment is not only to meet the practical needs of those who make and test satellites, but more importantly, to determine a reliable and accurate value of a fundamental physical quantity for the benefit of those who need it in many scientific fields, and to fill a rather conspicuous gap in man's knowledge of the physical world.

The value of the solar constant most often quoted, at least in the United States, is 2.00 calories per square centimeter per minute. This value was deduced by Francis S. Johnson[5] at the Naval Research Laboratory, Washington, D. C. in 1954. It is interesting to note that the solar constant has frequently been revised, and most revisions prior to 1956 have yielded a higher value than those accepted previously. Some of the more significant revised values are given in Table 1 in units of calories cm^{-2} min^{-1} and mW cm^{-2}. Some of the authors give the value in thermal units, others in electrical units. Conversion from one system to the other is based on the assumption that the mechanical equivalent of heat, J, is 4.1840 joules per calorie. The joule is the absolute joule and the calorie is the thermochemical calorie; this conversion factor constitutes the definition of the thermochemical calorie.[6]

The value given by C. W. Allen[14] in his Symons Memorial Lecture of 1958 is based on one of the more significant studies of all earlier ground based measurements. He gives a table of values and a curve of the solar spectrum outside the earth's atmosphere, and determines the value of the solar constant to be 1.978 cal cm^{-2} min^{-1}. In this work he reconsidered his earlier data[10] with the help of discussions by Deirmendjian and Sekera,[19] Johnson, Purcell, Tousey and Wilson,[20] and Johnson.[5] Some account was also taken of the measurements of the intensity at the center of the solar disc in the continuum between Fraunhofer lines by Makarova,[21] Peyturaux[22] and Labs.[23]

Table 1

Significant Revisions of the Solar Constant.

Author	Year	Solar Constant	
		cal cm^{-2} min^{-1}	mW cm^{-2}
P. Moon[7]	1940	1.896	132.2
L. B. Aldrich and G. C. Abbot[8]	1948	1.90	132.5
W. Schuepp[9]	1949	1.96 to 2.03	136.7 to 141.6
C. W. Allen[10]	1950	1.97	137.4
L. B. Aldrich and W. H. Hoover[11]	1952	1.934	134.9
F. S. Johnson[5]	1954	2.00	139.5
C. S. Allen[12]	1955	1.97 ± .01	137.4 ± 0.7
R. Stair and R. G. Johnston[13]	1956	2.05	143.0
C. W. Allen[14]	1958	1.978	137.9
A. J. Drummond et alii[15]	1968	1.950	136.0
D. G. Murcray[16]	1969	1.919	133.8
D. Labs and H. Neckel[17]	1968	1.957	136.5
M. P. Thekaekara et alii[18]	1968	1.937	135.1

The four last entries in Table 1 are relatively recent. The value of Labs and Neckel is based on measurements from Jungfraujoch in the range 0.33 to 1.25 μ, and revisions of earlier data. These measurements were of the continuum radiance of the center of the solar disc, with corrections for limb darkening and Fraunhofer absorption. The other three entries are based on measurements made at high altitude.

Table 1 shows that the values of the solar constant given in literature vary from 1.90 to 2.05 cal cm^{-2} min^{-1}. The disagreement between authors is due largely to the difficulties of making measurements through the highly variable smoke, dust, haze and cloud cover of the earth's atmosphere.

The discrepancies between different investigators are even greater in the case of solar spectral irradiance measurements. Tables of solar spectral data have been published by Moon,[7] Johnson,[5] Stair and Johnston,[13] Allen,[14] Labs and Neckel[17] and others. Some of the more significant data have been collated and published by Gast[24] in the "Handbook of Geophysics," where he makes the following observation: "As an example of a more important uncertainty, in the ultraviolet region (300 to 359 mμ), the discrepancy between various observations is about 10 percent, and there have been reported variant observations as large as 40 percent which can be neither ignored nor explained." Dunkelman and Scolnik[25] have published charts which show these differences in a striking manner. It is seen that at 3400Å Petit's value is about 4 times that of Gotz and Schonman, and at 6000Å the Smithsonian value is 40 percent higher than that of Reiner. Even more discouraging is the difference between relatively recent measurements, as for example, between

Stair and Johnston, and Dunkelman and Scolnik. A detailed report on the state of our knowledge of the solar constant and solar spectral irradiance has been published by M. P. Thekaekara.[26]

The uncertainties in our presently accepted values of spectral irradiance are considerably greater than for the total irradiance. In the wavelength range beyond 0.7 μ where the atmospheric water vapor bands are many and strong, most authors, following P. Moon, have assumed the solar spectrum to be that of a 6000°K blackbody. The wide differences between authors in the shorter wavelength range, and the relative lack of experimental data in the longer wavelength range, strongly indicated the need of a new method which is free of many of the uncertainties of ground based measurements. Hence it was that the NASA 711 project was undertaken.

At the flight altitude of 38,000 feet the observers were above nearly 80 percent of the permanent gases of the atmosphere, and more importantly, above nearly 99.9 percent of the water vapor and all of the dust and smoke which form the highly variable and absorbent constituent of the atmosphere. The combination of 12 different instruments, complimenting each other in wavelength range, spectral resolution and measuring techniques, calibrated and operated by different experimenters, and carried in an airborne laboratory at 38,000 feet, practically free of atmospheric absorption, is considered a valuable feature in enhancing the level of confidence in the final result.

This report gives the results from the 11 instruments operated by the two Goddard Space Flight Center (GSFC) groups. The Cary 14 monochromator operated by the Ames group was also used during several later flights of the aircraft, and its results are reported in a separate publication.[27] This report consists of four parts. The first part describes the project as a whole, the airborne solar irradiance laboratory, general features of the instrumentation, the flight paths, atmospheric correction techniques and associated problems common to all the flight experiments. The second and third parts discuss the measurements of total and spectral irradiance respectively. These instruments were operated by the Thermodynamics Branch, Test and Evaluation Division and the Thermophysics Branch, Spacecraft Technology Division, GSFC. The experimental procedure, data analysis and results of each instrument will be discussed by the persons who operated them. The fourth part combines the results of the eleven instruments to present a new value of the solar constant and a new solar spectral irradiance curve for zero air mass.

B. The Aircraft and Experiments

The aircraft was a NASA-owned, modified Convair 990, four-engine jet, called the NASA 711 Galileo. The team for solar irradiance measurements consisted of 18 experimenters, scientists and technicians to operate the instruments, and nine aircraft personnel. An inflight view of the aircraft is shown in Figure 1. Prominent among the special features making it an airborne science laboratory are the large extra windows on the roof of the plane and the replacement of some of the passenger windows by optical quality material. Other special features are electrical power outlets at each experimenter's station, defrosters for observation windows, time code generator, and precise navigational equipment for the determination of latitude, longitude and solar zenith angle.

Figure 2, giving a view of the front section, port side of the plane, was taken while the plane was in the hangar. The figure clearly shows where the double plexiglass cover of four passenger windows has been replaced by aluminum plates with small apertures. These apertures are covered by optical material suited to the instrument behind each window.

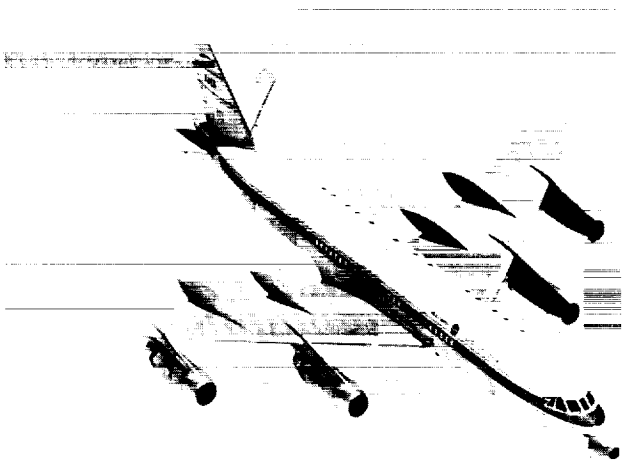

Figure 1—NASA 711 Galileo, Convair 990A, the airborne laboratory in flight.

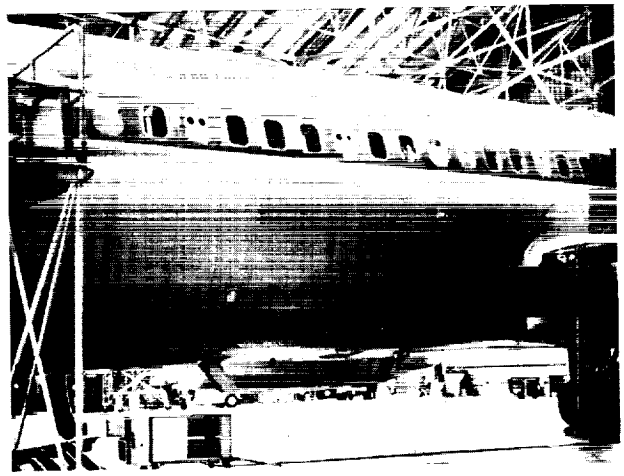

Figure 2—Port side view of NASA 711, showing passenger windows changed to observation ports.

The location of the experiments is shown in Figures 3 and 4. Figure 3 gives the floor plan of the aircraft. Passenger seats which are used during takeoff, outward flight, and landing are in the tail. Figure 4 shows photographs of each of the instruments as mounted in the aircraft. The instruments used for observing the sun are on the port side of the aircraft, as are some of the electronic chassis and chart recorders. On the starboard side of the aircraft are located the tape recorders and the larger items of electronic equipment, namely those for the three monochromators. A listing of the instruments in the order in which they were located, starting from the nose of the airplane, is given in Table 2, and also some basic data on each. These instruments were selected partly because they had all been tested and were believed to be sufficiently reliable at levels of solar irradiance, and partly because they could be readily mounted and operated almost as well on an airplane as in the laboratory. A general description of the instruments is attempted here, to bring out the specific function and distinguishing characteristics of each, and also to show how, based on different techniques, they complement each other.

Five of the instruments—Hy-Cal and two Ångström pyrheliometers, and the Eppley and Cone radiometers—measure the total irradiance; the others measure spectral irradiance. The Hy-Cal pyrheliometer and Eppley radiometer measure the radiation in terms of the thermo-electric e.m.f. generated by them; conversion to units of irradiance is by means of the calibration supplied with the instruments. The calibration is with reference to standards maintained by the respective manufacturers: the Hy-Cal Engineering Company, Santa Fe Springs, California and the Eppley Laboratories, Newport, Rhode Island. The primary standard for the Hy-Cal pyrheliometer is a blackbody, and for the Eppley radiometer the international pyrheliometric scale. The two Ångström radiometers,

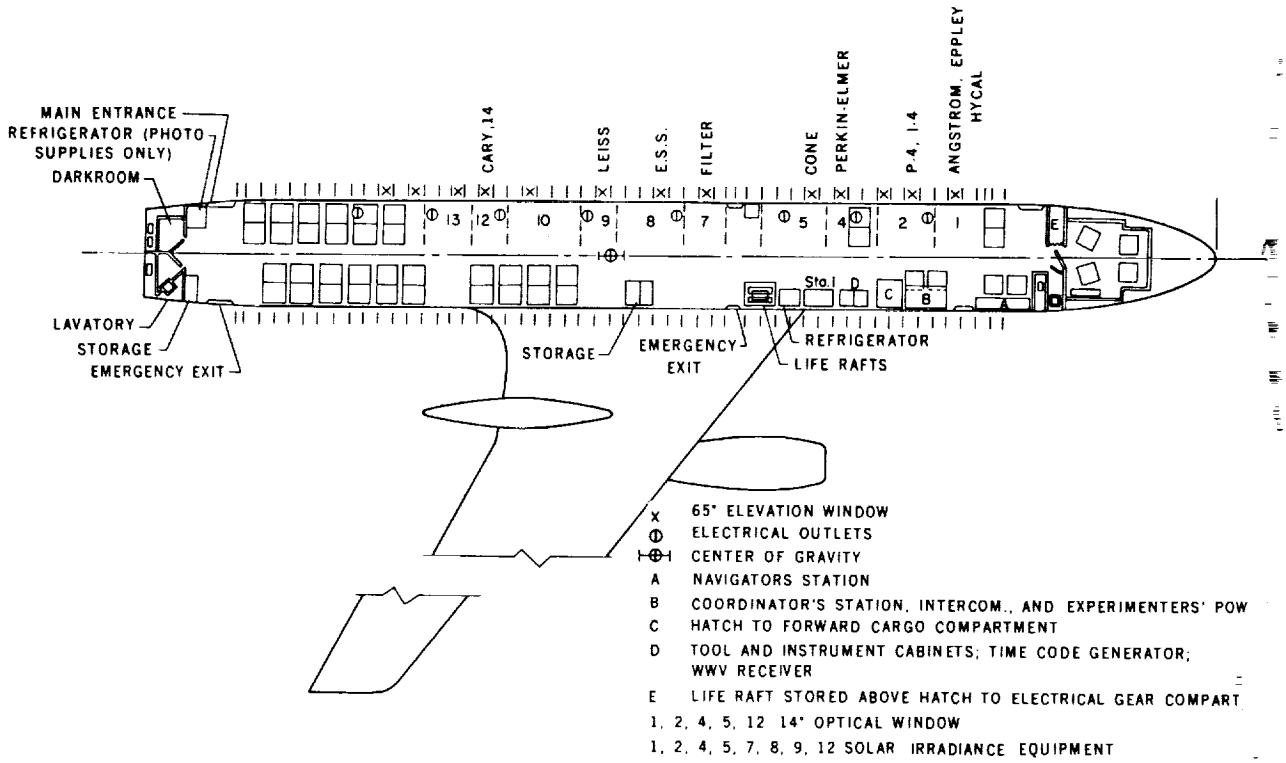

Figure 3—Floor plan of NASA 711 "Galileo", showing solar irradiance equipment and solar scanning instruments to port, electronic chassis and tape recorders to starboard.

distinguished by their serial numbers, were also obtained from the Eppley Laboratory. The principle of measurement is that of balancing the temperature of two metal strips—one of which is exposed to radiation, and the other is heated by an electric current. The calibration is with reference to the international pyrheliometric scale. The Cone radiometer is an absolute instrument which was designed and developed in the Thermodynamics Branch, GSFC. The irradiance is determined from the difference in electrical heating power supplied to the wire-wound cone with and without the external radiation. The angular aperture of these instruments is limited by the diaphragm mounted in front of each at some distance from the sensitive surface, so that the incident energy is due only to the sun and a known small fraction of the circumsolar sky. The irradiance of the circumsolar sky at 38,000 feet was computed, from data published in literature,[28] to be about 5×10^{-4} (1/20 percent) of that of the sun. In Table 2 the wavelength range of these instruments is given as .3 to 4 μ, the lower limit being due to atmospheric ozone and the upper limit to the quartz window of the aircraft.

Seven instruments were used for measuring the spectral distribution of solar irradiance. They represent a wide variety of size, design, construction, measuring process, data analysis, wavelength range and resolution. There are three monochromators—Perkin-Elmer (Perkin-Elmer Corporation, Norwalk, Connecticut), Leiss (Leiss Instrument Co., West Germany), and Cary 14 (Cary Instruments, Monrovia, California); two interferometric spectrometers (Block Engineering, Inc., Cambridge, Massachusetts), the P-4 for the range up to 2.5 μ and the I-4 for the IR range up

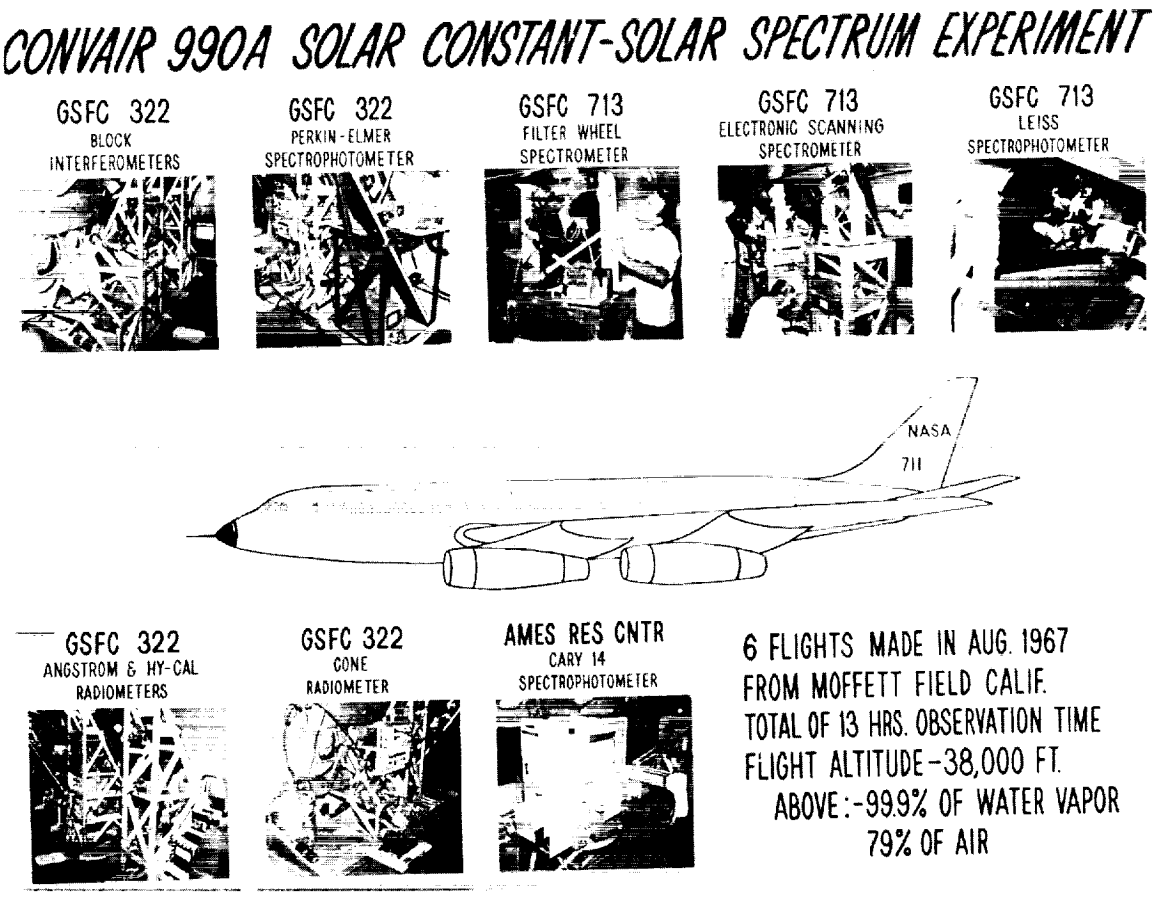

Figure 4—Location of experiments on board NASA 711.

to 15 μ; one electronic scanning spectrometer (International Telephone and Telegraph Industrial Laboratories, Fort Wayne, Indiana); and a filter radiometer designed and constructed by the Thermophysics Branch, GSFC. The wavelength range covered by the instruments was determined by the material of the dispersive element and by the detector. The visible range, .3 to .65 μ, was scanned by all instruments except the I-4 interferometer. Photomultipliers are highly sensitive in this range. The near infra-red, .7 to 2.5 μ, was covered by the Leiss and Cary 14 monochromators, P-4 interferometer, and partly also by the filter radiometer. The detectors were a phototube in the case of the GSFC filter radiometer and PbS cells in the other three. The Perkin-Elmer monochromator, having an LiF prism and thermocouple detector, covered the range up to 4 μ. The I-4 interferometer spanned the range 2.6 to 15 μ. The material for the aircraft window was selected according to the range covered by the respective instrument: Irtran 4 for the I-4 interferometer, sapphire for the Perkin-Elmer monochromator, and fused quartz for the others. For the five instruments at the tail of the aircraft the entire window was covered by a quartz plate, grade Dynasil 4000 or Corning 7940, size 12" × 14", thickness 1"; these windows were available from earlier solar eclipse expeditions of NASA 711. The observation windows in the nose were covered by aluminum blanks with 4"-diameter holes containing infrasil quartz or sapphire, and 2"-diameter holes containing Irtran-4. These windows were made specifically for these solar irradiance flights. The infrasil ensured better transmittance in the H_2O bands and the small apertures lessened the

Table 2

Data on Instruments Used for Solar Irradiance Measurements
On Board NASA 711 Galileo, August 1967.

Instrument	Energy Detector	Type of Instrument	Aircraft Window Material	Wavelength Range	Experimenters
1 Hy-Cal Pyrheliometer	Thermo-electric emf	Total	Infrasil	0.3 to 4 μ	McNutt, Riley
2 Ångström Pyrheliometer 6618	Resistance Strip	Total	Infrasil	0.3 to 4 μ	McNutt, Riley
3 Eppley Normal Incidence Radiometer	Thermo-electric emf	Total	Infrasil	0.3 to 4 μ	McNutt, Riley
4 Block P-4 Interferometer	1P28 or R136 PbS Tube	Soleil Prism Soleil Prism	Infrasil Infrasil	0.3 to 0.7 μ 0.7 to 2.5 μ	Rogers, Ward
5 Block I-4 Interferometer	Thermistor Bolometer	Michelson's Bi-mirror	Irtran 4	2.6 to 15 μ	Ward, Rogers
6 Perkin-Elmer Monochromator	1P28 Tube Thermocouple	LiF Prism LiF Prism	Sapphire Sapphire	0.3 to 0.7 μ 0.7 to 4 μ	Thekaekara, Winker, Stair
7 GSFC Conc Radiometer	Resistance Wire	Total	Infrasil	0.3 to 4 μ	Kruger, Winker, Ward
8 GSFC Filter Radiometer	Phototube	Dielectric Thin Film Filters	Dynasil	0.3 to 1.2 μ	Stair, Lester
9 Ångström Pyrheliometer 7635	Resistance Strip	Total	Dynasil	0.3 to 4 μ	Duncan
10 Electronic Scanning Spectrometer	Image Dissector Tube	Grating	Dynasil	0.3 to 0.48 μ	Webb
11 Leiss Monochromator	E.M.I. 9558 Q.A. PbS Tube	Quartz Double Prism	Dynasil	0.3 to 0.7 μ 0.7 to 1.6 μ	McIntosh, Park, Stair
12 Cary 14 Monochromator	1P28 Tube PbS Tube	Grating and Prism	Corning 7940	0.3 to 0.7 μ 0.7 to 2.5 μ	Arveson, Griffin, Kinney

scattered light within the aircraft. The pointing accuracy of the instruments towards the sun was ensured in azimuth by the aircraft itself which maintained a flight path constantly at right angles to the sun. Accuracy in elevation was ensured for the Perkin-Elmer and Cary 14 monochromators by external reflecting optics which tracked the changing elevation of the sun, and for the other 10 instruments by the instrument itself rotating about a horizontal axis parallel to the length of the aircraft. For instruments 8 through 11 on Table 2, the fixture design permitted observation through the upper windows only. The other instruments could be shifted to the lower windows for low solar elevation. The normal to the upper windows was at 65° to the horizontal; the normal to the lower windows was at 14° to the horizontal.

The spectral irradiance instruments display a wide diversity in their principles of operation, and in their data acquisition and analysis. The three monochromators, though greatly different in external and internal optics, have in common a dispersing element. In the filter radiometer, 30 narrow-band filters are interposed in succession between the incoming light and the detector. The electronic scanning spectrometer operates on a principle similar to the Vidicon camera; the spectrum is displayed on an X-Y plotter. The P-4 and I-4 interferometers record an interferogram on a magnetic tape from which a spectrum is later obtained by computerized Fourier analysis.

All spectral irradiance measurements are on a relative scale, since the output at any given wavelength depends not only on the incoming light but also on the transfer function of the instrument, which is dependent on the wavelength. This function is determined by measuring a standard of known spectral irradiance. The most reliable standards now available in the .25 to 2.5 μ range are the 1000 w quartz iodine lamps, formerly issued by the National Bureau of Standards and now issued by the Eppley Laboratory. Two blackbody sources were used to extend the wavelength range beyond 2.5 μ. One source, operating in the temperature range 800° to 1400°K, was manufactured by Infrared Industries, Santa Barbara, California, and the other source, operating in the temperature range 1700° to 3000°K, was manufactured by Astro-Industries, Santa Barbara, California.

C. Mounting and Fixture of the Instruments

All the instruments for measuring total and spectral irradiance are standard items of a radiometric laboratory. All of them, except the I-4 Michelson-type interferometer which required a special shockproof mounting, are also relatively insensitive to the levels of shock and vibration encountered on an aircraft. Only minor modifications were needed in the instruments themselves to change them from measurement of laboratory sources to measurement of the sun. However, for several months prior to the flight, a major effort in design and construction was needed to provide for each instrument and item of equipment a mount which would meet the specifications of the aircraft for loading and safety. Loads are borne by the two pairs of rails on either side which serve as the seat tracks in passenger planes. All mounting frames and instruments were attached to these rails either directly or with a one-inch plywood pallet. For the instruments operated by the Thermodynamics Branch, Numbers 1 to 7 in Table 2, the design of the mounts and racks and a detailed stress analysis were undertaken by Fairchild-Hiller, Germantown, Maryland.[29] Fairchild-Hiller Corporation built the instrument mounts; the GSFC Fabrication Division built the electronics racks. The design and fabrication of the mounts for instruments operated by the Thermophysics Branch (Numbers 8 to 11) was done jointly by Metcraft, Inc., Baltimore, Maryland, and the GSFC Fabrication Division. The construction of the Cary 14 mounts, and the final modifications required for all the other mounts and racks during the two weeks before the flight, were undertaken by the workshops attached to the Airborne Sciences Office at Ames Research Center.

The design and fixture of the mounts, and their arrangement in NASA 711 Galileo, can best be shown with the aid of Figures 5 to 8 which are reproductions of photographs taken on board the aircraft. These were taken while the plane was on the ground, or in flight to the location.

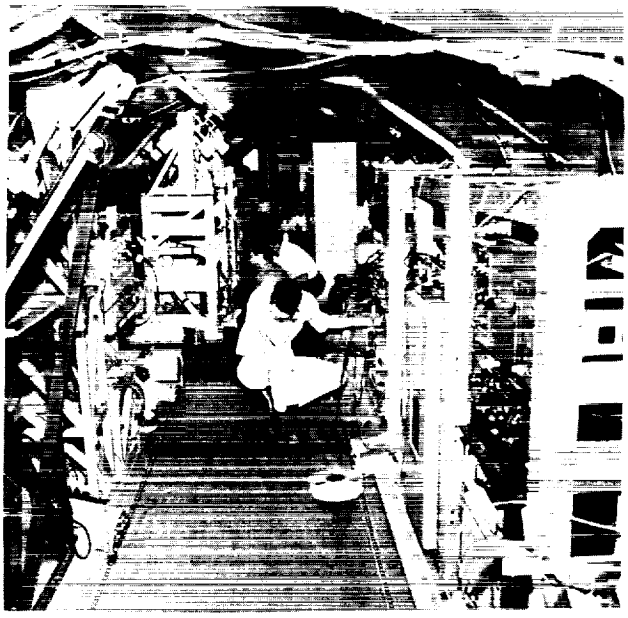

Figure 5—View down the aisle towards the tail of the aircraft.

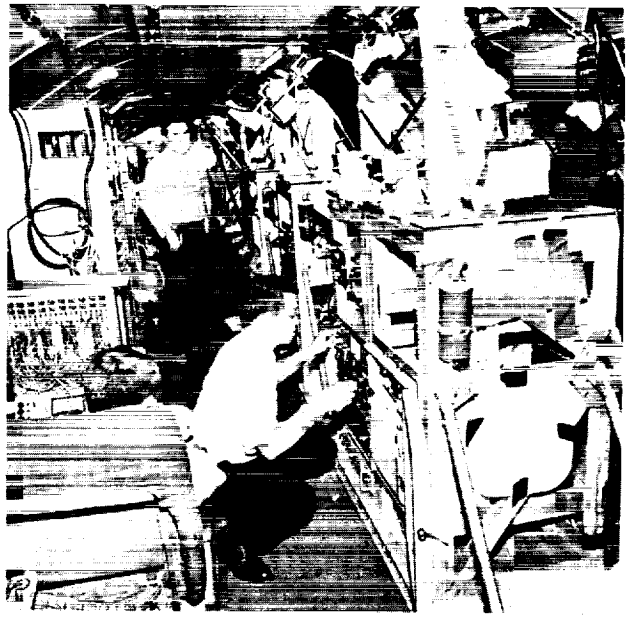

Figure 6—View up the aisle towards the nose of the aircraft.

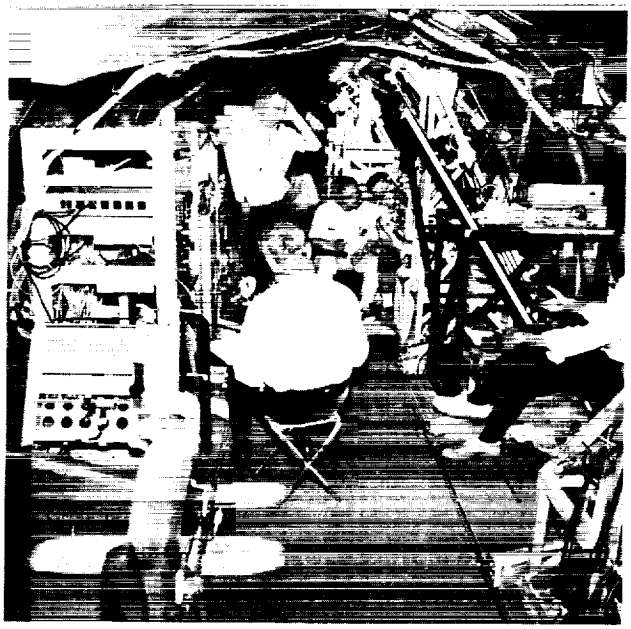

Figure 7—Front section of the aircratt cabin, showing experimenters during in-flight calibration of the equipment.

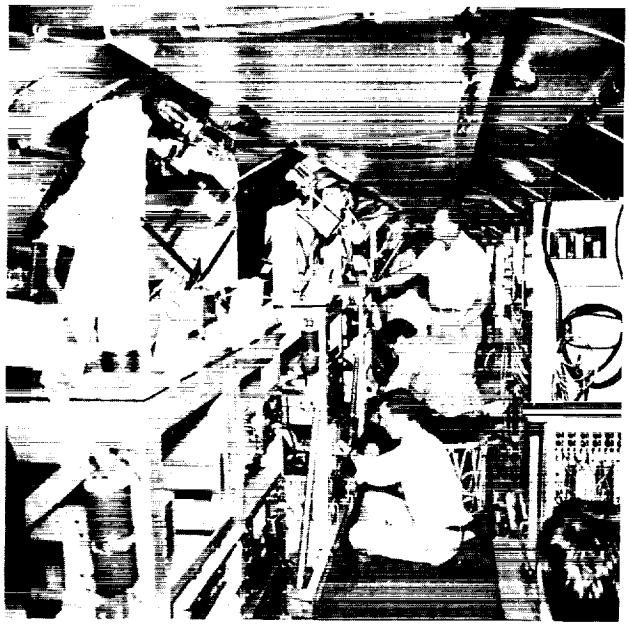

Figure 8—Mid section of the aircraft cabin, showing experimenters during in-flight calibration of the equipment.

Figure 5 gives a view from the nose of the plane, looking down the aisle. Most of the instrument mounts, and the racks for the power supply and the electronics, can be identified in this picture. On the port side of the plane in front are seen the black-painted slant rails of the

Perkin-Elmer monochromator. Behind it are the upper and lower mounts for the cone radiometer, the mounts for the filter radiometer, the electronic scanning spectrometer (E.S.S.), and the Leiss monochromator. On the starboard side are the control console for the Perkin-Elmer monochromator, the tape recorder, the control console for the Hy-Cal pyrheliometer and the cone radiometer. The experimenters are, front to rear, McNutt, Lester and Park.

Figure 6 which gives a view up the aisle from the rear of the aircraft serves as a complement to Figure 5. The instruments seen on the port side are, front to rear, the Leiss monochromator, E.S.S., filter radiometer, cone radiometer, and Perkin-Elmer monochromator. The experimenters are Park and Lester. The pseudo-polar axis mounts of the first three instruments, the handles used for tracking the sun, and the standard lamp holders can be clearly distinguished.

Some of the instruments and the experimenters at their respective stations are seen in Figures 7 and 8. Figure 7 shows some of the instruments of the Thermodynamics Branch; the experimenters are, left to right—Thekaekara, back to camera, Maichle, Kruger, Ward and Winker. Figure 8 shows the instruments operated by the Thermophysics Branch; the experimenters are, left to right—Webb, Lester and Duncan, standing. These pictures were taken during flight while making calibrations with standard lamps, prior to the solar measurements.

J. Flight Altitude and Atmosphere Above the Aircraft

The flights of NASA 711 for the solar irradiance measurements were made at an altitude of 38,000 ft, except for the first flight of August 3 which was at 38,300 ft. This altitude was chosen as a compromise between the minimum amount of atmospheric air above the aircraft, and maximum length of observing time. An altitude of 40,000 ft, which had been maintained in the eclipse flights of NASA 711, had first been projected for the solar irradiance flights, but that would have entailed a sacrifice of about 40 minutes of observing time per flight. The weight of the plane without any load is 118,000 lbs., and that of fuel for 7 flying hours is 85,000 lbs. Compared to these the weight of less than 7000 lbs. for men and equipment is relatively small. The total weight is the major factor determining the ceiling of the flight; thus at 195,000 lbs. weight the aircraft can reach 37,000 ft, and at 170,000 lbs. the ceiling is 39,000 ft. It was decided early in the planning stage that the aircraft would depart Moffett Field with a full load of fuel, fly out to a distant point, thereby expending fuel and bringing the total weight down, make a U-turn and then start the data-taking portion of the flight. During this portion, the bearing of the aircraft would be normal to the incoming solar rays. The observations would stop at about 15 minutes flying time from Moffett Field. The higher the altitude chosen for the observation, the less fuel would be available, and hence the shorter would be the duration of the data-taking portion of the flight. The altitude of 38,000 ft proved to be a satisfactory compromise. Altitude is determined from the pressure outside the aircraft as indicated by an aneroid barometer. The conversion from pressure to altitude is made on the assumption of the U.S. standard atmosphere for pressure-altitude variation. Thus, the reading of the aircraft's altimeter represents not so much the exact value of the height above sea level as the weight per unit area of the atmosphere vertically above the aircraft. Since this intervening atmosphere causes attenuation of the solar energy, maintaining a constant altimeter

reading ensured the constancy of an important parameter in the solar measurements—the air mass above the aircraft.

The atmospheric pressure at 38,000 ft is 208 millibars, which is 20.5 percent of the pressure at sea level. At 40,000 ft the pressure is 18.6 percent. The difference, though not negligible, was considered a small enough tradeoff for the extra observation time which would be available for each flight at the lower altitude. A major consideration is that at these high altitudes the atmosphere consists almost entirely of the permanent gases, and the relative composition and hence also the attenuation due to Rayleigh and aerosol scattering is independent of geographical location. The factors which contribute most to the uncertainties in ground-based measurements, namely, dust, smoke and water vapor, become vanishingly small at the high altitudes. Tables of typical moisture content at different altitudes are available in literature;[30] from these data it is seen that the annual average of precipitable water vapor above 38,000 ft is about 30 microns. This is less than 0.2 per cent of the total annual average of precipitable water, 17.9 mm, in the atmosphere above sea level for mean latitudes. An independent measurement was made in September, 1967 by the Environmental Sciences Service Administration (ESSA) in the vicinity of Moffett Field from an aircraft at 38,000 ft. From the depth of the main H_2O absorption band at 6 μ, the amount of precipitable water vapor above the aircraft was calculated and found to vary between 12 and 18 μ. Our own findings (discussed later) show that the H_2O content, though varying with date and location of flight, was of the same order of magnitude. This is of great significance for measurements of solar spectral irradiance in the wavelength range longer than 7000 Å which contains about half the solar energy. The strong predominance of H_2O absorption bands in this range is illustrated in Figure 9, which shows four curves related to solar spectral irradiance. It is reproduced from "Solar Radiation" by Gast[24] in the *Handbook of Geophysics*. The lowest of the four curves, with a large number of absorption bands, is the solar spectral irradiance as seen from sea level for air mass one, that is, for rays entering the atmosphere normally to the earth's surface. The so-called atmospheric windows are few and narrow, and even in these windows the assumption that the energy is transmitted without any water vapor absorption is open to doubt. For measurements at ground level,

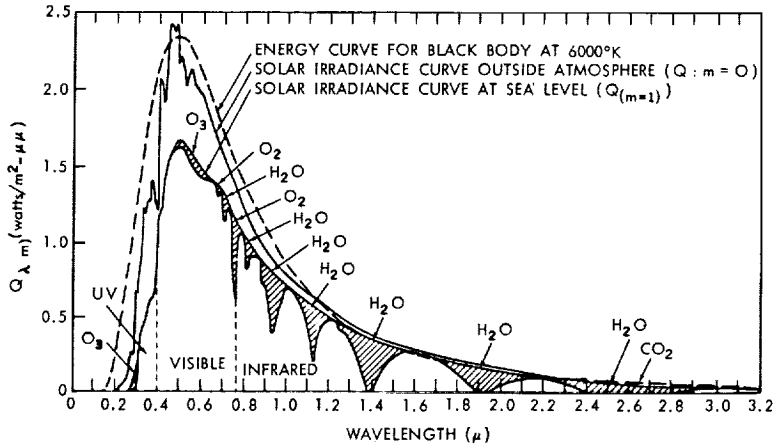

Figure 9—Spectral irradiance curves related to solar energy.

water is not only a strong absorber but also a highly inconstant absorber. Hence the measurements from a high-altitude aircraft can yield a degree of accuracy which is impossible at ground level.

The amount of water vapor within the aircraft is also a factor to be considered. Two independent methods were used to determine this. Readings of the wet and dry bulbs of a psychrometer were taken at different locations within the aircraft and on different days. An alternate method was to fill three previously evacuated cans with samples of cabin air, and analyze these with a C.E.C. 613 mass spectrometer. Values of relative humidity were between 5 and 10 percent, which correspond to between .7 and 1.4 μ of precipitable water vapor per meter of path length. Residual gas analysis of cabin air confirmed this result; the values were .99 μ, .98 μ and 1.04 μ respectively for the samples collected during the last three flights. The relative percentages of the permanent gases O_2, N_2, and A were shown by the residual gas analysis to be the same as in normal atmospheric air. CO_2, which is only .0314% in normal air, was found to be several times higher than expected, namely 16.9, 11.1 and 7.3 times the normal mixing ratio, on the three days. In an attempt to check this anomaly, three other samples of cabin air were taken during later flights of NASA 711 in February 1968. Again the agreement between psychrometric and RGA data was confirmed for water vapor, and CO_2 was found to be 3 to 7 times higher than the normal mixing ratio. It should be noted that this type of residual gas analyzer does not distinguish between CO_2 and N_2O, which in normal air is 1/6 percent of CO_2.

The effect of the permanent gases in the atmosphere above the aircraft, though small compared to that at ground level, is not negligible, and requires a closer study. Data, based on Elterman's computations, are available in literature (Reference 28, pp 7-3 to 7-36) for the extinction optical thickness from height h to ∞ for altitudes at intervals of 1 km for different wavelengths. The transmittance of the atmosphere for any given wavelength is related to the extinction optical thickness by the equation

$$T_{h\infty} = \exp\left(-\tau_t' \sec z\right), \qquad (1)$$

where z is the zenith angle of the sun, τ_t' is the extinction optical thickness, and $T_{h\infty}$ is the ratio of energy transmitted to altitude h to that incident above the atmosphere. τ_t' is the combined effect of Rayleigh scattering, aerosol scattering and ozone absorption. The parameters given by Elterman were computed for U.S. standard atmosphere under certain simplifying assumptions. Table 3 gives the values of τ_t' and $T_{h\infty}$ for sea level and for the altitudes of NASA 711 flights. The values of wavelength are those given by Elterman. Beyond .90 μ the six values given are for the optical windows of the atmosphere. The extinction optical coefficients for 38,000 ft and 38,300 ft were computed by interpolation from Elterman's values for 11 km (36,090 ft) and 12 km (39,370 ft). An important feature revealed by the table of values of transmittance is that at all wavelengths, even in the infrared, there is a considerable difference between the values at sea level and at the altitude of the aircraft. The difference in transmittance for 38,000 ft and 38,300 ft is negligible except at .3 μ. For wavelengths less than .3 μ the ozone absorption is so strong that practically no energy reaches the aircraft. The transmittance, which is only 4.5 percent at .3 μ, increases rapidly

Table 3

Extinction Optical Thickness and Attenuation Due to the Atmosphere at Sea Level and at the Altitude of NASA 711 Galileo.

Wavelength (μ)	Extinction optical thickness from ∞ to h			Attenuation from ∞ to h for normal incidence		
	Sea Level	38,000 ft	38,300 ft	Sea Level	38,000 ft	38,300 ft
.28	37.806	32.618	32.560	3.801×10^{-17}	6.83×10^{-15}	7.24×10^{-15}
.30	4.968	3.110	3.100	6.96×10^{-3}	.0446	.0451
.32	1.551	.4656	.4624	.212	.628	.630
.34	1.046	.1690	.1668	.212	.845	.847
.36	.872	.1179	.1162	.351	.889	.890
.38	.744	.0943	.0929	.476	.910	.911
.40	.619	.0743	.0736	.539	.928	.929
.45	.455	.0479	.0473	.635	.953	.954
.50	.370	.0411	.0406	.691	.960	.960
.55	.331	.0487	.0483	.718	.952	.953
.60	.305	.0553	.0550	.737	.946	.946
.65	.252	.0298	.0297	.777	.972	.972
.70	.217	.0154	.0153	.805	.985	.985
.80	.187	.0084	.0083	.829	.992	.992
.90	.166	.0034	.0034	.847	.997	.997
1.06	.151	.002	.002	.860	.998	.998
1.26	.141	.001	.001	.869	.999	.999
1.67	.126	.001	.001	.882	.999	.999
2.17	.109	0	0	.897	1.0	1.0
3.5	.089	0	0	.915	1.0	1.0
4.0	.080	0	0	.923	1.0	1.0

to 63 percent at .32 μ and 95 percent at .45 μ. The absorbance of the permanent gases becomes negligible only for wavelengths greater than 2 μ.

Thus, practically over the whole wavelength range of solar spectral irradiance there is a non-negligible absorption effect due to the atmosphere. The parameters on which these computations are based are not sufficiently accurate, and the U. S. standard atmosphere is not exactly valid for the locations of the flights, so that it is necessary to make observations for different zenith angles and to extrapolate to zero air mass using the conventional method of plotting logarithm of the signal versus air mass.

E. Flight Paths and Air Mass

NASA 711 made six flights between August 3 and August 19, 1967. Summary data on the starting and finishing points of the measurement portion of the flights are given in Table 4. The flight of August 3 was originally intended for checking out the performance of the instruments. All instruments were found to function properly from the very beginning and hence usable data were obtained all through the 2 hours and 10 minutes during which the flight path was normal to the sun's rays. The measurements started at a point which was 1227 miles from Ames Research Center in a direction 14.5° west of south. These values of distance and direction are approximate. The latitude and longitude given in Table 3 were known quite precisely from measurements made on board the aircraft by the navigator. The measurements started at 4:40 p. m. Pacific Daylight Saving Time. The zenith angle of the sun and the air mass given in Table 4 were computed from the known parameters of latitude, longitude, time and date as will be discussed later. The measurements ended at a point 135 miles from Ames in a direction 17.6° south of west and at time 6:50 p. m. Similar data for the flights of the other five days are also given in the table.

The second flight started later in the afternoon and observations were continued until the sun was 6.86° above the horizon. The third was an early morning flight for which the experimenters and crew were in the airplane at 3:30 a. m. As the sun began to rise over the mountains of Canada,

Table 4

Summary Data on Starting Point and Finishing Point of Measurements on Board NASA 911 Galileo.

Flight (period of day)	Date (1967)	Distance to Ames (miles)	Direction with Reference to Ames (degrees)	Time (Pacific Daylight Saving Time)	Latitude (degrees N)	Longitude (degrees W)	Zenith Angle (degrees)	Air Mass at 38,000 ft
STARTING POINT								
1. Sunset	Aug 3	1277	14.5°W of S	4:40 p.m.	19.533°	127.167°	43.83°	1.3858
2. Sunset	Aug 8	1449	20.7°W of S	5:16 p.m.	17.833°	130.000°	50.14°	1.5596
3. Sunrise	Aug 10	1262	11.3°W of N	7:10 a.m.	55.333°	128.500°	81.26°	6.5290
4. Afternoon	Aug 14	1403	1.3°W of S	2.32 p.m.	17.133°	122.750°	18.53°	1.0545
5. Mid-day	Aug 16	1297	20.6°N of E	11:06 a.m.	44.000°	98.583°	31.01°	1.1665
6. Afternoon	Aug 19	1413	4.0°W of S	2:31 p.m.	17.000°	123.667°	18.01°	1.0514
FINISHING POINT								
1. Sunset	Aug 3	135	17.6°S of W	6:50 p.m.	36.750°	124.267°	73.15°	3.4420
2. Sunset	Aug 8	183	19.8°S of W	7:40 p.m.	36.333°	125.250°	83.14°	8.2713
3. Sunrise	Aug 10	250	6.4°S of W	9:43 a.m.	37.000°	126.717°	54.74°	1.7313
4. Afternoon	Aug 14	176	13.5°S of W	5:02 p.m.	36.833°	125.250°	52.86°	1.6555
5. Mid-day	Aug 16	333	20.8°E of N	1:30 p.m.	41.917°	119.883°	28.18°	1.1406
6. Afternoon	Aug 19	294	34.3°S of W	5:00 p.m.	35.003°	126.500°	52.23°	1.6319

the plane started to make a U-turn, and the observations began at 7:10 a. m. with the sun at an elevation of 8.74° above the horizon. During these three flights we had the advantage of measuring the solar irradiance over a wide range of zenith angles, 43.83° to 83.14°, the corresponding air masses being 1.386 and 8.271. All the instruments which had mounts designed for use with both upper and lower windows were directed to lower windows. Measurements were made with the other instruments during the portion of the flight when the elevation of the sun was sufficiently high to illumine the integrating sphere from the upper window.

The fourth flight was an early afternoon flight when all 12 instruments could be directed towards the sun during the whole of the data-taking portion of the flight. The zenith angle changed from 18.53° to 52.86°. At the start all instruments were turned towards the upper window, but in the course of the flight, the Cary 14 monochromator and the seven instruments in the front section of the aircraft had to be changed from the upper to the lower window. This was accomplished without any significant loss of time. But another factor which could not have been provided for made this flight break the perfect record of clear skies and usable data which had been established thus far. There was a hurricane over the Pacific Ocean west of Mexico that day and the weather forecasts on which we had relied for the exact location of the hurricane proved to be in error. This is not surprising since our flight was in an area little traveled by commercial aircraft and hence deficient in weather reports. During the first hour of the data-taking portion of the flight the aircraft was closer to the eye of the hurricane than had been anticipated and there were large masses of cirrus clouds above the aircraft. Hence we decided to change our original plans for the final flight of the series and to schedule for that day a similar flight path with the same range of solar zenith angle and air masses. We had originally intended for the flight of the final day a series of three elongated ellipses over much the same geographical area south of Ames. This "race track" flight path would have shortened the total observing time but would have served as a check on the variation of atmospheric opacity, if any, over the 1000 or more miles of each of the other flights. However, getting usable data during all of an afternoon flight and from all 12 instruments seemed more important for the whole program than investigating the (probably small) effect due to the latitude variation of the ozone layer. The increased observing time was another consideration for changing the "race track" plan.

The fifth flight on August 16 was in an east to west direction, with the sun shining from the south. Because of the requirement that the data-taking portion of the flight should end near Ames, the flight path was not over the ocean but over the western United States, from South Dakota, across the states of Wyoming, Utah and Nevada, and over the Rocky Mountains. Our fears of meeting more cirrus clouds over land than over water proved to have been wrong. In fact this flight gave us the clearest skies, and the least aircraft-roll, so that the signals received by the instruments were quite strong throughout the flight.

The final flight of the series for repeating the zenith angle range of August 14 was made on August 19. The flight started from Oakland Civil airport since Moffett Field had been reserved by the U. S. Navy for a major annual airshow that morning. High altitude cirrus clouds again caused a minor change in flight path, but useable data were obtained all during the flight.

During each flight, at intervals of ten minutes, the flight navigator made measurements of the latitude and longitude of the aircraft location. Figure 10 is a map of the geographical area covered in the six flights, with curved lines showing the route taken during the data-taking portion of each flight. Each flight path is indicated by the date and by the time in Pacific Daylight Saving Time (P.D.S.T.) of start and finish of data acquisition.

The flight navigator also supplied detailed aeronautical charts of each flight. He used these charts for planning the flight path. The actual route of the aircraft differed slightly from the projected route because of varying windspeed, and the essential condition of the flight that the aircraft bearing should be at right angles to the sun. The positions of the aircraft are shown at ten-minute intervals during the return flight. The chart for the sunrise flight of August 10 is shown on a reduced scale in Figure 11. Note that the path actually flown started slightly to the east and ended slightly to the west of the computer-generated, planned flight path. The

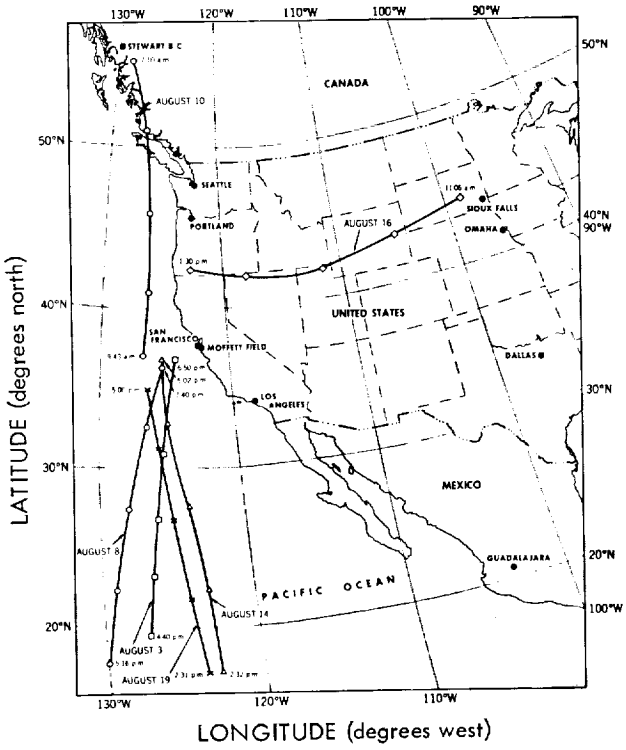

Figure 10—Flight paths of NASA 711 Galileo for solar irradiance experiments, August 1967.

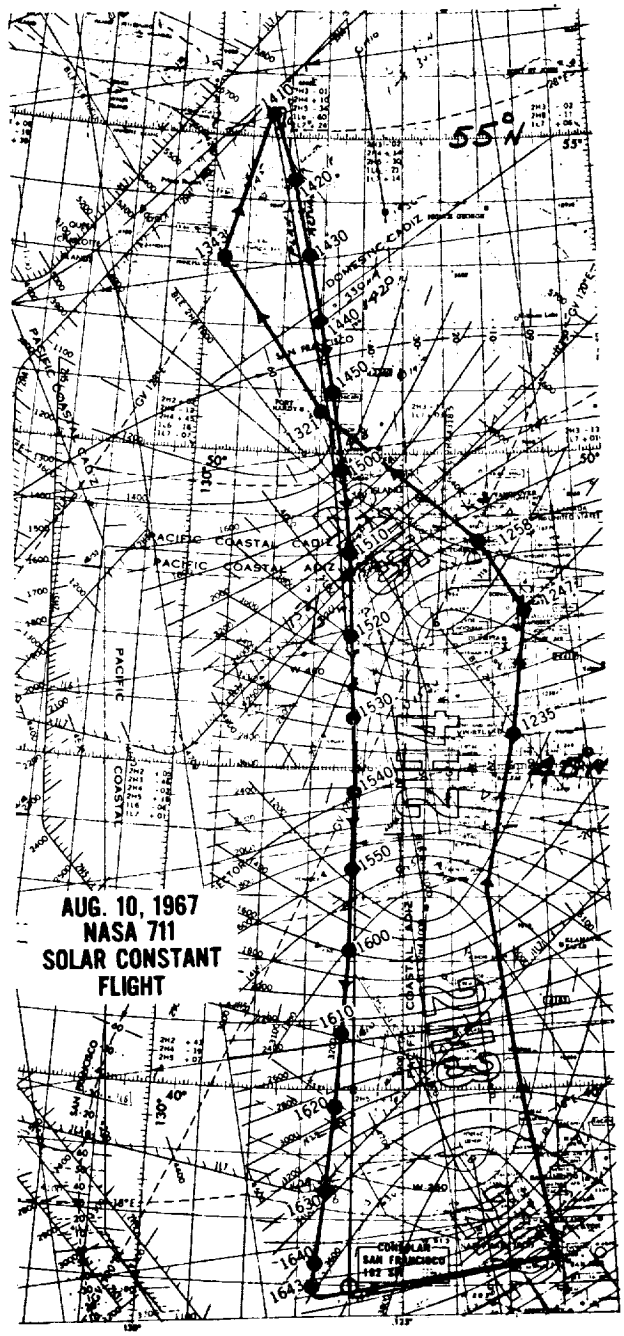

Figure 11—Navigator's chart, showing the flight path on August 10.

time in hours and minutes given in these figures is G.C.T., Greenwich civil time or universal time. It is eight hours ahead of P.D.S.T., in terms of which the data in Table 4 are recorded.

The position data provided by the navigator using Loran A and doppler radar are considered accurate to within 10 nautical miles. These data were used in a computer program to calculate the zenith angle of the sun and the air mass above the aircraft at one-minute intervals. Air mass data are needed to determine the solar irradiance for zero air mass, that is, in the absence of the earth's atmosphere. Air mass is defined as the ratio of the distance travelled by the rays of the sun in the atmosphere for a given zenith angle of the sun and altitude of observer to the distance for same altitude and zenith angle zero. Air mass is unity when the sun is vertically above the observer. For other positions of the sun,air mass is the secant of the zenith angle in the first degree of approximation. The zenith angle may be directly measured by a sextant or may be computed from the known values of latitude, longitude and time. Since the aircraft was a moving platform, it was decided that instantaneous computed values of position over the ground would be more reliable than measured values.

The zenith angle z is related to latitude ϕ, declination of the sun δ and the hour angle of the sun h by the equation

$$\sec z = (\sin\phi \sin\delta + \cos\phi \cos\delta \cos h)^{-1} . \tag{2}$$

Basic data for computing δ and h at any given location and time are available in *The American Ephemeris and Nautical Almanac*.[31] Values of δ are given for 0^h G.C.T. (Midnight Greenwich civil time) for every day of the year, from which by linear interpolation δ for time t P.D.S.T. can be found. The hour angle of the sun is 15° times the difference in hours between the time of the day and the time when the sun crosses the meridian. The time of the day in this case is the local true solar time which is slightly different from the local mean solar time. The difference between the two is the equation of time. The local mean time varies with the longitude, being exactly equal to the Pacific standard time at longitude 120° west, and decreasing by 4 minutes for every degree increase in longitude. Taking these correction factors into account, it can be shown that the hour angle in degrees is given by

$$h = |t - 4\theta + \epsilon - 300| \times 0.25 , \tag{3}$$

where t is time, P.D.S.T., since midnight in minutes, θ is longitude in degrees, ϵ is equation of time in minutes (true solar time—mean solar time).

The variables (declination at 0^h G.C.T., change in declination per hour, and equation of time) for each day of the flight were obtained from the *American Ephemeris and Nautical Almanac*. An expression for zenith angle dependent on these three variables, and on the three variables of the flight path—latitude ϕ, longitude θ and time in P.D.S.T.—was derived and programmed for the computer. The input data for computing ϕ and θ were the values of 10-minute intervals supplied by the flight navigator. The first three pairs of consecutive values of ϕ and t were fitted to an equation

of the second degree to give ϕ for increments of one minute. Then the first pair of ϕ and t was replaced by the 4th pair to extend the interval by 10 minutes. Thus in every interval except the first and last, two values of ϕ are available for a given t; any difference between the two is due to slight deviations from the parabolic path or more likely to rounding off errors in reading the latitude. A similar method was employed for finding θ at one-minute intervals.

Equating the air mass to the secant of the zenith angle is valid only in the first degree of approximation, and does not take into account the decreasing air density in the upper layers of the atmosphere and consequent bending of the sun's ray as it passes from a rarer to a denser layer. Two formulae are available for obtaining a more accurate value of the air mass for ground-based measurements, one due to Bemporad[32] published in 1907 and widely used by many of the early observers of solar irradiance and a more recent one due to Kasten[33] published in 1964. The latter is computed from the air density profile of the U. S. standard model atmosphere proposed in 1959 by the Air Force Research and Development Command, and is considered more accurate. However, for measurements at 38,000 ft, above 80% of the atmosphere, Kasten's formula is over-corrected. The value of air mass at 38,000 feet which we have used as being most satisfactory is a weighted average of the secant of the zenith angle and the value given by Kasten's formula, with relative weights in the ratio 4 to 1. Figure 12 shows the variation of air mass with time on the six days of the flight. On August 16 the air mass was practically constant. There was a small change on

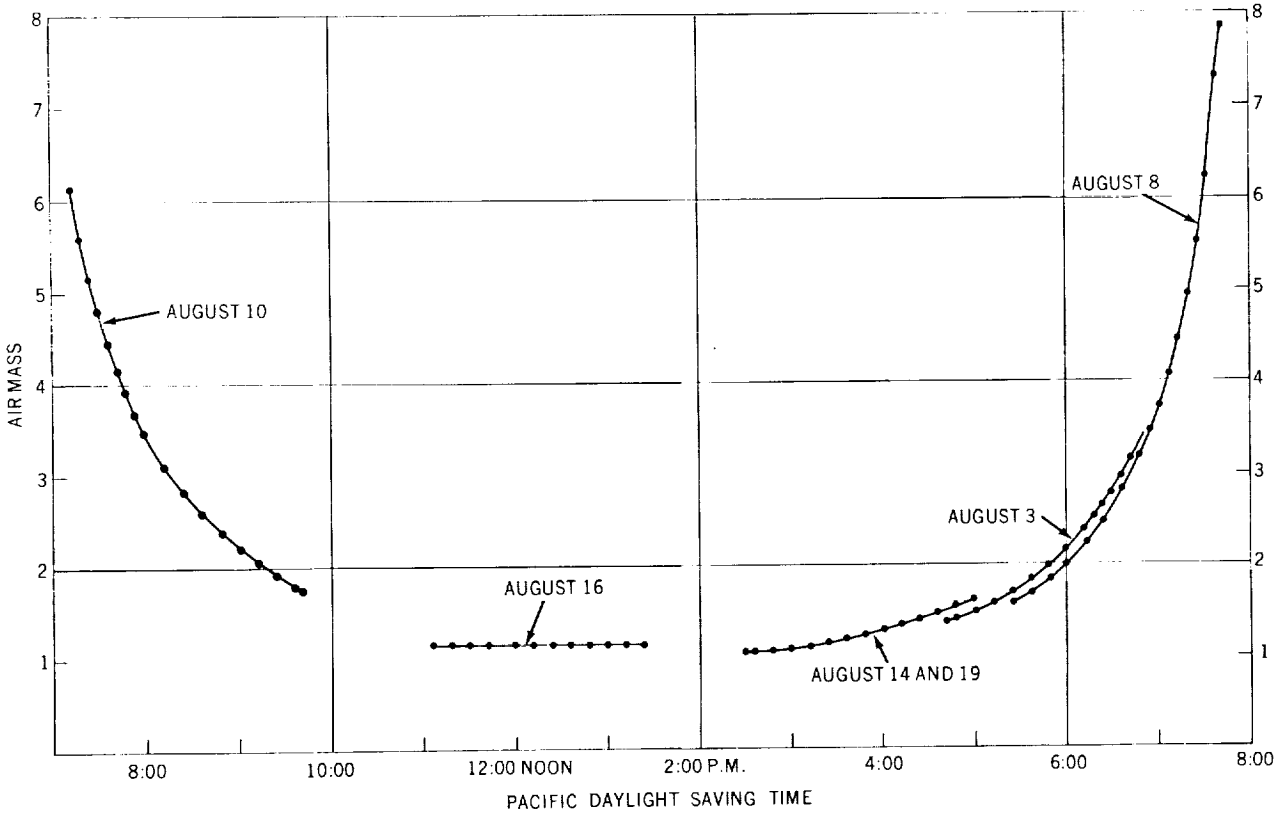

Figure 12—Variation of air mass with time for the flights of NASA 711.

August 14 and 19. On the other days the change was over a wide range. Early in the morning on August 10, and late in the evening on August 8, the air mass changed very rapidly with time.

A sample of the table giving aircraft location and air mass, which was prepared soon after the flights and distributed to all the experimenters, is shown in Table 5. Only 10 minutes of flight time from August 8 are shown here. The first and last entries of the latitude and longitude are from the flight navigator; the rest are by parabolic interpolation. The average zenith angle and the air mass at 38,000 ft given in the last two columns are based on two sets of interpolations. The final column, as stated earlier, is $(0.8 \sec \theta + 0.2\, l_k)$ where l_k is air mass from Kasten's formula.

Another factor which has to be considered as a correction factor common to all the instruments is the distance of the earth from the sun. The solar constant and spectral irradiance are defined for the mean sun-earth distance, which is the semimajor axis of the earth's orbit or one astronomical unit (A.U.). During the days of the flights, the ratio of the sun-earth distance to one A.U. had the following values: August 3: 1.0146; August 8: 1.0139; August 10: 1.0136; August 14: 1.0128; August 16: 1.0125; August 19: 1.0119. These values were obtained by interpolation from those given in U. S. Nautical Almanac for every day at zero hour G.C.T., with due corrections for actual flight time and the difference between G.C.T. and P.D.S.T. It is seen that, since the sun was at a distance greater than average during the flight days, the values obtained from our observations must be increased by percentages varying between 2.9 and 2.4 to give the true solar constant and spectral irradiance.

Table 5

Air Mass Computation from Location of the Aircraft and Time of Day—
Sample Data for 10 Minutes of Flight Time on August 10, Sunrise Flight.

Time (Pacific (D.S.T.)	Latitude (degrees (north)	Longitude (degrees west)	Zenith Angle of the Sun (degrees)	Air Mass (Bemporad's formula)	Air Mass (Kasten's formula)	Average Zenith Angle from 2 Interpolations	Air Mass at 38,000 ft
7:20 a.m.	54.383°	127.833°	79.72°	5.4564	5.4395	79.72°	5.5705
7:21	54.272°	127.778°	79.57°	5.3833	5.3668	79.575°	5.4947
7:22	54.157°	127.726°	79.42°	5.3125	5.2963	79.43°	5.4210
7:23	54.039°	127.675°	79.28°	5.2438	5.2281	79.29°	5.3516
7:24	53.919°	127.627°	79.13°	5.1773	5.1619	79.14°	5.2793
7:25	53.796°	127.581°	78.98°	5.1128	5.0977	78.995°	5.2113
7:26	53.669°	127.537°	78.84°	5.0501	5.0354	78.85°	5.1450
7:27	53.540°	127.495°	78.69°	4.9893	4.9750	78.70°	5.0782
7:28	53.407°	127.456°	78.55°	4.9303	4.9163	78.56°	5.0175
7:29	53.272°	127.418°	78.41°	4.8729	4.8592	78.415°	4.9561
7:30	53.133°	127.383°	78.27°	4.8171	4.8037	78.27°	4.8962

PART II

SOLAR TOTAL IRRADIANCE EXPERIMENTS

A. The Cone Radiometer—R. Kruger and M. P. Thekaekara

1. Description of Equipment

The wire wound cone radiometer was one of the instruments used on board NASA 711 for measuring the total solar irradiance. Figure 13 shows all the total radiation detectors, unmounted and placed side by side to indicate their relative size. Left to right are seen, after the limiting diaphragm of the cone radiometer on the extreme left, 1) the cone radiometer in its vacuum enclosure, 2) the Ångström pyrheliometer, 3) the Hy-Cal pyrheliometer, and 4) the Eppley normal incidence thermopile.

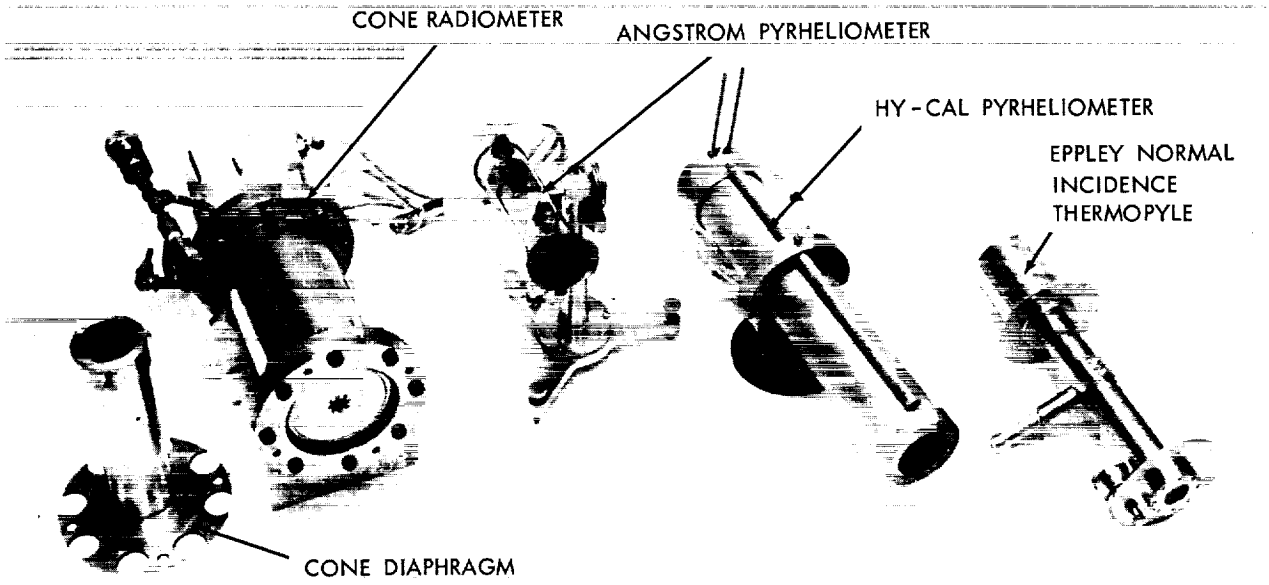

Figure 13—Total radiation detectors.

The cone radiometer is designed to operate as an absolute total radiation detector, using an electrical power substitution method. It is therefore referenced to the scale of absolute electrical units. The radiometer is designed to operate in vacuum, where gaseous conduction and convection may be neglected.

The theory behind the operation is relatively simple. If an electric current is passed through a wire wrapped in the shape of a cone with the base open, the energy dissipated will be radiated

out through the base and outer surface of the cone. If the slant outer surface is enclosed in a housing whose temperature is maintained constant, the energy incident from this enclosure to the slant surface may be considered constant. The energy incident on the base of the cone is a function of the environment viewed by the base. If, after stable conditions are reached, the energy reaching the base is changed, the wire temperature and resistance will change. If these are returned to their original values by varying the current through the wire, the change in electrical power is then a measure of the net change in the radiant energy falling on the base of the cone.

The detector used in this program was made by wrapping a fine wire (0.002 inch diameter insulated nickel wire) on a 30° apex angle conical mandrel. The wire was then thinly coated with an aluminum filled epoxy, removed from the mandrel, and painted inside and out with Parsons' black matte lacquer. The unit had a mean base diameter of 9.65 mm. The effective absorbance of the detector was taken as 0.9945, based on the work of Gouffé.[34] This value is open to question but is, however, used in this report. A value of 0.99 for a cone would result from the method of Campanero and Ricolfi.[35] The actual value of the area times the absorbance used in this report is 0.7364, which includes corrections for the area of the rim of the cone and its absorbance (0.9), and a 1.9% correction which will be discussed later. If the value of 0.99 is chosen for the conical absorbance and 0.96 for rim absorbance, the area times absorbance is less than 0.1% different than the value used for this report.

The detector is mounted by fine wires at four points inside a housing or block which is cooled by liquid nitrogen, and made of copper to improve isothermality. Figure 14 is a drawing of the radiometer configuration. The block is shaped so as to prevent reflection from the front surface into the detector. The interior is conically shaped to decrease to a negligible amount that light which passes through the annulus between the detector and the front of the block and is reflected onto the slant surface of the cone. The interior of the cavity is coated with 3M Velvet flat black paint.

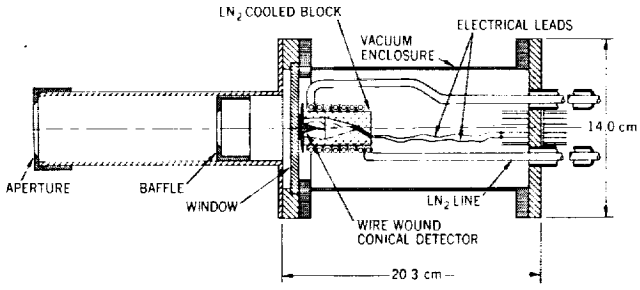

Figure 14—Cross-sectional view of cone radiometer.

The block and detector are enclosed in a vacuum-tight chamber with a sapphire window. This material was chosen for the window because of its mechanical and optical transmission characteristics (no absorption bands from 0.2 to 6 μ). The chamber itself is constructed of stainless steel with Viton o-rings used on the sealing surfaces and teflon used for both thermal and electrical insulation.

The aperture system is designed in accordance with the method of A. Ångström.[36] Two acceptance angle apertures were manufactured, one with approximately a 3° acceptance angle and a second giving an angle of 5-1/2°. The 5-1/2° aperture was used for most of the flight. The other unit was used for a short period during the test but no difference was detected.

Figure 15 is a schematic representation of the electrical system. The conical detector forms one leg of the Wheatstone bridge. Resistor R_v is varied according to the energy level to be detected. For this series of tests, the cone resistance was about 206 ohms which happens to correspond to a temperature of 23°C. A voltage-to-current converter provides the bridge voltage and detects the null. Changes of null are sensed by the converter and the bridge voltage is varied to return the system to null.

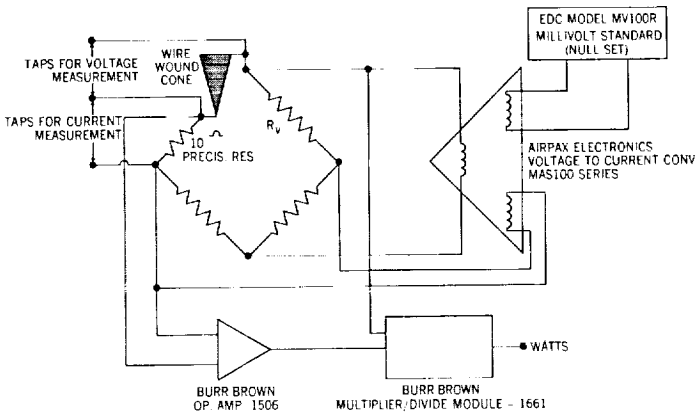

Figure 15—Electrical schematic diagram of cone radiometer.

The data for this report were hand recorded. A Dana digital voltmeter, model 5600, was used to measure the voltage across the cone and across the 10-ohm precision resistor to determine current. Data were also recorded on tape from the Burr-Brown multiplier/divider unit, model 1661, which yields a direct measurement of electrical power by supplying the product of voltage and current.

The mounts for the cone radiometer are shown in Figure 16. The control panels for the electrical circuitry were attached to the lower window mount.

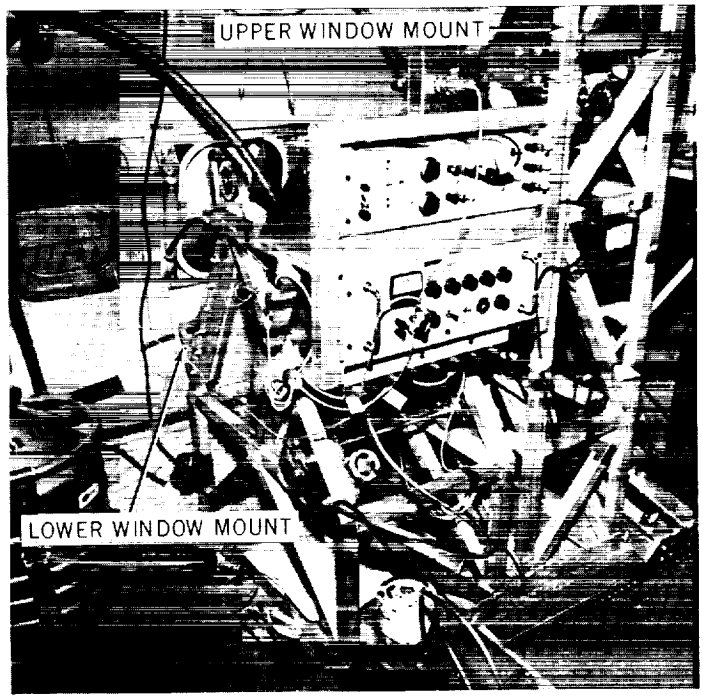

Figure 16—Cone radiometer mounting.

2. *Experimental Procedure*

Prior to each flight, the electrical system was checked to assure that it was operating. The liquid nitrogen dewar and pressurization system were filled. A mechanical pump was used to evacuate the radiometer housing; this would normally bring the unit to the order of 15 μ pressure. The system was then valved shut and liquid nitrogen fed to the cooled block. This caused a further reduction of pressure by cryopumping to a final value ranging between 0.7 and 2.8 μ pressure as measured by a Hastings thermocouple gage. Although this is not sufficient vacuum to eliminate gaseous conduction and convection, these terms are reduced to where they are small and nearly constant. The use of the zero readings provides a method for decreasing the effects of pressure variations.

On the flight out to the data-taking leg, liquid nitrogen flow was stabilized and the block operated during the tests at -185°C ± 2°. The electronics were given one to two hours to warm up.

During the data-taking leg, the system was checked for null, and hand recordings were made of time, voltage and current through the cone, off-null current, bridge voltage, millivolt standard output, block temperature, and chamber pressure. The latter four values were only checked occasionally to assure that no gross changes occurred. Data from the Burr-Brown model 1661 were recorded on the Ampex CP-100 tape recorder; time, synchronized with WWV, was also recorded on the magnetic tape. The output of the Burr-Brown model 1661 was corrected several times each flight to equal the power as calculated from the digital voltmeter readings.

During the flight, tracking was manually accomplished as explained in Part I of this report. Aside from occasional large excursions due to aircraft motions, the system could normally be kept aligned to within 1/2° of angle.

3. *Data Analysis*

a. Data Selection

The data for this report are taken entirely from the hand recorded data. While the tape recorded data was accurate to within 1%, the multiplier/divider unit was found to be in error by 2% on some occasions when corrections were being made. The tape recorded data did provide information of a qualitative nature in particular as to whether the electronic system was stable; also the voice channel was used as a log.

Of the hand recorded data, some have been discarded for various reasons. 25 readings were omitted when a review of the data showed a marked shift and increase in scatter for these points. This happened on the two days when the instrument was moved from the upper to the lower window; the erratic data occurred when the detector was moved to the lower window. A careful layout of the equipment indicated a high probability that light could be scattered off the window aperture edge and into the detector. 20 readings were eliminated when log notations indicated light haze and other atmospheric disturbances. Other data were discarded for reasons such as cone resistance outside an error limit, electrical system being unstable, and a question of whether the radiometer window was parallel to the aircraft window. This last item is very angle-sensitive and would cause an increase in transmittance of over 1%.

b. Zero Readings

In order to obtain a best estimate of the net power change in the detector, the zero readings were plotted and a smooth curve drawn through them. The particular value of this curve at the time of the solar observation was then used as the tare power value.

c. Reduction to Zero Air Mass

A method of data reduction was developed in order to obtain from the irradiance values at different zenith angles the value of the solar constant and the irradiance at the average sun-earth

distance in the absence of the atmosphere. This method is applicable to all the total irradiance instruments used on board the aircraft.

Let P° be the solar constant, and P be the irradiance measured by the radiometer for air mass ℓ. P is the integral

$$\int_0^\infty P_\lambda \, d\lambda ,$$

where $P_\lambda \, d\lambda$ is the energy in the narrow wavelength band λ to $\lambda + d\lambda$. Let $P_\lambda^\circ \, d\lambda$ be the zero-air-mass solar irradiance in the same band. P_λ° and P_λ are related by the equation

$$P_\lambda = P_\lambda^\circ \tau_\lambda A_\lambda^\ell , \tag{4}$$

where τ_λ is the transmittance of the window at wavelength λ (in the case of the cone, the transmittance of the combination of the quartz window of the aircraft and the sapphire window of the cone casing) and A_λ is the attenuation due to the atmosphere above the aircraft for a ray of wavelength λ incident normally.

Hence the irradiance as measured by the radiometer is

$$P = \int_0^\infty P_\lambda \, d\lambda = \int_0^\infty P_\lambda^\circ \tau_\lambda A_\lambda^\ell . \tag{5}$$

The value of τ_λ varies monotonically and slowly with λ, except at the two ends of the spectrum and in the absorption bands of quartz. The theoretical values of A_λ are given in Table 3. A_λ also varies slowly with λ. But there are exceptions, mainly in the wavelength ranges where ozone and water vapor are strong absorbants. The effect of water vapor is discussed later in Part III, Section E of this report.

Since both A_λ and τ_λ change gradually with λ over most of the wavelength range where the zero air mass solar spectral irradiance, P_λ°, is not extremely small, the integral in Equation (5) can be replaced by a summation. Taking the logarithm to the base 10 for both sides, we have

$$\log_{10} P = \log_{10} \sum_{i=1}^{n} F_i \tau_i A_i^\ell , \tag{6}$$

where we have written F_i for the fraction of P° in a finite wavelength range; τ_i and A_i are average values of the window transmittance and atmospheric attenuation over the same range; n is the total number of wavelength ranges into which the spectrum is divided, and i is a running subscript. The larger the number n, the closer is the approximation to the integral on the right-hand side of

Equation (5). In practice the value 20 for n was found to be more than adequate. A larger number was not justified by the experimental uncertainties in the determination of P.

The value of τ_i can be determined to a high order of accuracy. This was computed theoretically from the index of refraction and adjusted by experimental data in the absorption bands. Account was taken for the inter-reflection between parallel surfaces of sapphire and quartz. Variation of reflectance with angle was also computed. Over the wavelength ranges where water vapor does not cause significant absorption, A_i can be determined both from the results presented in Table 3 and from the experimental data of the spectroradiometric instruments. In the wavelength ranges of water vapor absorption the parameters A_i are to some extent uncertain, all the more so since the amount of precipitable water vapor above the aircraft for the different locations and times of the data points could not be determined with sufficient accuracy. We chose different sets of values of A_i and evaluated the right-hand side of Equation (6) as a function of air mass ℓ. A solar spectral distribution function is needed for F_i. When the data from the total irradiance instruments were being reduced, the results of our spectroradiometers were not yet available. Hence we chose the Johnson curve for the spectral distribution. Later it was found that changing this distribution to ours did not produce any significant change in the summation.

The right hand side of Equation (6) can be evaluated for different values of ℓ, and the points plotted with ℓ on the X-axis and $\log_{10} \Sigma F_i \tau_i A_i^{\ell}$ on the Y-axis. The points do not lie on a straight line as would be the case for a Langley plot for a single wavelength, but on a curve which is concave up. Changing the assumed value of the solar constant shifts the curve up or down parallel to the Y-axis without changing its shape. Changing the parameters A_i changes the shape of the curve, making it more concave or less so. The solar irradiance at the two extremes of the spectrum is not observed by the instrument, in the UV due to ozone absorption and in IR due to quartz window absorption. This amounts to about 2%. The relative amounts of energy in these two ranges are included in the first and last terms of the summation. An erroneous assumption about the percentage of energy in these two ranges would also change the shape of the curve.

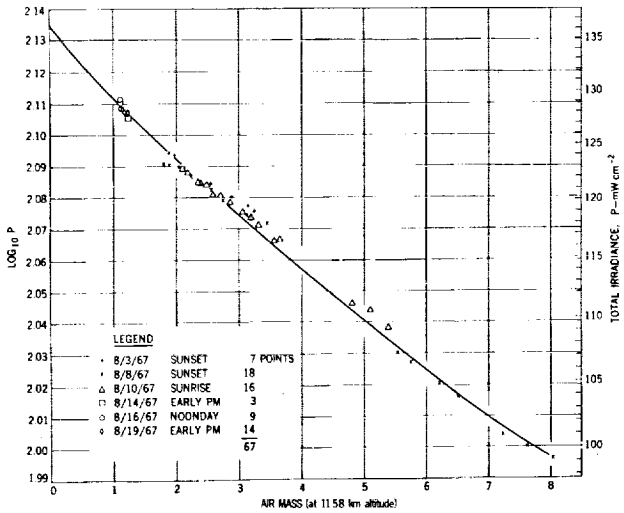

Figure 17—Data from the cone radiometer.

The irradiance values as measured by the cone radiometer, corrected to the mean sun-earth distance, are plotted on a large sheet of graph paper with $\log_{10} P$ on the Y-axis and air mass ℓ on the X-axis. The data points are shown in Figure 17. The right hand side of Equation (6) is evaluated by a computer for different values of ℓ and an assumed set of values of A_i. These points are plotted on a transparent sheet of paper to the same scale as the data graph, and a smooth curve is drawn through them. This sheet is slid over the data graph to test for closeness of fit. In practice it was found necessary to generate several curves with

different values of A_i. The curve which best fits the data points is chosen as the one which corresponds most closely to the atmospheric conditions. The intercept of this curve on the Y-axis gives the logarithm to the base 10 of the solar constant.

Since a family of curves may be built up by varying the value of A_i in any interval, it was decided to vary A_i in the interval between 1.2 and 1.6 μ in order to obtain a curve which best passed through all the data points. Using this approach, a value of 136.4 mW cm^{-2} was found as the value of P, the total irradiance.

A second approach was used which took advantage of the other available data. In this technique, the value of A_i was varied in those three intervals containing the 1.4, 1.9, and 2.7 μ water vapor absorption bands. The data from the Perkin-Elmer monochromator in those bands were reviewed for five periods—three on August 10, 1967, one on August 14, 1967, and one on August 16, 1967. The values were 131.9, 134.0, 133.8, 135.6, and 136.0 mW cm^{-2}, respectively. It is of interest to note that the readings are arranged in order of decreasing air mass: 5, 3.6, 2.25, 2.13, and 1.13, and also increasing amounts of precipitable water: 9, 12, 18, 22, and 28 μ.

d. Sources of Error

The following is a tabulation of sources of error and estimates of their magnitude in terms of the total irradiance P:

1.0% — Uncertainty in window transmittance.

1.0 — Value of A used in extrapolation.

0.2 — Effect of error in time of day of measurement on air mass; varies from 0.7 at air mass 8 to less than 0.1 at air mass 1.5. The value 0.2 was chosen as including most of our data.

0.1 — Position over the ground as determined by Loran A and doppler radar.

0.8 — Zero reading shift due to pressure rise in vacuum enclosure while taking a reading; derived from laboratory tests.

0.5 — Area times cone absorbance.

0.5 — Precision derived from laboratory tests applying the inverse square relationship to energy sources.

0.5 — Light reflected from front face of cooled block back to aperture tube and thence to detector; analytically derived but could not be measured in the laboratory.

0.1 — Error in measurement; digital voltmeter was checked at Ames Research Center accurate to within 0.01%.

A number of other sources of error, less than 0.1%, have been neglected. These include the effect of being off-null and the effect of light passing through the annulus between the cone and the cooled block. The latter was shown analytically to cause an error in the order of 0.02%.

Applying the method of the square root of the sum of the squares, one arrives at an overall error in the order of 1.8%.

One error which has been corrected for was a bias of 1.9% caused by a slightly rounded edge on the front face of the cooled block. This edge reflected light into the detector and was noticed during laboratory tests after the flight. The 1.9% figure was arrived at by conducting laboratory tests with the shiny edge painted black.

A major uncertainty is the absolute accuracy of the cone. For comparison purposes, tests were run with a standard 1 kW lamp source (Eppley Laboratories, Rhode Island, lamp serial ETK-6704). In order to have sufficient signal at the detector to give reliable readings, the unit was placed at 100, 75, and 50 cm from the source and the calibrated value of 1726 μW cm^{-2} at 200 cm was adjusted by the inverse square relation to 6.904, 12.274, and 27.616 mW cm^{-2} at the three distances, respectively. The radiometer indicated 7.070, 12.581, and 28.399 mW cm^{-2} at the three distances, or errors of +2.4%, +2.5%, and +2.8%. A review of the errors does not indicate differences of this order.

4. Results

Since five values have been indicated for the solar constant in the previous section, a weighting has been applied to arrive at a single value. This weighting is highly subjective. The value of 136.4 mW/cm^2 is the result of a best fit curve through all the data points. 60% of the final value is derived from this number. The remaining 40% is derived by accounting for the air mass so that the proportion of the number making up the final value is inversely proportional to the air mass. That is, those values derived from the higher air mass curve fits are given lower weighting. The value of air mass 5 has been deleted because of the large extrapolation. Tabulating the data results in the following:

$$136.4 \text{ mW cm}^{-2} \times 60\% = 81.8 \text{ mW cm}^{-2},$$
$$136.0 \text{ mW cm}^{-2} \times 17 = 23.1 \text{ mW cm}^{-2},$$
$$135.0 \text{ mW cm}^{-2} \times 9 = 12.1 \text{ mW cm}^{-2},$$
$$133.8 \text{ mW cm}^{-2} \times 9 = 12.1 \text{ mW cm}^{-2},$$
$$134.0 \text{ mW cm}^{-2} \times 5 = 6.7 \text{ mW cm}^{-2}.$$

The final value of the solar constant would then be 135.8 mW cm^{-2} ±2.4 mW cm^{-2}, or 1.8% uncertainty, based on the error analysis.

B. Hy-Cal Normal Incidence Pyrheliometer—A. McNutt and T. A. Riley

1. Description of Equipment

The Hy-Cal Engineering normal incidence pyrheliometer consists of a detector at the end of a tube 14 in. long and 2.75 in. in diameter with circular apertures. The acceptance angle is about

2° half angle. The detector surface is a thin metal disk, coated with Hy-Cal high emissivity graphite coating. The disk is mounted in a cylindrical copper block of 1.5 in. diameter and 0.75 in. length, with a quartz window. The spectral range of the window is 0.2 to 3.5 μ. The output from the detector is a dc millivolt signal which varies linearly with incident irradiance up to 2 solar constants. A calibration curve of millivolt output versus incident radiation is supplied with the pyrheliometer. Hy-Cal Engineering calibrated the pyrheliometer by comparison to a standard pyrheliometer calibrated with reference to a blackbody cavity.

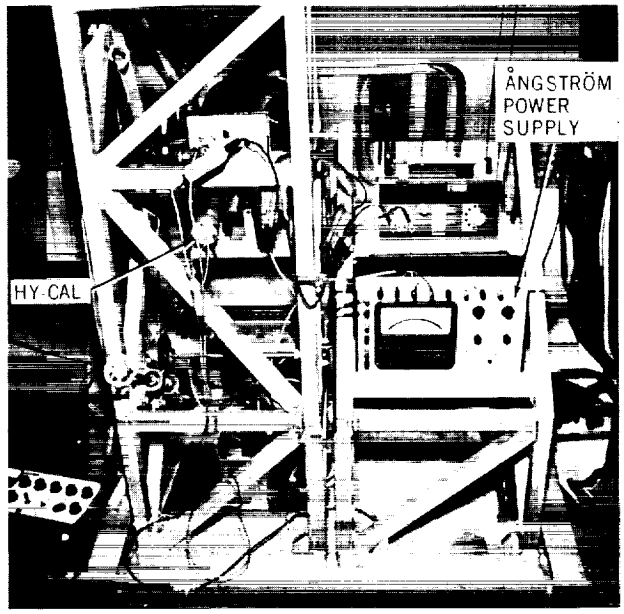

Figure 18—Mounting of the Ångström and Hy-Cal pyrheliometers.

2. Experimental Procedure

The Hy-Cal and Ångström 6618 pyrheliometers were mounted on the same stand. Figure 18 shows, to the left, the mounting rack for the detectors (the rear of the Hy-Cal pyrheliometer is clearly seen), and to the right the rack for the power supply and galvanometer for the Ångström 6618 pyrheliometer. The output of the Hy-Cal pyrheliometer was monitored in two ways. First it was read directly from the instrument using a Dana digital voltmeter, model 5600, about 3 or 4 times during each flight. The rest of the time it was amplified by an operational amplifier and recorded on one of the channels of the Ampex CP-100 tape recorder. The time, synchronized to WWV, was recorded on another channel of the same tape, so that a continuous record of signal versus time was available.

3. Data Analysis

The Hy-Cal pyrheliometer irradiance values were calculated using the formula:

$$I = 27.36\,V, \tag{7}$$

where

V = signal in millivolts,

27.36 = calibration constant, and

I = irradiance in mW cm^{-2}.

The analog flight tapes were sampled five times a second by a computer and averaged over a ten second period. The ten second averages were printed out, giving a table of signal in millivolts versus time at ten second intervals. The analog flight tapes were also played into a stripchart

recorder, giving a continuous graph of the analog signal as a function of time. The stripchart was used to select periods of time when the instrument was not sighted on the sun or when the signal was erratic for other reasons. The ten second averages during these times were omitted. A total of 170 irradiance values was obtained this way. The values obtained from the computer printout agree with the values taken at the corresponding time on the plane with the Dana digital voltmeter to within ±0.5%. The 170 irradiance values were plotted as a function of time and showed a scatter of ±1.0%. The irradiance values were then corrected for window transmission and the mean distance of the earth from the sun in the same way corrections were made for the Ångström pyrheliometer. A plot was made of the $\log_{10}$ of the corrected irradiance values versus air mass (Figure 19). Theoretical curves were fitted to the data as discussed earlier in the section on the cone radiometer.

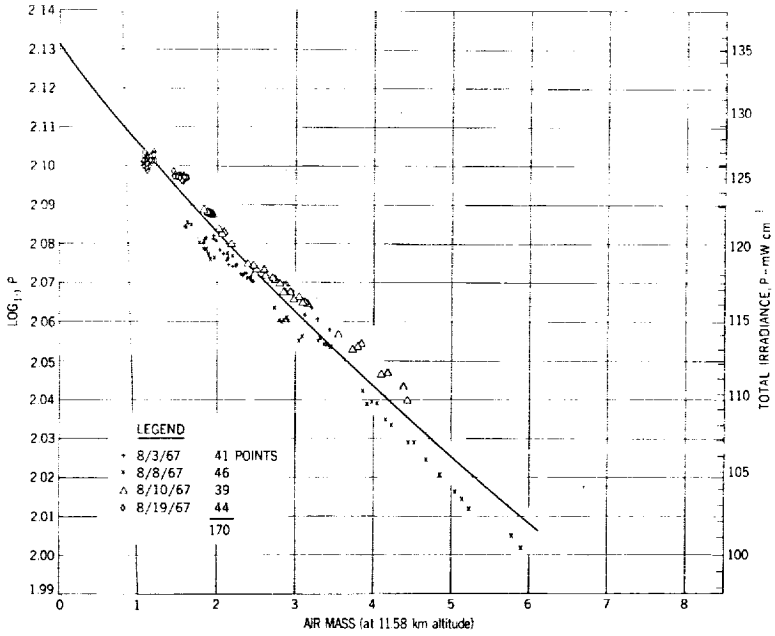

Figure 19—Data from the Hy-Cal pyrheliometer.

4. Results

The data are presented in Figure 19. The intercept for zero air mass is 2.131 which corresponds to 135.2 mW cm^{-2}. The error is 1.6% or ±2.2 mW cm^{-2}.

C. Ångström Compensation Pyrheliometer 6618—A. McNutt and T. A. Riley

1. Description of Equipment

Another total radiation detector was an Ångström Compensation Pyrheliometer 6618. It consists of two ribbon detecting surfaces located at the rear of a tube, nine in. long and two in. in diameter, containing rectangular apertures and a shutter. The shutter allows the left or right or

both ribbons to be exposed to the incident radiation. The ribbon is located about 5" behind the front of the instrument. The front aperture is such that each ribbon has plane angles of 4.2° and 10.6° as measured from the center of the ribbon to the edges of the aperture which admits radiation to it. The detector ribbons are manganin, sprayed with Parsons' matte black optical lacquer. Each strip has a copper-constantan thermocouple in thermal but not electrical contact with it, and can be heated electrically by passing current through it. Measurements are made by exposing the left ribbon to the incident radiation and heating the right ribbon electrically until both are the same temperature. The current necessary to heat the ribbon is measured. The shutter position is then changed so that the right ribbon is exposed and the left is electrically heated and the current is again measured. The average of the two measured currents, and a calibration constant (furnished with the instrument and determined by comparison to a standard pyrheliometer) gives the value of the incident radiation. The auxiliary equipment consists of a Kipp and Zonen galvanometer, model AL-1, which indicates when the ribbons are at the same temperature, and a battery power supply and meter for measuring the current. They were mounted on a separate stand, as shown to the right in Figure 18.

2. Experimental Procedure

A measurement was made every two to four minutes during a flight and took about one minute to get both a left and right ribbon exposure. The time of measurement was accurate to the nearest minute. The time and the current measurements were recorded by hand.

3. Data Analysis

The irradiance values measured by the Ångström pyrheliometer were calculated using the equation

$$P = Ka^2 , \tag{8}$$

where

P = irradiance in cal per min per cm^2,

K = calibration constant, and

a = average of left and right currents in amps.

The calibration constant K was checked by A. J. Drummond of Eppley Laboratory at Table Mountain, California on August 25 and 26 after the series of flights, and was found to be 6.08, a 1.0% change from the original value of 6.02. The value K = 6.08 was used in the reduction of the flight data. The current was measured with an accuracy of ±0.5%, but a plot of irradiance versus time showed a scatter of ±1.5%, so the accuracy of the raw data was assumed to be about ±1.5%. The irradiance values were corrected for transmittance of the aircraft window and the mean distance of the earth from the sun. One correction factor for the mean distance was used per flight for each of the six flights. One value for the window transmittance was used for all flights and all

angles of incidence for both upper and lower windows. This was done since the transmittance changed by only 0.5% over the full range of angles of incidence. The method for obtaining the window transmittance is described in the cone radiometer data analysis section of this report. Figure 20 shows the values of $\log_{10}$ of the irradiance plotted as a function of the air mass.

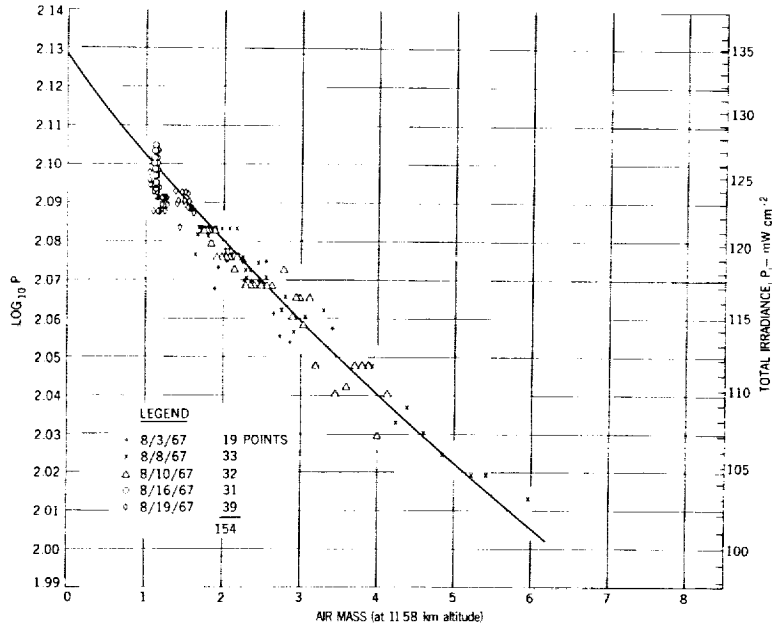

Figure 20—Data from the Ångström Pyrheliometer No. 6618.

Instead of fitting a straight line to the data by the method of least squares, a family of theoretical curves was generated to see which curve best fit the data, as described in the cone radiometer data analysis section of this report. The uncertainties in the time and position of the plane which affect the air mass value are negligible compared to the uncertainty in the irradiance values. The uncertainty in the window transmittance is of the order of ±1.0%. There is an uncertainty in choosing which curve to use, and where to fit it.

4. Results

The best fitting curve is shown in Figure 20. The intercept for zero air mass is 2.128 which corresponds to 134.3 mW cm^{-2}. The error is 1.9% or ±2.6 mW cm^{-2}.

A third total radiation detector, also operated by the GSFC Thermodynamics Branch, was an Eppley Laboratory-manufactured normal incidence radiometer. It was used in place of the Hy-Cal pyrheliometer for the first hour of the August 16 flight. It is an apertured instrument with a quartz window. The output is a dc millivolt signal from a thermocouple. A total of four readings was taken using the Dana digital voltmeter. The irradiance is calculated by multiplying the millivolt signal by a calibration factor. The four irradiance values were compared to the irradiance values of the Ångström pyrheliometer at the same time. They averaged 1.9% lower. No check was made,

however, on the calibration of this instrument since it was used for such a small portion of the total flight time.

D. Ångström Compensation Pyrheliometer 7635—C. H. Duncan and J. J. Webb

1. *Description of the Equipment*

This type of instrument is described in the preceding section of this report concerning the Ångström pyrheliometer 6618. This unit was originally not among the planned instrumentation. It was adapted to mount on the filter radiometer frame after the first flight, and data were recorded for the remaining flights. The pyrheliometer can be seen in the photograph in Figure 21.

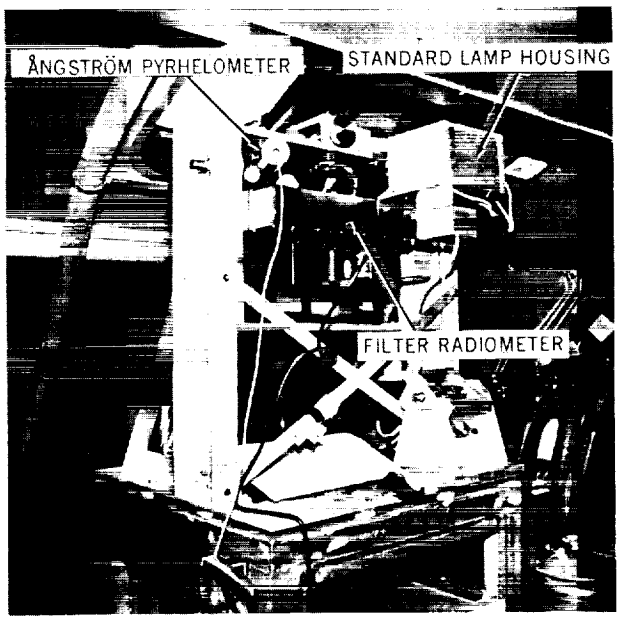

Figure 21—Mounting of the filter radiometer and Ångström pyrheliometer 7635.

2. *Data Analysis*

After the flight program, Ångström pyrheliometer 7635 was calibrated both at Table Mountain and later at the Eppley Laboratories. The instrument was not stable during the two days at Table Mountain and A. J. Drummond of Eppley, who was present during the calibration measurements, recommended an average value of 6.17 be used for the calibration factor.

A total of 42 measurements was made during the five flights but the readings of August 14 were discarded because of intermittent cloud conditions. The remaining data were corrected and the data were analyzed in the same way as for the other total radiation instruments.

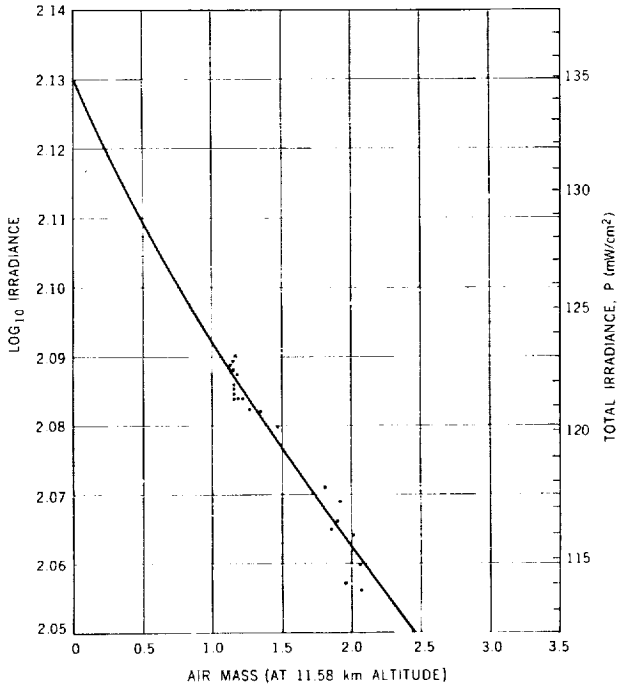

Figure 22—Data from the Ångström pyrheliometer No. 7635.

3. *Results*

The distribution of the data points is shown in Figure 22. The resulting value of total irradiance was 134.9 mW cm^{-2}, which is in good agreement with the other Ångström pyrheliometer. The errors in the system (particularly in view of the calibration) are on the order of 3% or ±4.0 mW cm^{-2}.

PART III

SOLAR SPECTRAL IRRADIANCE EXPERIMENTS

A. Perkin-Elmer Monochromator —M. P. Thekaekara, R. Stair, A. R. Winker

1. Description of the Equipment

A Perkin-Elmer monochromator model 112, with a sapphire window for the aircraft and a lithium fluoride prism as the dispersing element, was one of the instruments used on board NASA 711 to measure the spectral irradiance of the sun. Figure 23 shows an optical schematic of the instrument. Light from a diffusing mirror enters the instrument through an adjustable slit and is rendered parallel by a paraboloid mirror. A system of plane mirrors causes the beam to traverse the prism four times, thereby increasing fourfold the resolution obtainable from a single prism. After traversing the prism, the beam is focused on an exit slit, after which it is detected by either a thermocouple or a photomultiplier tube. Scanning the spectrum is done by a littrow mirror located behind the prism; the wavelength falling on the detector is indicated by the count on the drum which controls the rotation of the mirror.

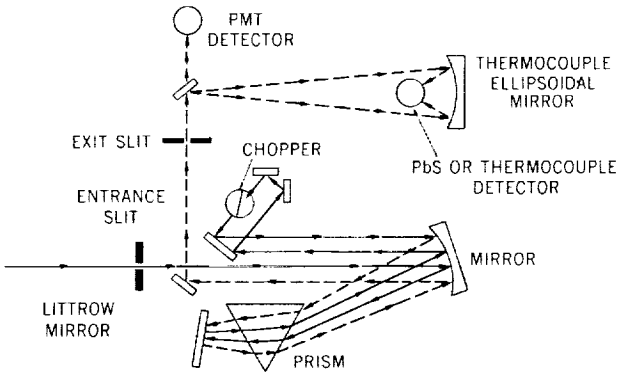

Figure 23—Optical schematic of the Perkin-Elmer monochromator.

An electronic console carries the amplifiers for the detectors, high voltage power supply for the PM tube, strip chart recorder, step-switch for gain setting of the amplifier and speed control of the littrow mirror, and several other features which make the Perkin-Elmer monochromator a highly versatile and automated instrument. A few modifications were introduced to make the instrument more suitable for the solar irradiance measurements. A helical potentiometer with a voltage divider was attached to the drum in order to generate a voltage which changed linearly with the drum count. Another voltage divider was connected to the gain control switch to generate a step voltage which changed by pre-set increments as the gain setting was increased. The output signals from both of these, and also from the detector amplifier circuit, were recorded on three of the channels of a tape recorder. A block diagram of the detection amplification system is shown in Figure 24. Modifications introduced at GSFC for recording the data on magnetic tape are enclosed in heavy lines.

The Perkin-Elmer monochromator was mounted on the plywood top of a rigid frame as shown in Figure 25. Sunlight falls on a diffuse mirror in front of the slit. This mirror was prepared at

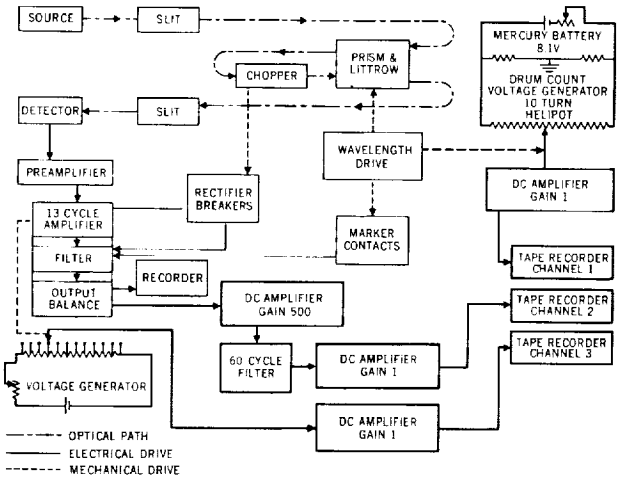

Figure 24—Block diagram of Perkin-Elmer data system.

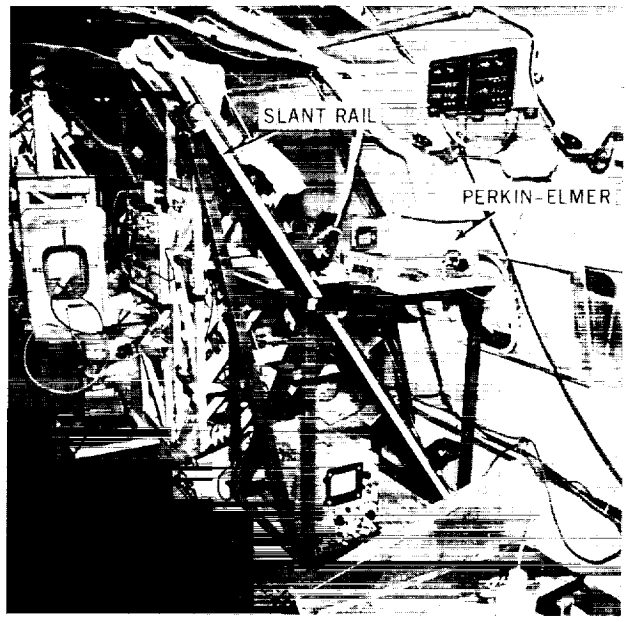

Figure 25—Mounting of the Perkin-Elmer monochromator.

GSFC by evaporating aluminum onto a ground glass surface. Tests had previously been made on two other types of diffusing surfaces—magnesium carbonate block, which many observers have used in previous solar irradiance measurements,[25] and gold evaporated onto frosted glass. Aluminum was found to have a higher reflectance over the whole wavelength range of the LiF prism. Some type of diffusing surface is essential for the solar measurements since the conventional method in spectroscopy of focusing the source on the entrance slit would have limited the observation to a very narrow strip on the solar disc and our interest is in the irradiance due to the whole disc. A plane diffuser was preferred to the integrating sphere because it increases the energy about ten-fold;[37] in the wavelength range 2 to 4 μ where solar energy is quite weak, low signal-to-noise ratio would have made the integrating sphere wholly unacceptable. The diffusing mirror is not, however, illuminated in the same manner by the collimated light of the sun as by the divergent beam from the quartz-iodine standard lamp. The standard lamp illumines the whole mirror, whereas the sun, shining through the 4" window of the airplane, illumines a limited elliptical area on the mirror and this area shifts a little with the pitch and roll of the plane. Hence a rectangular diaphragm of adjustable area was mounted a short distance in front of the entrance slit. The maximum area of this diaphragm was used only for portions of the flight which were free of all turbulence. Sunlight was reflected to the diffusing mirror by one of two plane mirrors mounted on a pair of slant rails which also carried the diffuse mirror. The three mirrors with their dust cover on can be readily identified in Figure 25. The height and angle of the plane mirror were adjusted during the flight, and the upper or lower mirror was used according to the position of the sun in the sky. The diffuse mirror was fixed in height, and its angle had one of two possible values according to the aircraft window which viewed the sun.

2. Experimental Procedure

During the six flights of NASA 711 Galileo, a total of 71 spectral scans of the sun was made. Nearly all the scans followed the same uniform procedure. The range of drum count was 2000 to 1100, wavelength .2945 μ to 2.53 μ, except during the mid-day flight of August 16 when the sun shining through the upper window permitted the range up to 600 drum counts, 3.884 μ wavelength, to be scanned. Each scan started with the PM tube as detector, slit width 0.1 mm, drum setting a few counts more than 2000. At count 2000 the drum voltage was turned on. At count 1550, wavelength .63 μ, the wavelength scan was stopped, slit-width changed to 2 mm, detector changed to thermocouple, and the scan was continued. At the end of the scan, the drum voltage was turned off, and height and angle of the plane mirror were readjusted to begin the next scan. The change-over from PM tube to thermocouple and from one scan to the next could be made in less than 30 seconds, so that spectral scans were made almost continuously from the time the aircraft completed the U-turn to view the sun till it turned away from the sun to start the descent to Ames. The scanning speed was 100 counts per minute, so that each scan was made in a little over 9 minutes. The scans of August 14 took 14 minutes each. The 1.25 in. per minute chart speed on August 3 was increased to 5 in. per minute for the five later flights.

Figure 26 shows a typical strip chart record in the PM tube range. It is a tracing based mainly on the scan made from 12:28 to 12:33 p. m. on August 16. Short sections from two other scans have been added to complete the record at the changes in gain setting. All the spectral scans are quite similar to the one shown here, except that the pen displacement is less for the lower position of the mirror and for the larger values of the air mass. The effect of the ozone becomes especially noticeable in the wavelength range 2950 to 3050 Å for large air mass. The curved lines showing intensity in Watts cm^{-2} μ^{-1} have been superposed on the strip chart record.

The calibration with reference to the standard lamp was made several times when the aircraft was in flight to the location, or in the hangar. The calibration scans made in the aircraft were

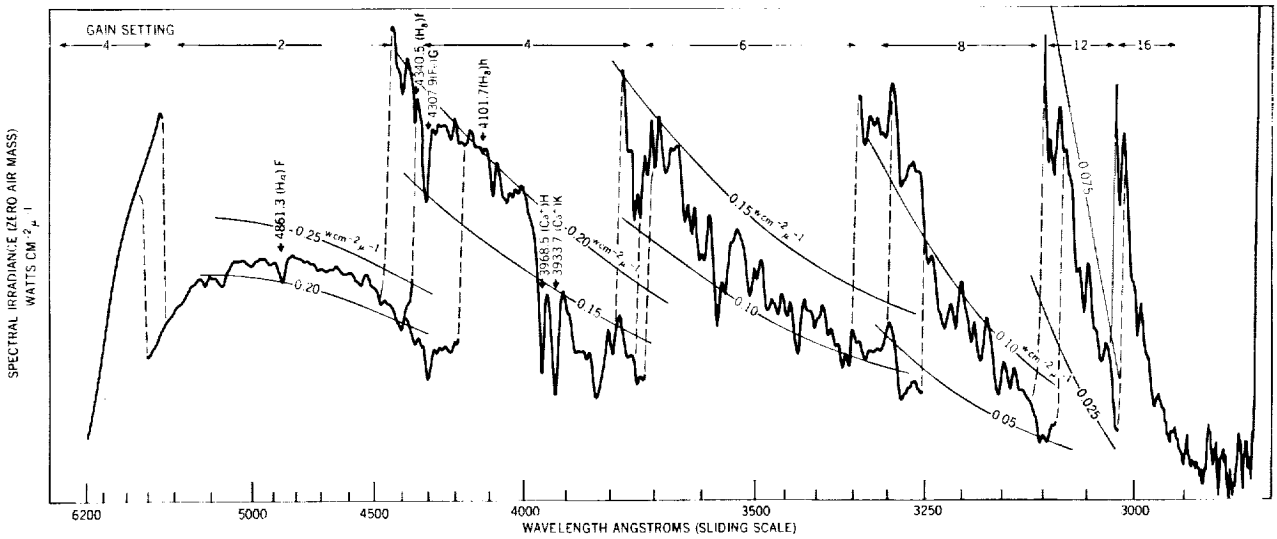

Figure 26—Perkin-Elmer strip chart in the photomultiplier range.

subject to a small error due to light from the roof of the aircraft. This error was corrected later, by comparison with scans made at GSFC. The transfer function of the instrument was highly constant in the photomultiplier range, but in the thermocouple range small fluctuations had apparently occurred due to a misalignment in the instrument.

3. Data Analysis and Results

The conventional method of determining irradiance from spectrum charts is to compare the chart of the unknown source with that of a standard of spectral irradiance. If the external optics are the same for both charts, the detector output at any given wavelength is proportional to the irradiance, and the following basic equation can be applied:

$$P_x = \frac{A_x G_x}{A_s G_s} P_s , \tag{9}$$

where the subscripts x and s refer to the unknown source and standard source respectively, P is the spectral irradiance, A is the amplitude (deflection of the pen or signal on the tape) and G is a multiplication factor to convert amplitude at a given setting to that at a standard gain setting of 20.

Equation (9) is valid only if the measurements of the sun and of the standard lamps are made under the same conditions, with the same external optics, and that is not the case on board the aircraft. The standard lamp shines directly on the diffuse mirror, but the sunlight undergoes attenuation by passing through the atmosphere above the aircraft, and then through the sapphire window of the aircraft, and finally being reflected by the specular mirror. Hence, a correction factor is necessary to determine what the signal A_x would be in the absence of such attenuation. Thus, A_x in Equation (9) has to be replaced by $A_x F$, where F is the correction factor.

F is the ratio of the amount of solar energy at a given wavelength incident above the atmosphere to the corresponding energy reflected from the specular mirror. It is the product of three factors—F_w for the sapphire window, F_m for the specular mirror, and F_a for the atmosphere. All three factors are highly dependent on wavelength, angle of incidence and other parameters. They are of importance also for other experiments besides the Perkin-Elmer and hence will be discussed in some detail.

The easiest to evaluate is F_w. It is equal to $1/\tau$, where τ is the transmittance of the window. Over the wavelength range where the material of the window does not absorb the light, losses are due only to the reflectance at the window's two surfaces. For the sapphire window, this holds true for the whole wavelength range of the Perkin-Elmer. For normally incident light the reflectance is given by the Fresnel formula[38]

$$r = \left(\frac{n-1}{n+1}\right)^2 , \tag{10}$$

where n is the refractive index. For light transmitted normally through a plate with parallel sides, taking into account reflection losses from the two surfaces and multiple reflection between the two

surfaces, the transmittance is given by[39]

$$\tau = \frac{2n}{n^2 + 1} .$$

Hence

$$F_w = \frac{n^2 + 1}{2n} . \tag{11}$$

In the case of oblique incidence the expression is more complex. The accuracy of the theoretical values was checked by experiments made in the laboratory, in the aircraft, and on the ground in direct sunlight. The correction factors for oblique incidence were found to be small for the range of angles for the Perkin-Elmer scans. In the aircraft, measurements were made during one of the flights using the filter radiometer with and without the sapphire plate in front of it. The laboratory measurements on transmittance were made with a Beckman DK2A spectrophotometer and the Perkin-Elmer monochromator. The experimental and theoretical values were found to be in close agreement. The theoretical values were used for the computer analysis as being more accurate.

The factor F_m is the reciprocal of the reflectance R of the aluminized mirror.

$$R = \frac{1}{2} \left(R_p + R_s \right) ,$$

where R_p and R_s are the reflectance for light polarized in the parallel and perpendicular planes, respectively. The expressions for R_p and R_s are available in standard literature.[39] Let n_a and k_a be the real and imaginary parts of $(n_a + i k_a)$, the complex index of refraction of aluminum; ϕ is the angle of incidence on the mirror; α and β are two other parameters defined in terms of n_a, k_a and ϕ by the equations

$$\alpha^2 - \beta^2 = n_a^2 - k_a^2 - \sin^2 \phi , \qquad \text{and} \qquad \alpha\beta = -nk .$$

Then

$$R_p = R_s \left\{ \frac{(\alpha - \sin\phi \tan\phi)^2 + \beta^2}{(\alpha + \sin\phi \tan\phi)^2 + \beta^2} \right\} ,$$

and

$$R_s = \frac{(\alpha - \cos\phi)^2 + \beta^2}{(\alpha + \cos\phi)^2 + \beta^2} . \tag{12}$$

Values of n_a and k_a were taken from the data published by G. Haas[40] in the American Institute of Physics (A.I.P.) Handbook. The computed values of reflectance were compared with those obtained experimentally, using a DK2A with a Gier Dunkle attachment. Measurements were made with both freshly evaporated, and relatively old but clean, samples of aluminized surfaces. The wavelength range 0.3 to 2.5 μ was covered, with different angles of incidence covering the range of the mirror positions on the aircraft. Within the limits of error of these measurements the experimental values and the theoretical values were in close agreement. Hence we decided to supply the computer with a table of values of n_a and k_a and have the factor F_m evaluated for each scan as a function of wavelength.

The factor F_a is the reciprocal of the factor A_λ^ℓ introduced in Equation (4). The method of determining the air mass ℓ from the position of the aircraft and the time of day has been discussed in Part I of this report. The atmospheric attenuation A_λ was determined from computed values, but with corrections based on our own measurements, as shown later.

Thus, determining the factor F requires six parameters: A_λ, n, n_a and k_a, which are dependent on wavelength but are the same for all scans, and ℓ and ϕ, which change from one scan to another but are independent of wavelength.

Computed values of the attenuation due to the atmosphere are available in literature[28] as stated in Part I of this report (Table 3). These values are valid for the U. S. standard atmosphere. Thirteen of the Leeds and Northrup charts of the flight of August 10 in the photomultiplier range were analyzed, using the manual data reduction method to check the validity of the theoretically computed atmospheric attenuation coefficients. The deflections of the pen were read for 77 selected wavelengths. The values were then plotted manually in terms of $\log_{10}$ of deflection versus air mass, and the points were joined by the best fitting straight line for each wavelength. The atmospheric attenuation and the signal for zero air mass were determined from the slope and zero intercept, respectively, of these graphs. These Langley plots for 8 of the wavelengths are shown in Figure 27. Figure 28 gives the values of atmospheric attenuation at the selected wavelengths.

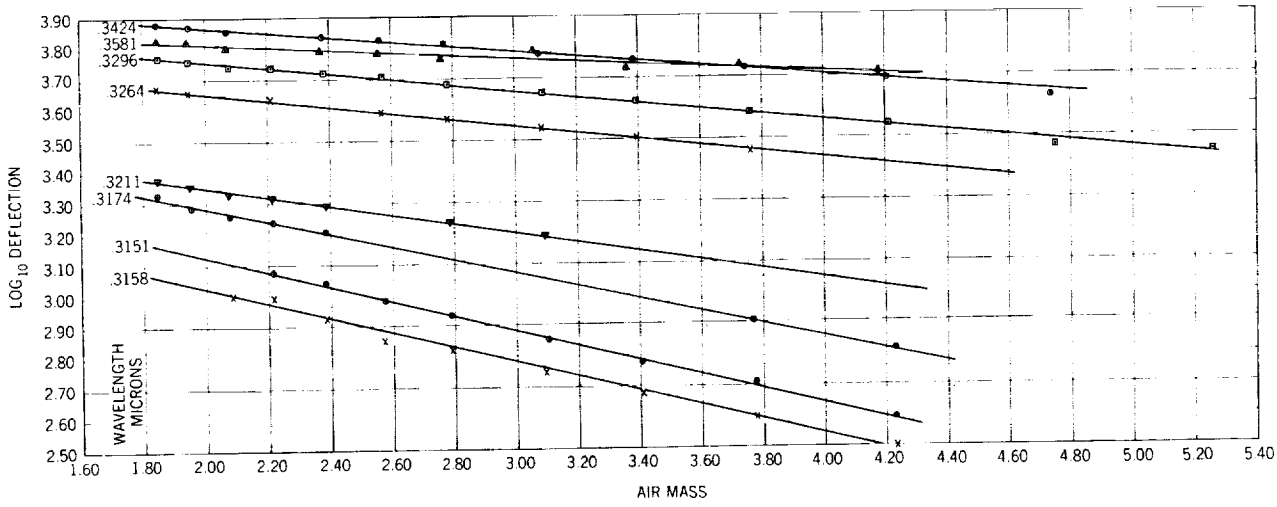

Figure 27—Log_{10} deflection of Perkin-Elmer monochromator vs. air mass.

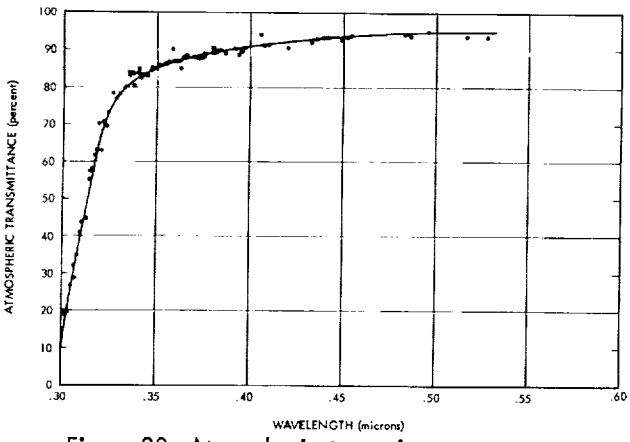

Figure 28—Atmospheric transmittance versus wavelength from Perkin-Elmer monochromator.

The Y-axis in Figure 28 is the percentage ratio of the spectral energy transmitted normally to the altitude of the aircraft to that incident above the atmosphere. The results of these computations of atmospheric attenuation were used to correct the theoretical values of Table 3, and to prepare a revised table which was used in the computerized data analysis of all the solar scans made by the Perkin-Elmer and Leiss monochromators.

The manual data reduction method was used also to obtain the solar spectral irradiance at the 77 selected wavelengths, based on the Perkin-Elmer monochromator scans of August 10. The detector signals for zero air mass, obtained from the Langley plots, were corrected for reflection of the specular mirror and transmittance of the aircraft window. The spectral irradiance was computed at these wavelengths using Equation (9) with the necessary correction for solar distance. The curved lines showing irradiance in absolute units in Figure 25 are based on these computations.

The manual data reduction method is obviously too time consuming, and further does not take into account the finer details of the Fraunhofer structure of the solar spectrum. Hence a computer program was prepared for handling the data recorded on the magnetic tapes, and calculating from each spectral scan the solar spectral irradiance for zero air mass. The following operations are performed: the analog signals of drum voltage, gain setting and detector signals are read every 1/5 second of scanning time, values are converted from analog to digital, and five successive values are averaged. From initial and final values of drum voltage, the individual scans are recognized. The signals are converted to a uniform gain setting of 20. Drum voltage is converted to the drum reading and then to wavelength. The correction factors for the atmosphere, window, and mirror are computed at each wavelength, as also the irradiance and signal of the standard lamp by interpolation from tables supplied to the computer. Spectral irradiance at each wavelength is calculated from Equation (9). The integrated values of the irradiance over bands of designated width are computed. For most of the scans the bandwidth chosen was 100 Å for the photomultiplier range and 1000 Å for the thermocouple range. For a few selected scans and over limited wavelength ranges, the integrated area under the spectral curve was computed also for bandwidths of 10, 5, 2 and 1 Ångström, thus displaying the Fraunhofer structure more clearly. The program provides for a printout of the energy in each band, the integrated value of the energy up to the end of that band, and for normalization with reference to a standard solar irradiance curve. The standard chosen was the Johnson curve.

A total of 71 spectral scans of the sun were thus reduced. The data from some 30 percent of the scans could not be used in the final average for reasons such as frosting of the aircraft window, cirrus clouds above the aircraft, maladjustment of the mirror system, roll of the

aircraft, or changing of magnetic tapes during a scan. The data from the other scans were in fairly close agreement.

The final results are presented in Figures 29, 30 and 31. The computer-generated graphs and tables were the main source for these figures. Some of the fine structure was added by comparison with the Leeds and Northrup charts. Figure 29 covers the range .3 to .42 μ, where the Perkin-Elmer monochromator has maximum wavelength resolution, and Figure 30 covers the rest of the photomultiplier range. These figures present essentially the same data as the Leeds and Northrup chart shown in Figure 26, with the differences that the wavelength increases from left to right, and that the wavelength scale and irradiance scale are linear. The data from the thermocouple range are shown in Figure 31 by the circles with centered dots. The black dots refer to the results from the P-4 interferometer discussed in Part III, section E, and the crosses refer to F. S. Johnson's curve.[5] The results in the wavelength range longer than 2.3 μ are included in Table 5 and in the figures which represent a weighted average of all the spectral irradiance instruments.

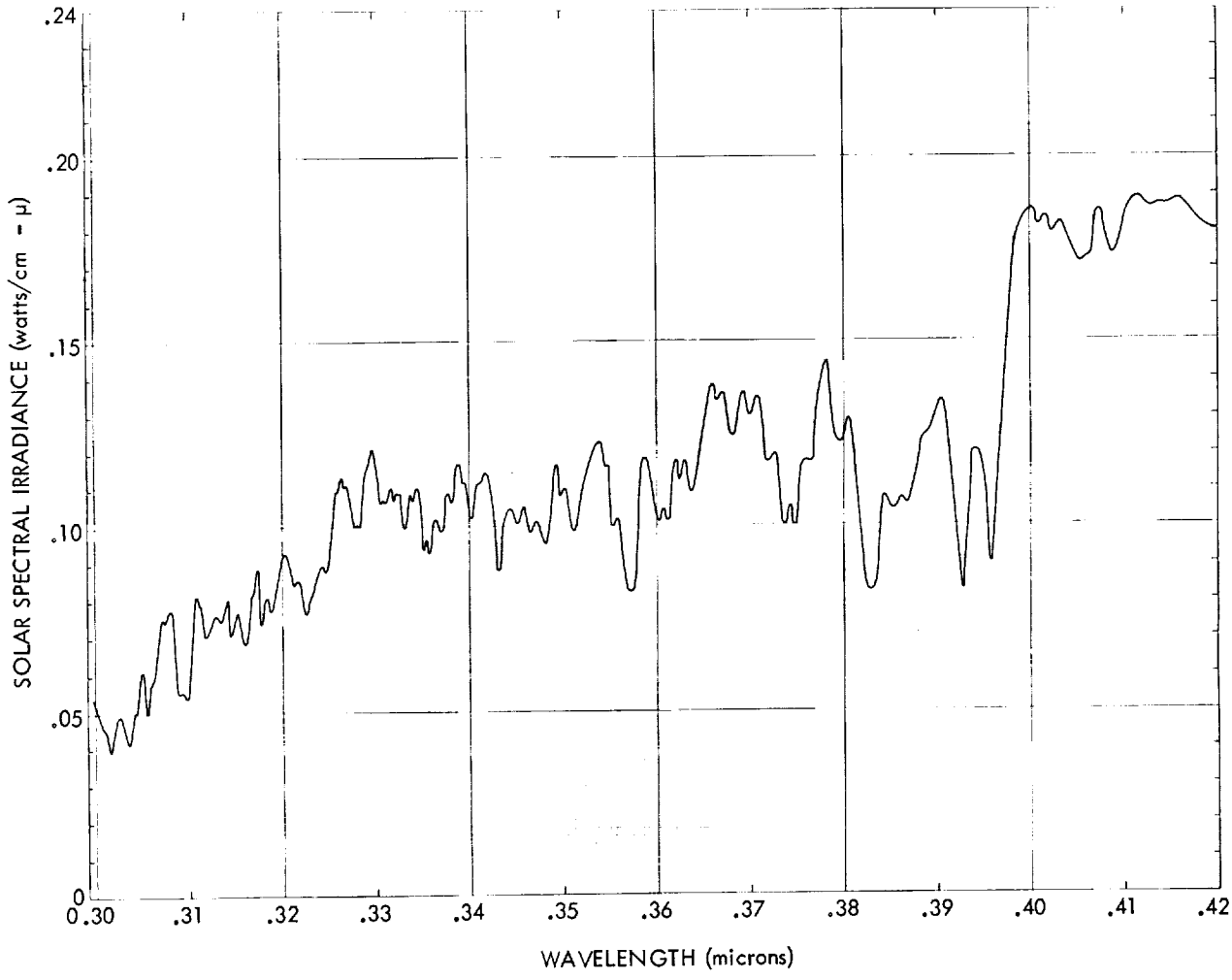

Figure 29—Perkin-Elmer data in the wavelength range .3 to .42 μ.

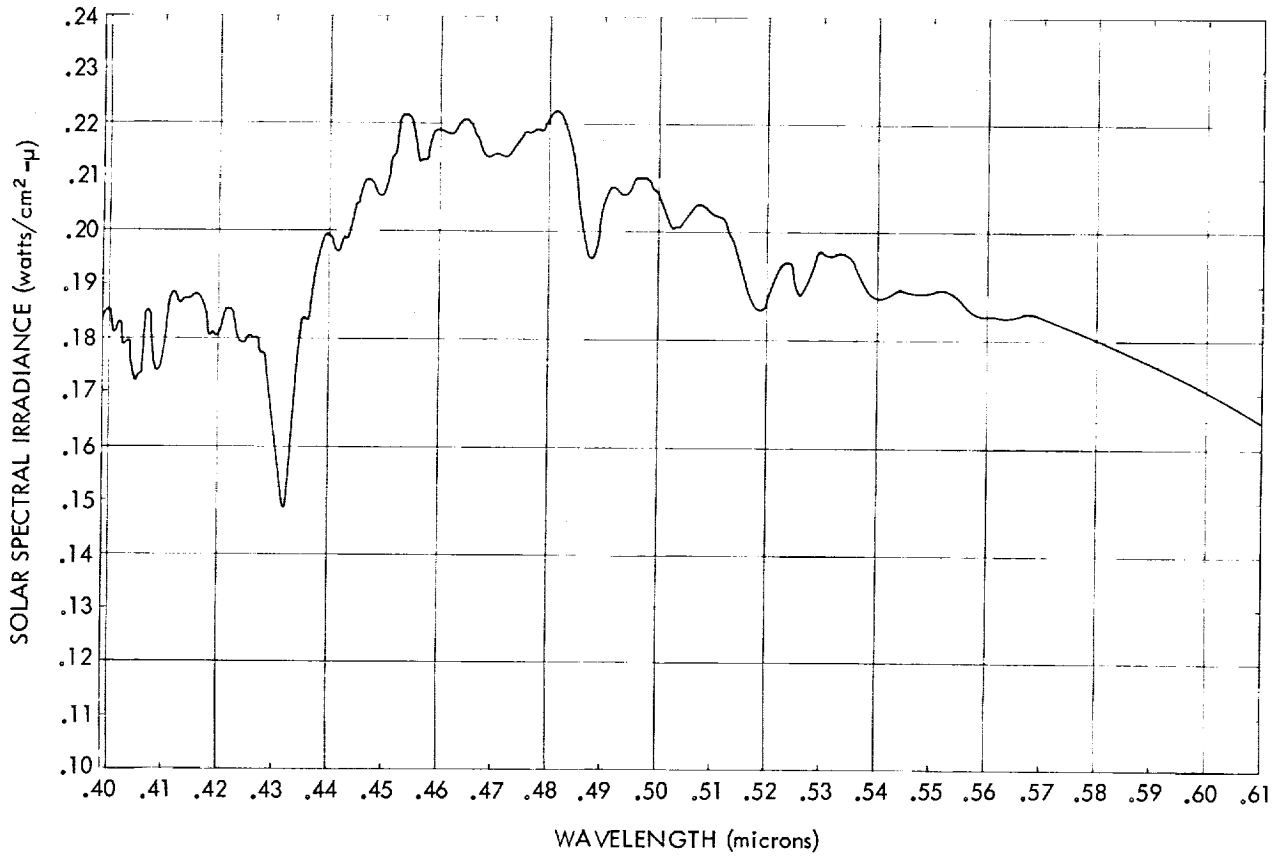

Figure 30—Perkin-Elmer data in the wavelength range .4 to .61 μ.

The wavelength resolution of the Perkin-Elmer system was determined by two independent methods, first by measuring the half-widths of very narrow emission lines of mercury with different slit-widths, and second by comparing the half-widths of the H and K lines of calcium as seen on our Leeds and Northrup charts and in the Utrecht Altas.[42] The two values were in close agreement. The half-width of the lines increases from relatively small values of 2.7 Å at 3000 Å, and 4.4 Å at 3500 Å to 11 Å at 5000 Å. The wavelength resolution, $\lambda/\Delta\lambda$, where $\Delta\lambda$ is the observed half-width or instrumental profile, decreases from 1100 at 3000 Å to 455 at 5000 Å. In the thermocouple range where the slit-width is 20 times greater, the resolution is considerably less; it increases from 11 at 7000 Å to 90 at 4 μ.

The major sources of error are scattered light from the roof of the aircraft shining on the diffuse mirror and the small degree of instability in the positioning of the mirror directly in front of the thermocouple detector. Detailed analysis of the solar and calibration scans made at different times, and both in the laboratory and in the aircraft, was made to determine the magnitude of this error. The accuracy of the spectroradiometric measurements is estimated at about ±5%.

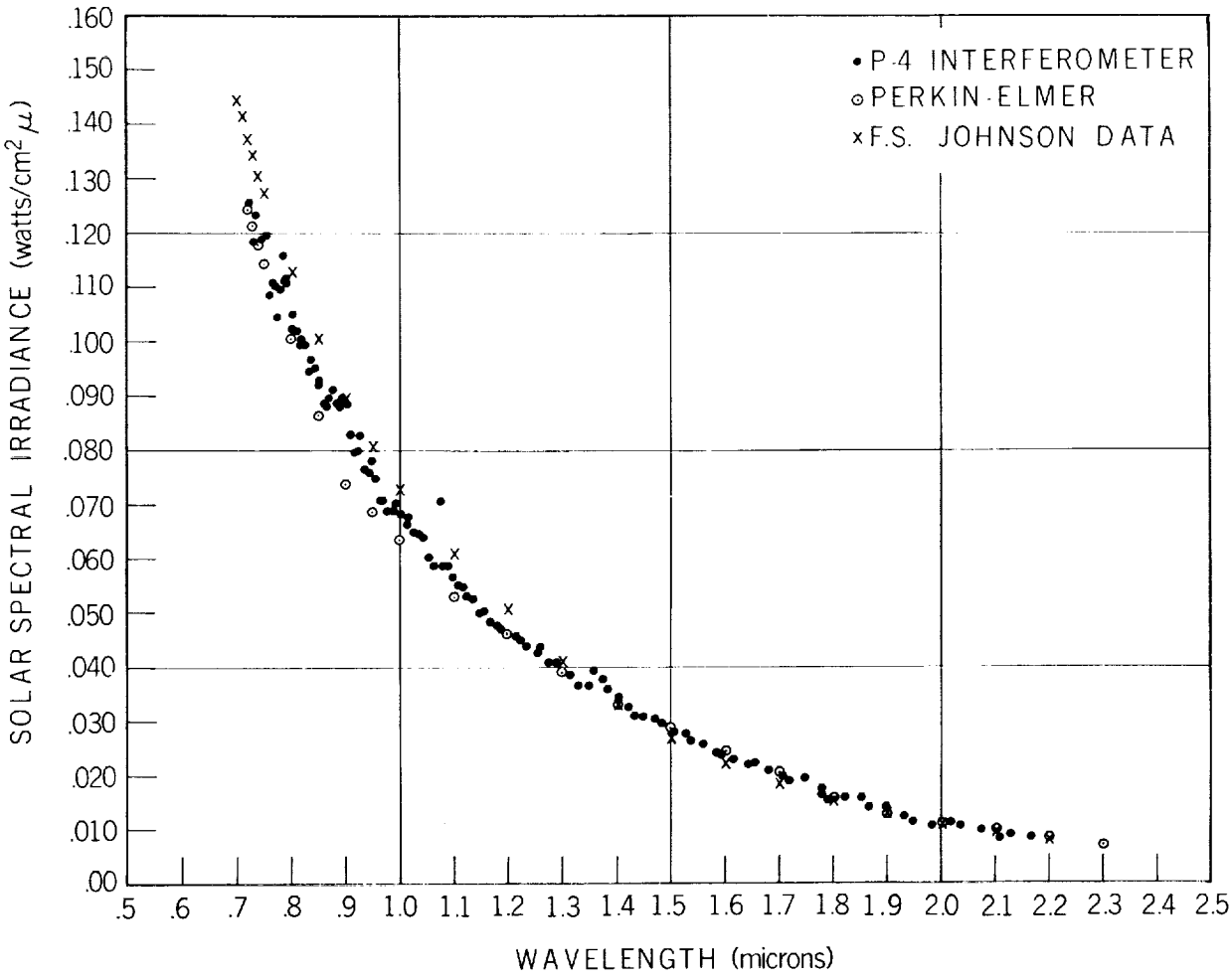

Figure 31—Solar spectral irradiance in the infrared wavelength range 0.7 to 2.5 μ, Perkin-Elmer and P-4 data.

B. Leiss Monochromator —R. McIntosh and S. Park

1. Description of the Equipment

The three following sections discuss the spectral irradiance instruments operated by the Thermophysics Branch, Spacecraft Technology Division, GSFC. They are a Carl Leiss double prism monochromator, an Eppley Filter Radiometer and an ITT Electronic Scanning Spectrometer. Each instrument was designed for observing the solar beam through the upper aircraft windows at solar altitudes ranging from about 20° to 70°. No auxiliary mirrors were employed as each instrument was mounted on a pseudo-polar axis such that an integrating sphere intercepted a direct beam of solar radiation which, after diffusion, completely filled the optical aperture of each spectral instrument.

Each instrumentation system is described, along with the results and some comparisons to previous ground-based measurements.

The Carl Leiss double prism monochromator was used for forty solar scans, each of wavelength from 0.3 to 1.6 μ. The relative spectral distributions agreed closely with published values and with the filter radiometer discussed in section C. However, calibration difficulties necessitated a normalization to the energy value obtained from the total irradiance measurements, 135 mW cm^{-2}.

The Leiss monochromator is a double prism instrument designed to provide high dispersion and minimal stray light. The instrument used in this experiment (see Figure 32) was equipped with two ultrasil quartz prisms. The three slits (entrance, intermediate, and exit) were set wide enough to provide sufficient energy while maintaining good resolution.

Figure 32—Mounting of the Leiss monochromator.

Because the Leiss monochromator was designed as a laboratory instrument, some modification was necessary to make it suitable for airborne operation. The mirror and prism mounts were stiffened and the entire instrument was enclosed in a rugged, light-tight aluminum box having sufficient strength to provide for mounting in a cradle which could be swung by a gearing mechanism on its longitudinal axis to allow solar tracking. The housing also provided a heat sink and air current insulation. Provision was made for thermostatic temperature control by heating coils mounted inside the housing.

Two detectors were used—an EMI 9558 QA photomultiplier tube for the UV and visible regions, and a Kodak Ektron lead sulfide cell for the IR. These detectors were mounted in an auxiliary light-tight box secured to the primary instrument housing. The detectors were mounted so that they could be quickly interchanged by rotating a lever. For maximum stability the PbS cell was thermoelectrically cooled to a constant temperature of approximately 0°C. The EMI tube was chosen for its low noise and dark current, extended red response, and high sensitivity.

A three-inch diameter integrating sphere was coated with a GSFC-developed magnesium oxide (MgO) paint, and then lightly smoked (1-2 mm) with magnesium oxide. The paint was used instead of a thick smoked coating because it was felt that the shock and vibration within the aircraft might damage a smoked coating because of its very fragile nature. The sphere was positioned so as to provide a diffuse source of illumination for the entrance slit of the monochromator. It was mounted on an axis perpendicular to the plane of the entrance slit and could be rotated by means of a hand driven worm gear to observe either the sun or the standard of spectral irradiance. This adjustment was at right angles to that of the main elevating mechanism and provided the second degree

of freedom for tracking the sun. The use of the sphere also minimized the effects of roll and yaw of the aircraft.

The sphere was posi oned immediately behind the aircraft window in direct sunlight, thus eliminating the need for mirrors. The determination of the reflectance characteristics of such mirrors as a function of angle of incidence is often difficult and tedious, and the additional frame design requirements necessary to directly view the sun were felt justified.

The monochromator was aligned on the sun by using a six-inch long tube with a pin hole and graduated target. This tube was attached directly to the sphere. The operator manually adjusted the elevation and azimuth angles of the monochromator. Figure 32 shows in detail the sphere and cranking mechanism, as well as the mounting frame used to support the equipment. The working standard lamp and housing can also be seen.

The wavelength drum which rotates the prisms was operated by a small a.c. synchronous motor and gear drive at one rpm. This made it possible to make one complete measurement (0.3 to 1.6 μ) in five minutes (including the changing of detectors). A cam and relay attached to the drum produced wavelength markers on the strip chart recordings.

2. Electronics

The electronic instrumentation for the Leiss monochromator consisted of the following components: a Brower model 129 synchronous amplifier tuned to 33 Hz, a specially built chopper and electronics module mounted inside the Leiss following the intermediate slit, a Power Designs model 5165 high voltage power supply, a Leeds and Northrup Type G Speedomax recorder, an E. G. and G. Thermoelectric module power supply, and various control and monitoring circuits. The high voltage power supply used to drive the photomultiplier tube has a voltage stability of 0.001%, resulting in a tube constancy of better than 1%.

The electronics for the Leiss monochromator as well as for the filter radiometer and the ESS were wired into an Elgar model 3001 transient regulator, because the aircraft's power converters were somewhat noisy and not regulated well enough for some of the instruments. The standard lamp power supply was wired into a Sorenson line voltage regulator which provided extremely stable lamp operation.

Figure 33 shows a block diagram of the entire instrumentation arrangement.

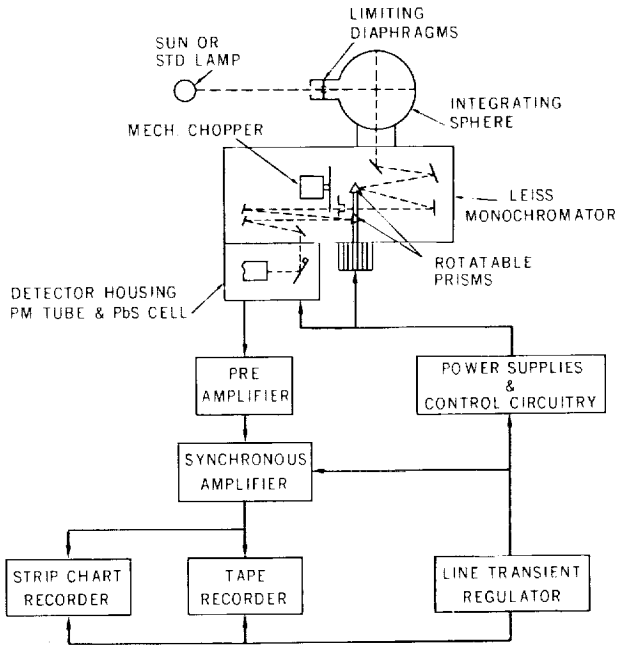

Figure 33—Block diagram of the instrumental setup of the Leiss monochromator.

3. Calibration

The Leiss monochromator was calibrated through the use of a 1000 watt, NBS type standard of spectral irradiance.[43] A certified standard (Eppley no. 1145) was employed for the basic calibration. Another lamp of the same type was used as a working standard and mounted in an aluminum box on the Leiss frame. The lamp current was monitored with a calibrated shunt and digital voltmeter and could be easily maintained to within 0.01 amp. Since the working standard was mounted inside an aluminum box, its irradiance was somewhat higher than that of the primary standard because of the reflectance of aluminum and the slightly higher operating temperature of the lamp. This was very helpful in the ultraviolet, where the irradiance of these lamps falls off rapidly. Monochromator calibrations were performed in flight as well as on the ground.

4. Data Analysis

Data were taken for each flight—a total of 40 measurements. However, only data from flights two through five have been analyzed. After the first flight the slit settings were changed significantly to improve resolution. Therefore, these data are not included here. The data from the final flight were not used because of an error in flight calibration. Several other runs were discarded because of cloud cover and instrument difficulties. Only the results from the remaining 19 measurements are presented here.

During the flights the calibration signal appeared to drift, especially in the ultraviolet region. All efforts to correct this difficulty in the field were futile. After the expedition, many measurements were made to determine the exact cause of this drift, but it has not yet been discovered. Since the repeatability of the working standard was verified, the drift was almost certainly caused by some heating effect in the Leiss optical system. It is interesting that the drift was quite reproducible (within 1%) as a function of time. Fortunately, no such drift could be observed in the solar data, or in any of the data from the filter radiometer or ESS which used similar instrumentation.

Because of these difficulties it was impossible to obtain absolute measurements of the solar spectral irradiance from these data. Therefore all of the data obtained by the Leiss monochromator were normalized to the value of the total irradiance of the sun as measured by the total irradiance instruments, 135.1 mW cm^{-2}. Since this value represents the total energy of the sun, and the Leiss monochromator covered only the wavelength range 0.3 to 1.6 μ, it was necessary to normalize the data to the energy in that range only. The spectral distribution function of Gast,[24] which is essentially the same as that of Johnson, was used to determine the energy in the range 0.3 to 1.6 μ. It was found to be 118.4 mW cm^{-2}. The spectral irradiance of the sun for zero air mass was computed at each flexion point of the Leeds and Northrup chart; the area under the curve of spectral irradiance versus wavelength was integrated over the wavelength range .3 to 1.6 microns, and the normalization was performed using the value 118.4 mW cm^{-2}. The technique used for reducing the data was the same as in the case of the Perkin-Elmer monochromator. The same method was used to evaluate the correction factors F_w for the spacecraft window and F_a for the atmosphere. The factor F_m for the mirror was not needed here. The normalization factor 118.4 mW cm^{-2} was found later to be very close to the value of the energy in the range 0.3 to 1.6 μ according to the

two spectral distribution curves given in Part IV of this report. The weighted average of all the spectral irradiance instruments of NASA 711, normalized to that of the total irradiance instruments, is given in Table 6. Table 8 gives the proposed standard curve, which is the NASA 711 curve modified slightly to take into account the high altitude data of Drummond.[15] According to these two tables the energy in the range 0.3 to 1.6 μ is 118.03 mW cm^{-2} and 118.15 mW cm^{-2}, respectively. The differences between these values and 118.4 mW cm^{-2} are 0.31% and 0.21%, respectively.

5. Results

The Leiss results are depicted in Figures 34, 35 and 36. Figure 34 compares the Leiss monochromator, filter radiometer, and Perkin-Elmer monochromator data. As can be seen, the agreement is good between the Leiss monochromator and the filter radiometer. Figure 35 compares the Leiss data to the most recent ground-based measurements of Stair[44] at Mauna Loa, Hawaii. The agreement here is again good in the ultraviolet region. Figure 36 compares the Leiss data to that of Johnson.[5] Johnson's visible spectrum is higher partly because of his higher total irradiance value of 139.5 mW cm^{-2}. The 4.5 mW difference occurs primarily in the visible region.

Two interesting features—the humps in the curve at about .9 and 1.3 microns—appear on the Leiss data. No previously reported data show these. However, very little data is available for this region of the solar spectrum. Attempts have been made to account for these anomalies on the basis of a possible system error, but after careful examination this does not seem to be the case.

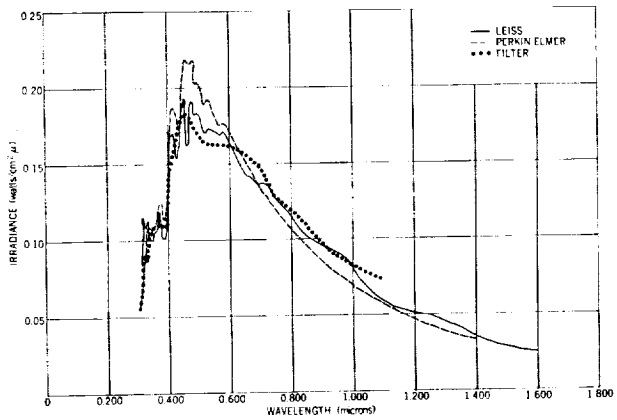

Figure 34—Comparison of data from the Leiss, Perkin-Elmer and filter radiometer.

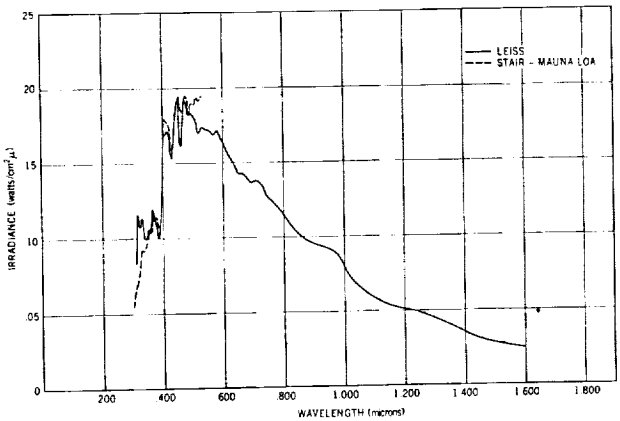

Figure 35—Comparison of Leiss monochromator and Stair (Mauna Loa) data.

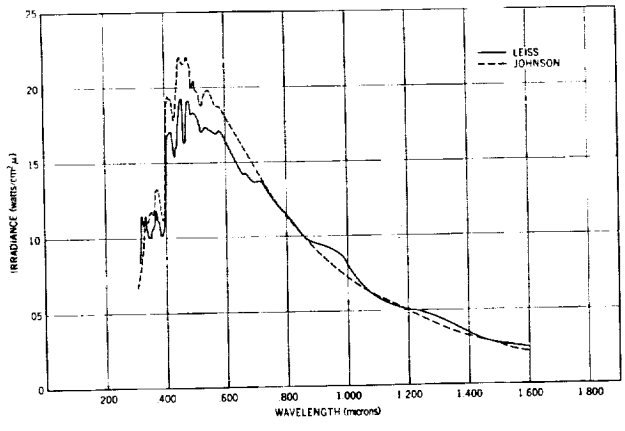

Figure 36—Comparison of Leiss monochromator and Johnson data.

The following is an estimate of the errors involved in the measurements:

Error in total irradiance (from Ångström pyrheliometer):	±3%
Error in irradiance outside the wavelength interval .3-1.6 μ:	±4%
Error due to window transmittance:	±1%
Instrumentation error:	±2%

The total RMS error is 5.5%.

C. Filter Radiometer–R. Stair, J. J. Webb and D. L. Lester

Introduction

A GSFC modified Eppley Mark V filter radiometer was used to make solar spectral measurements from 0.3 to 1.1 μ. Good agreement has been noted with the Leiss monochromator and with recent ground-based measurements.

1. Description of Equipment

The basic mechanism of an Eppley Mark V radiometer was employed in the photoelectric filter wheel radiometer. No commercial instrument of the required type was available. The thermoelectric detector, shutter and shutter drive, and other features not associated with the filter rotation mechanism were removed, or made non-active. The filter wheel rotation mechanism provided for the step rotation of two filter wheels, each containing 13 filter positions. Allowing for a zero position and for the interposition of two wide band filters or radiation (or isolation) screens, a total of 22 narrow band filters could be installed on the two wheels at one time. Such filters were set up on two wheels for use with an RCA type 935 phototube (S-5 response) to cover the ultraviolet (11 filters) and visible (11 filters) wavelengths within the range of 3100 to 6000 Å. On a third wheel, another set of 11 filters was arranged to cover the spectral range from 6000 to 11,000 Å. All three sets were used with an RCA type 917 phototube (S-1 response). Thus, to shift the instrument coverage from the ultraviolet and visible range to the visible and near infrared required the changing of one filter wheel and the interchange of detectors. Since this procedure required a significant amount of time, it was decided to use only one combination during any particular flight. This was done except for the flight of August 16, the constant air mass flight, when both ranges were covered by making the change at mid-flight.

The narrow band interference filters supplied by Eppley were chosen to cover the spectral range mentioned above. In the ultraviolet, each filter has a half-band width of approximately 100 Å and is centered at an even wavelength, e.g., 3100, 3200, 3300, etc. to 3900 Å. Those at longer wavelengths have wider half-band widths and, in general, are also centered on even wavelengths spaced at 500 or 1000 Å in the visible and infrared. Thus, each filter (except for several wide band filters) covers a portion of the solar spectrum extending in either direction from its central transmission peak such that, ideally, where the transmittance of one filter drops to one-half its greatest value, the next has increased to one-half its greatest value. The transmittance of each filter was measured on a Beckman DK-2A spectrophotometer.

2. Instrument Modifications

The Eppley radiometer mechanism was originally designed for manual operation in changing filters. This consisted of momentarily pressing a pushbutton switch for a single filter position change, or by holding the switch in the closed position until the desired filter was in place. Automatic operation could be had through fixing this switch in the closed position. This, however, left each filter in position for too short an interval (about one second or less) for precise recording. To alleviate this situation, a timing motor was set up to momentarily close a microswitch, wired across the button switch, once each 8-1/3 seconds, thus providing for automatic filter changes at that time interval.

The instrument was mounted in the aircraft in a frame similar to that used for the Leiss monochromator, i.e., a pseudo-polar axis mount. The mounting arrangement is shown in Figure 21. As with the Leiss monochromator, a manual elevating mechanism provided instrument adjustment for solar altitude and a worm gear mechanism rotated the integrating sphere. The sphere was the same size and used the same coating as the Leiss monochromator. A block diagram of the instrumental arrangement is shown in Figure 37.

3. Electronics

The primary electronics used with the filter radiometer consisted of a Keithley model 610R Electrometer and a Moseley model 7100B strip chart recorder. The current from the phototube was amplified by the electrometer and directly recorded by the Moseley. No modification of either instrument was required as each has several sensitivity settings.

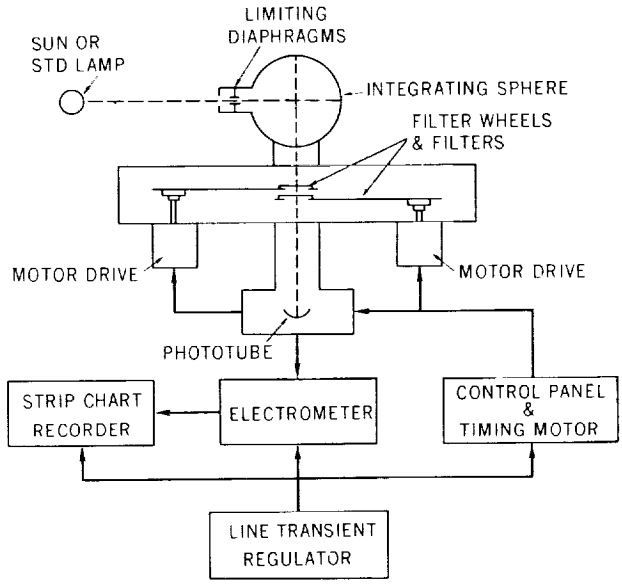

Figure 37—Block diagram of the instrumental set-up of the filter radiometer.

4. Calibration

Calibration was accomplished in the same way as with the Leiss monochromator. A 1000-watt NBS type quartz iodine standard of spectral irradiance was mounted in an aluminum box and attached to the instrument frame. The housing can be seen in Figure 21. The only difference in procedure was that, with the filter radiometer, wavelength calibration was not a problem since the filters themselves provided the wavelength range.

5. Results

The analysis involved in reducing the filter radiometer data is detailed and somewhat complex and will not be described here. The procedures and techniques used are given in a recent GSFC contract report.[45] The results presented here are also taken from this report.

The zero air mass solar spectral curve is shown in Figure 34, along with the results of the Leiss and Perkin-Elmer monochromator measurements. The comparison with the Leiss monochromator is very good in all but the regions around 3000 and 6500 Å. It is believed that these discrepancies are due to calibration uncertainties. The fact that the results of the two instruments agree closely despite their differences in optical characteristics seems to strengthen their validity. Also, the energy scale for the filter radiometer was obtained from the in-flight calibrations, not from normalization. Thus it seems that the normalization procedure was justified for the Leiss.

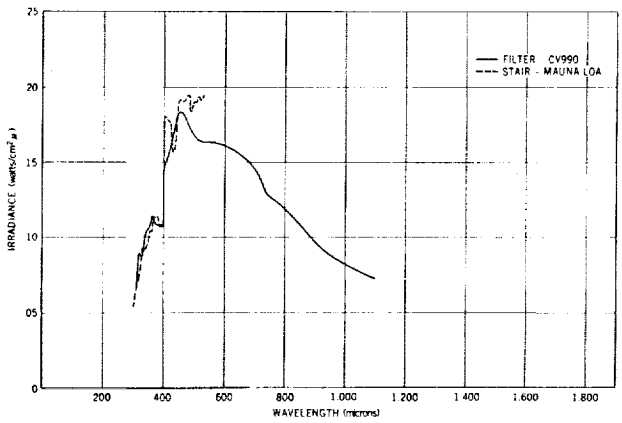

Figure 38—Comparison of filter radiometer and Stair (Mauna Loa) data.

Figure 38 shows a comparison of the filter radiometer and the most recent ground-based measurements available, those of Stair at Mauna Loa. A good agreement is again noted.

An uncertainty of approximately 5% is estimated, due mainly to the inaccuracies of the standard lamp and window and filter transmittance values.

D. Electronic Scanning Spectrometer—J. J. Webb

Introduction

An Electronic Scanning Spectrometer recorded solar data from 3000 to 4800 Å during all six NASA 711 flights. A total of 95 spectral runs were obtained, but only 17, randomly selected, were used in the data analysis. Resolution was not as good as expected, and the spectral energies are lower than results of other experiments.

1. Description

The Electronic Scanning Spectrometer (ESS), manufactured by ITT Industrial Laboratories of Fort Wayne, Indiana, is designed to measure either static- or rapidly changing spectral distributions in the ultraviolet and visible regions from 2500 Å to 5000 Å. Completely electronic and weighing only 21 lbs., the spectrometer scans the spectrum by means of a television-type camera tube called an image dissector. A long narrow slit aperture in the tube serves as the exit slit of the optical unit, which consists of two turning flats, a focussing mirror, and a grating (see Figure 39). A photoemissive surface (S-21) on the faceplate converts the optical spectrum into an electron spectrum in the tube. The electron image is formed within the tube in the plane of the tube's slit aperture. The spectrum is sampled by sweeping the electron image across the slit aperture by means of magnetic fields generated by coils surrounding the tube. The signal is then amplified in the tube exactly as in conventional photomultipliers.

2. Instrument Modifications

To adapt the instrument for solar measurements aboard the aircraft, certain modifications were necessary.

The rapid scanning feature was changed to a much slower speed because of a lack of a suitable recording device. The scanning was done by driving the field coils with a potentiometer and synchronous motor, which took about two minutes for one complete scan of the wavelength region.

An integrating sphere like those used with the Leiss monochromator and filter radiometer was mounted in front of the entrance slit.

A mechanical chopper was also installed in front of the entrance slit to allow the use of a tuned amplifier.

As was the case with the Leiss monochromator and filter radiometer, the ESS was mounted on a pseudo-polar axis and two degrees of freedom were provided for manual solar tracking.

Figure 40 shows the actual flight configuration.

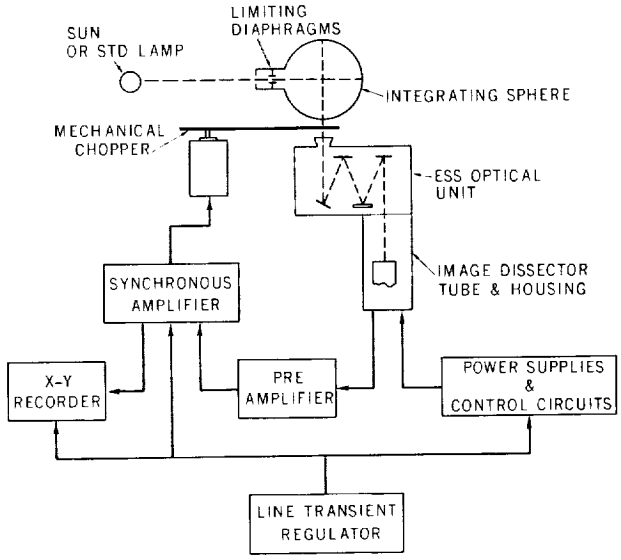

Figure 39—Block diagram of the instrumental set-up of the Electronic Scanning Spectrometer (ESS).

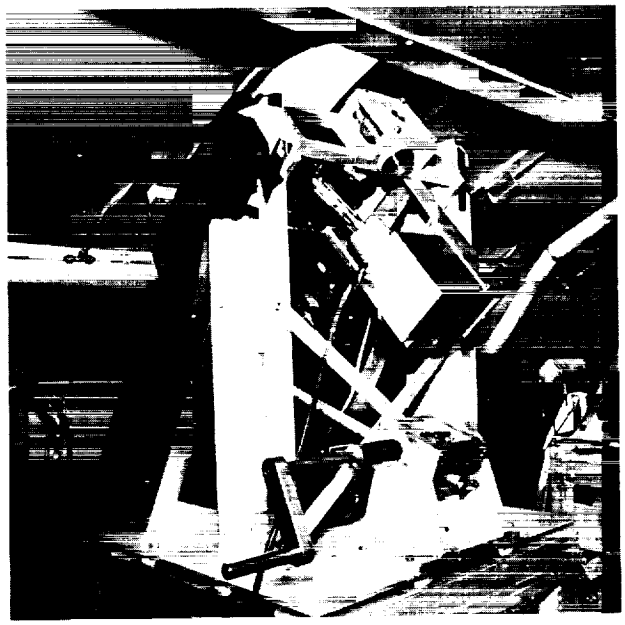

Figure 40—Mounting of the ESS spectrometer.

3. Calibration

Wavelength calibration and indexing was performed by using a low pressure Spectroline Cadmium lamp of known spectrum, and adjusting the time of the scan to align the spectral lines with the appropriate linear markings on the chart paper. For solar measurements the Fraunhofer lines provided excellent wavelength identification. Intensity calibrations were accomplished and in the same way as those for the Leiss monochromator and filter radiometer, i.e., with a 100-watt quartz iodine lamp.

The calibrations were made in flight prior to the solar data recording, and also on the ground between flights. These data agreed fairly well, and an average calibration curve was determined and used in the solar data analysis.

4. Results

The data were not as good as expected, primarily because of poor resolution and unreliable wavelength calibrations.

The integrating sphere was added just prior to the flights and no time was available for a thorough ground test. Apparently the sphere reduced the resolution from a previous 10 Å[46] to 35 Å by filling the optics in a different manner. Had the ESS been equipped with a variable entrance slit, the resolution could easily have been improved. However, the instrument was made with a fixed entrance slit either 50 or 100 microns wide, both of which were too large; therefore nothing could be done except observe the poor resolution.

As stated earlier, a total of 95 spectral scans were recorded during the six flights, but only 17 were used in the Langley method[12] of data analysis. Clouds during portions of the flights eliminated some runs, and lack of time and manpower made it impossible to utilize all the remaining runs. A random selection of the 17 runs was made, covering the air mass range as well as possible. Voltage readings were chosen from each run at the maximum, minimum, and inflection points. The logarithms of these voltages were then plotted versus the appropriate air masses for each of the chosen wavelengths. Some typical Langley plots are shown in Figure 41. The data appear to be good, i.e., they lie on straight lines except in the UV region where ozone absorption and low detector sensitivity increased the scatter. A least squares analysis was made for each wavelength, and the y intercept (at air mass 0) was determined. These values were then corrected for mean distance to the sun and window transmission, and reduced to absolute values with the calibration data.

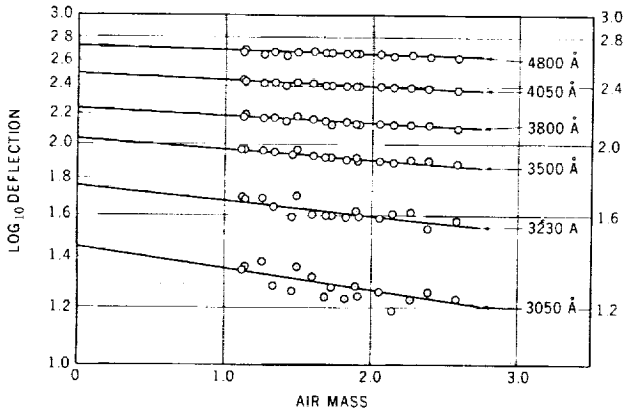

Figure 41—Typical Langley plots from ESS data.

A plot of the zero air mass data is shown in Figure 42. The ESS curve is considerably lower than the Johnson curve in the range 3000 to 4000 Å, and also somewhat lower than the curves obtained by the Leiss monochromator and the filter radiometer.

The data in all other respects appear to be reasonable, including the comparison shown in Figure 43 of the experimental attenuation coefficients (the slopes of the Langley plots) and the theoretical curve of the extinction optical coefficients for a turbid atmosphere[28] at 11.6 km. The theoretical curve represents Rayleigh and aerosol scattering, and ozone absorption. The fact that they do not exactly overlay indicates that the atmosphere above the observers was not homogeneous (an assumption made in the tables).

The in-flight wavelength calibration data did not show good repeatability from day to day, so an average value was used. However, the possibility of a wavelength shift in the data exists and

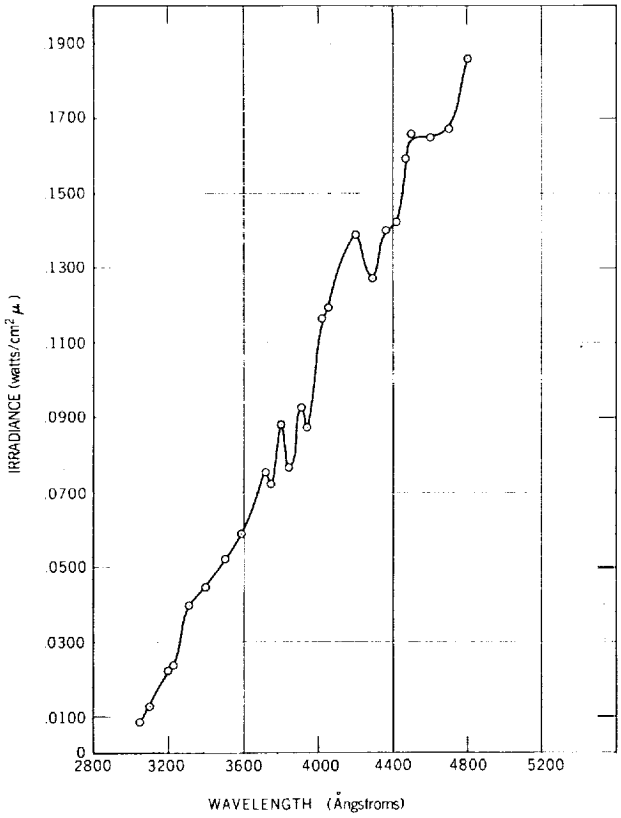

Figure 42—ESS zero air mass solar curve.

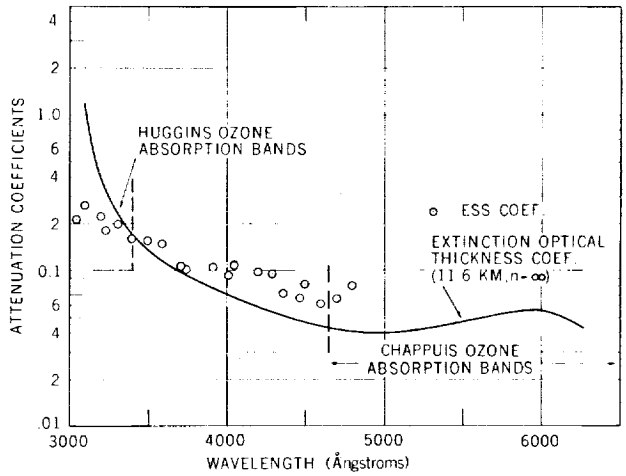

Figure 43—Comparison of experimental (ESS) and theoretical attenuation coefficients.

may be a cause of difficulty. In addition, a possible non-linearity in the ramp voltage drive mechanism may be a contributing factor.

Because of these problems, the ESS data were not given any weight in the determination of the final spectral curve presented in the conclusion of this report.

E. P-4 Interferometer —P. Ward and M. P. Thekaekara

1. Description of the Equipment

Two interferometer spectrometers manufactured by Block Engineering, Inc., Cambridge, Mass. were used to cover the spectral range from 0.3 to 15 μ. A Michaelson type, I-4, interferometer covered the region from 2.6 to 15 microns and a polarization, P-4, interferometer measured the spectral band from 0.3 to 2.5 microns. In this section we discuss the P-4 interferometer. The next section is devoted to the I-4 interferometer, where we also discuss in some detail the principles of Fourier analysis in spectroscopy.

Although interferometers have been valuable in the laboratory for many years, their application in spectroscopy and radiometry has been severely limited until recently because of the difficulty in performing the necessary mathematical calculations. With the advent of easy access to digital computers in the past ten years, the technique of Fourier spectroscopy has received a great deal of interest due to distinct advantages in radiation gathering power and improvement in signal to noise ratio.

Relative path retardation between two mutually interfering beams of light is the basic principle of interferometry. In the Michelson interferometer this is produced by a plane mirror moving in a direction normal to its surface. In the short wavelength region, where the P-4 interferometer operates, accurate alignment of a moving mirror system is difficult to achieve, so the relative path difference is introduced by a Soleil prism. An optical schematic of the instrument is shown in Figure 44. The incident beam is separated by a polarizer into two components of equal amplitudes in mutually perpendicular planes. The wave then passes the birefringent Soleil compensator that has a different index of refraction for each wave component; thus the two components traverse the compensator at different speeds, introducing an optical path difference between the two perpendicular components given by

$$B = d(n_o - n_e) , \tag{13}$$

where d is the thickness of the compensator and n_o, n_e are the indices of refraction in the "O" and "E" planes. The path difference is varied by moving the wedge-shaped section as shown in Figure 44, thus performing the function of the moving mirror in the Michelson interferometer. The radiation is recombined at the second polarizer and then separated at the beam splitter with approximately 90% of the energy transmitted to the lead sulfide detector and 10% sent to the photo-multiplier tube. The resulting interferograms are processed in a manner similar to the method described below in Section F.

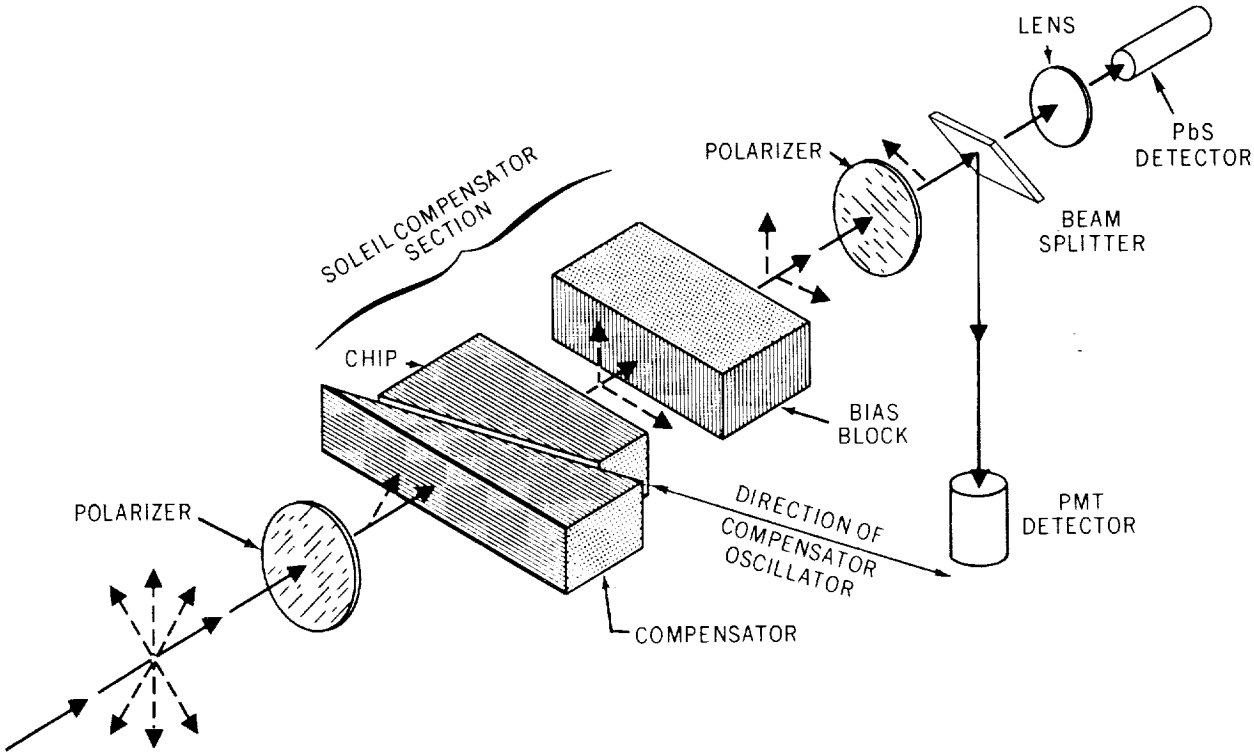

Figure 44—Optical schematic of the polarization interferometer.

2. Experimental Procedure

The mounting of the interferometers is shown in Figure 45. The P-4 interferometer is above and to the right; the I-4 interferometer is slightly below it and to the left. The P-4 interferometer views the sun through an integrating sphere and an aperture system. The aperture limits the field of view of the instrument to ±5°, thus minimizing the circumsolar sky radiation and making the angle of the incoming cone of light similar to that of the other total and spectral irradiance instruments on board the aircraft. The window material was infrasil quartz. The figure shows the instrument directed towards the upper window of the aircraft. The interferograms are recorded on analog tape.

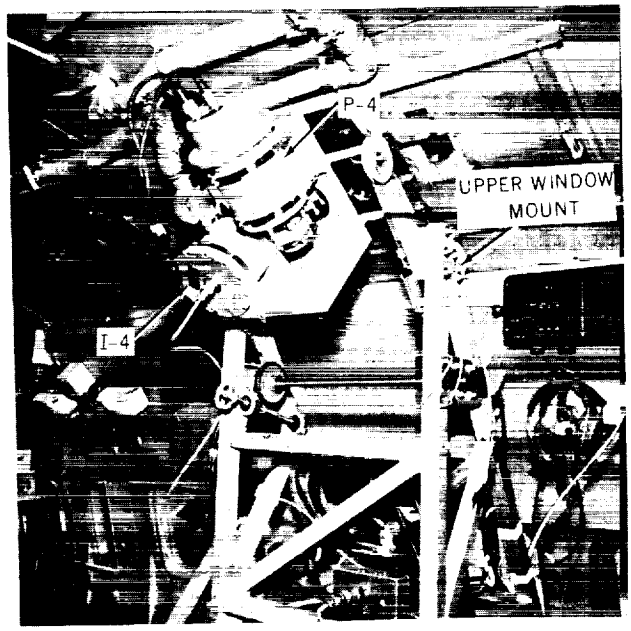

Figure 45—Mounting of the P-4 and I-4 interferometers.

Along with the interferogram, the signals from a Moiré fringe pattern are recorded on a separate channel. The purpose of these signals is to trigger the stripping of signals from the interferogram for conversion from analog to digital at equal increments of the path difference between the two rays. If the forward velocity of the chip in the Soleil compensator were constant, equal increments of path difference would occur at equal intervals of time. However, the drive mechanism of the chip is such that its velocity varies with position, being maximum at the middle of the stroke. Attached rigidly to the chip is a Moiré strip which moves relative to a fixed Moiré strip, with an indicator lamp on one side and a detector on the other side. The signals of the detector thus form a fringe pattern with successive maxima occurring at equal displacements of the chip. This enables the analog signals of the interferogram to be stripped at equal increments of path difference.

A complete to and fro motion of the chips takes 1.3 sec, of which 0.9 sec is for the forward motion and 0.4 sec for the reverse motion. Signals are stripped for 0.8 sec of the forward motion during each scan. A total of 1991 signals (samples) per scan is stripped for A-D conversion. The signals from a large number of successive scans are co-added to increase the signal to noise ratio. A sync pulse ensures that the first signal of each scan corresponds to the same position of the chip. The displacement of the chip during a scan is about two inches.

3. Data Analysis and Results

Selected portions of the P-4 interferograms have been reduced. In the photomultiplier range where the solar spectrum is several orders of magnitude stronger than that of the standard lamp, the absolute calibration of the instrument seemed to yield large uncertainties. Since this region

is adequately covered by the monochromators, we shall restrict ourselves here to the analysis of data in the PbS range.

For the analysis of data from the lead sulfide detector, 14 spectral scans of the sun and 7 spectral scans of the standard lamp were used. Each scan was the result of co-adding about 40 spectra obtained by Fourier transform of a large number of interferograms. The 14 solar spectra were distributed as follows among the flights: 2 from August 3, 4 from August 8, 7 from August 10, and 1 from August 16. Of the calibration runs, one was from interferograms made during the flight and the rest from those made later at GSFC. The air mass for the solar spectra varied from 1.13 to 5.10. The print-out data of the computerized Fourier transform give for each frequency value of the spectrum a value of the spectral amplitude S, and of the logarithm to the base 10 of S. It was found that the log S values were more convenient for mathematical computations. Values of log S in the frequency range 81 to 280, λ = 2.202 to .7236 μ, were tabulated from each of the solar and calibration spectra and for 120 of the computer generated frequency values. The log P values outside this range were considered less reliable due to the high noise to signal ratio. Frequency is converted to wavelength by means of the equation $f\lambda = (n_e - n_o)\, k$, where f is the frequency, λ is the wavelength, n_e and n_o are the extraordinary and ordinary indices of refraction of quartz, the material of the soleil prism, and k is a constant to be determined empirically. For our instrument k had been found to be 2.2607×10^8 Å sec^{-1}. In practice, for more accurate interpolation, the wave number was computed from a previously prepared table and the reciprocal was taken at each frequency.

The spectral irradiance P is related to the spectral amplitude S by the equation

$$\log P_S = \log P_L + \log S_S - \log S_L , \tag{14}$$

where the subscripts S and L denote the sun and the standard lamp, respectively. The values are available on a relative scale only, since calibration runs were made at different distances of the lamp from the P-4 interferometer, and the factors due to angular aperture, etc., could not be determined with sufficient accuracy. Comparison of log S_L values from different spectra showed that while the absolute values for any given λ varied over a wide range, (1.8 to 0 on the log scale or a factor of over 60) the differences between corresponding values of any two spectra were highly constant, independent of frequency, thus establishing the validity of Equation (14). The wavelength resolution varies from 15 Å at .72 μ to 170 Å at 2.2 μ. For each of the 120 selected wavelengths the average log S_L from the 7 calibration scans and the average log S_S from the 14 solar scans were computed. Since log S_S varies linearly with air mass, the average log S_S is the value corresponding to the average air mass, namely 2.719. To determine log S_S for zero air mass, the values of log S_S for each spectral scan and wavelength were plotted as a function of air mass. Although the points showed a wide scatter, due partly to the process of normalization, there was a clear indication of the slope of the line of log S_S versus air mass increasing to a maximum at each of the well known H_2O absorption bands. A significant result is that even in the so-called atmospheric windows, far from the absorption bands, the slope does not become zero; there is a continuum absorption which for unit air mass at 38,000 feet is about half a percent. Figure 46 shows

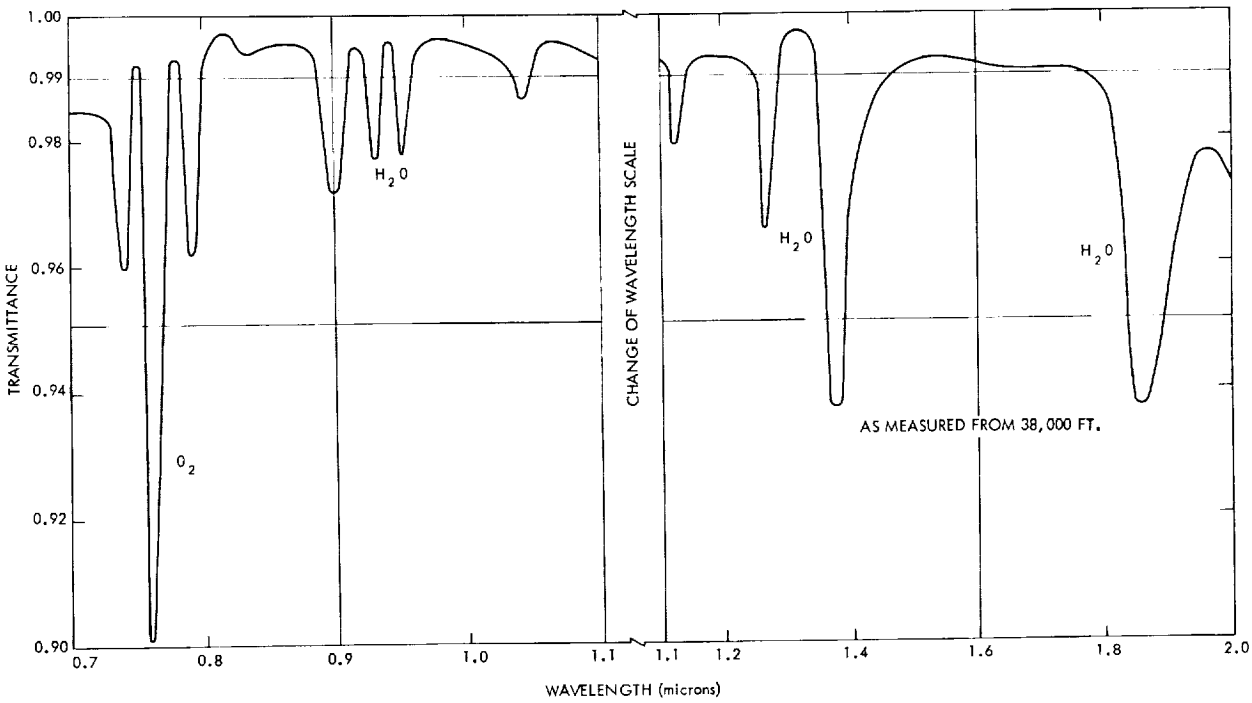

Figure 46—Transmittance of the atmosphere at 38,000 feet for normally incident solar rays, 0.7 to 2.0 μ, based on P-4 interferometer data.

the results of these studies. The slopes of the lines were plotted as a function of wavelength, and a smooth curve was drawn through the observed points. The Y-axis was scaled to show the transmittance of the atmosphere down to the aircraft altitude of 38,000 ft for normally incident solar radiation, that is, the ratio of solar spectral irradiance at 38,000 ft to that for zero air mass. This curve represents the average effect of the 14 P-4 interferometer scans which were analyzed.

4. Analysis of Water Vapor Absorbance

Figure 47 shows a comparison of the transmittance of the atmosphere at ground level to that at 38,000 feet. The dashed line is for 38,000 ft, and the continuous line is for ground level. Both lines are for solar rays incident normally on top of the atmosphere. The curve for 38,000 ft is based on the P-4 interferometer data and is the same as in Figure 46, with a tenfold decrease in the Y-axis. The curve for ground level is based on Parry Moon's data.[2] This is also the curve which would be obtained by taking the ratio of the ordinates of the two lowermost curves in Figure 9. A comparison of the two curves in Figure 47 shows that the absorption dips occur at the same wavelengths. One absorption band is due to O_2; the rest are due to H_2O. The difference in depth of the absorption dips in the two curves is considerably greater for H_2O than for O_2. The high wavelength resolution of the P-4 interferometer shows considerably more detail. At the two wavelengths near 1.4 and 1.9 μ where the transmittance of the atmosphere at ground level is zero, the transmittance at the aircraft altitude is about 94%. There is also a great difference in the width and transparency of the atmospheric windows as shown in Figures 46 and 47. The absorbance of about 1/2 percent in these windows as shown in Figure 46 is due to the wings of the H_2O bands,

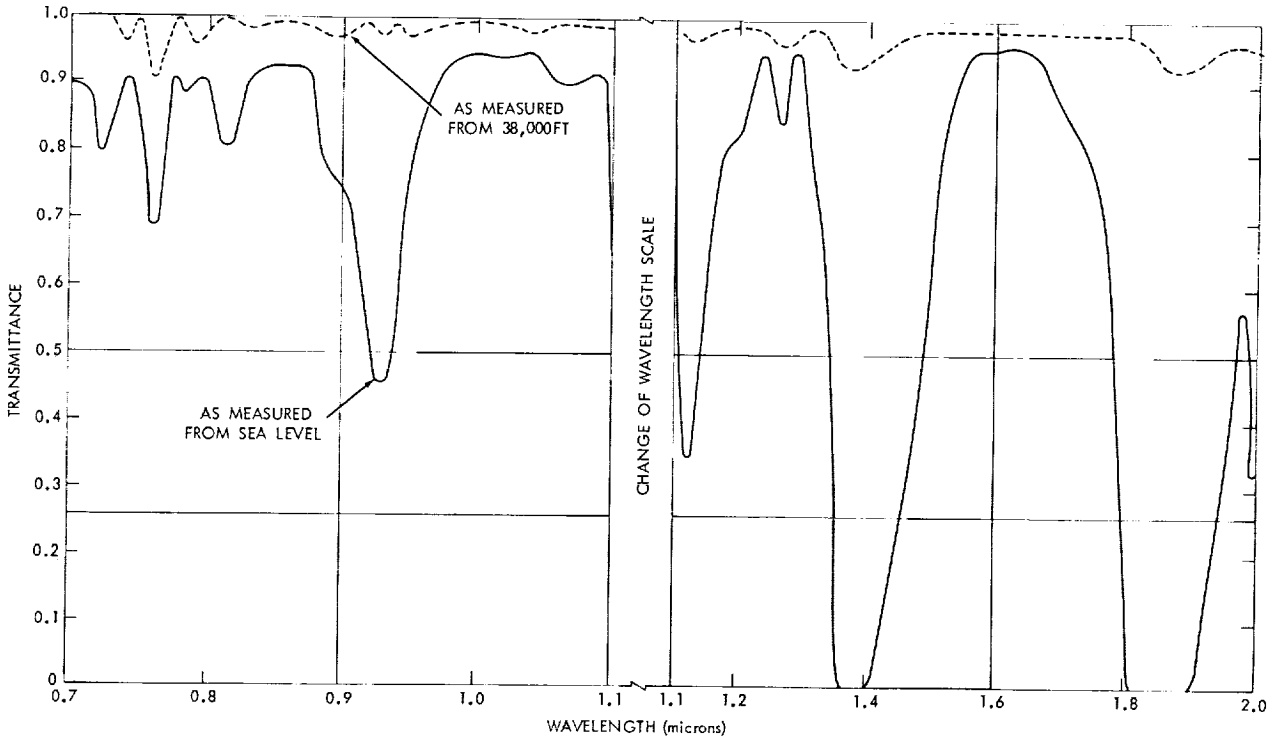

Figure 47—Transmittance of the atmosphere at ground level compared to that at 38,000 feet for normally incident solar rays, 0.7 to 2.0 μ, based on P-4 data.

but more significantly to the Rayleigh and aerosol scattering, as seen from a comparison of the observed values with the theoretical values of Table 3.

As stated earlier the transmittance curve of Figure 46 represents an average of data from several flights. Too few scans of the P-4 interferometer have been analyzed to yield more detailed data of the variations in the H_2O content above the aircraft for different dates and locations. The Perkin-Elmer monochromator data analyzed by the computer and integrated over wide wavelength bands also failed to show the finer details of H_2O absorption. As shown in Part II, Section A, total irradiance as measured by the cone radiometer gave clear evidence of increased atmospheric absorption at certain locations. A more careful study of the Leeds and Northrup charts of the Perkin-Elmer monochromator showed a correlation with the cone data. In order to obtain quantitative data on the amount of precipitable water vapor above the aircraft, a series of measurements was made in the laboratory to determine the absorption profiles of the water bands in the range 1.2 to 3.4. The Perkin-Elmer monochromator was used with the 2 mm slit width, as for the solar measurements on board NASA 711. The source was a 1000 w quartz iodine lamp. The beam was rendered parallel by a concave mirror, travelled a measured distance in clean, dust-free air of known relative humidity, and then was focussed on the entrance slit of the monochromator. Measurements were made for several pathlengths and the absorbance curves were normalized to 28 μ of precipitable water vapor (N.T.P.). The results are presented in Figure 48. The temperature and relative humidity in the laboratory were such that the amount of precipitable water vapor per meter of path length was 7 μ.

The absorption band near 1.8 μ was measured on a large number of the Leeds and Northrup charts made with the Perkin-Elmer monochromator on board NASA 711. The 2.7 μ band had been covered only on the flight of August 16. Computations based on these measurements and the laboratory data of Figure 48 showed that in general the amount of precipitable water vapor above 38,000 ft varies with latitude, not with longitude. Along the path of the transit flight of August 16, the amount of water vapor was 28 μ, while an increase from 10 μ to near 28 μ was observed during the sunrise flight of August 10. On the other hand very high values of water vapor, above 40 μ, were observed during the early part of the flights of August 14 and 19.

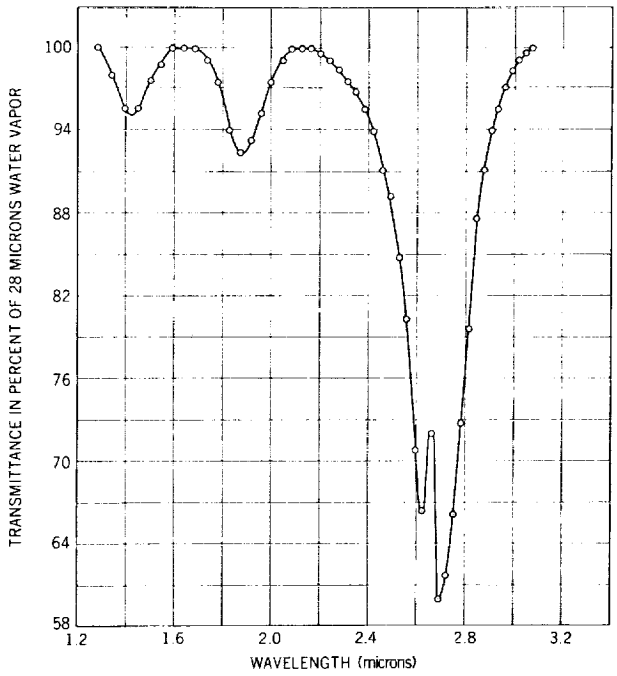

Figure 48—Transmittance of 28 microns of precipitable water vapor based on laboratory measurements with a Perkin-Elmer monochromator.

5. *Spectral Irradiance From the P-4 Interferometer*

The average value of log S_S (signal from the sun) as obtained from the P-4 interferometer was tabulated for 120 wavelengths in the spectral range .7236 to 2.202 μ. It was then corrected for the attenuation due to air mass 2.719, and by applying Equation (14), log P_S (solar irradiance) was computed. These values are on a relative scale since a limiting diaphragm had been mounted in front of the integrating sphere of the P-4. This made an absolute calibration on board NASA 711 with reference to the standard lamp impossible, because the diaphragm prevented the P-4 interferometer from viewing all of the standard lamp. The relative scale of the solar spectral irradiance was changed to an absolute scale by two methods. The Perkin-Elmer monochromator data in the thermocouple range were analyzed using a manual method at a large number of wavelengths, with due corrections for scattered light from the roof of the plane and atmospheric attenuation. The energy in the range of the P-4 interferometer, PbS detector was made to agree with that given by the Perkin-Elmer monochromator. A further slight adjustment was made when a composite curve of solar spectral irradiance based on all the spectral measurements was obtained and the area under the curve was made to agree with the weighted value of the solar constant as given by the total irradiance instruments. The normalized values of the spectral irradiances at each of the 120 selected wavelengths are indicated by the black dots in Figure 31.

F. I-4 Interferometer —J. F. Rogers and P. Ward

1. Description of the Equipment

The I-4 interferometer is of the Michaelson type and covers the wavelength range 2.6 to 15 microns (μ). Apart from the Perkin-Elmer monochromator, which could scan the lower end of this range below 4 μ, this was the only instrument on board for studying solar spectral irradiance in this long wavelength range. It was also the only instrument which required an Irtran 4 window for the aircraft and special shock-proof mounting for its fixture.

The moving coil of the Michaelson cube is actuated by a voice coil driven by a ramp function generator, so its velocity is practically constant through the data acquisition stroke. The data are in the form of an interferogram which is subsequently processed by a digital computer in order to obtain the amplitude spectrum.

Since interferometric spectroscopy is a relatively new field, we will discuss some of its basic principles. The principle common to all interferometers is that the incident radiation is made to interfere selectively with itself, thereby revealing information about the spectral energy distribution. Unlike dispersive instruments that isolate and measure a series of narrow spectral bands in succession, interferometers accept and analyze all wavelengths in their operating range at once. Hence there is a great improvement in signal to noise ratio.

For illustrating the operation of these instruments, the Michaelson interferometer is perhaps the simplest, and easiest to understand.

Consider a monochromatic ray of wave-number ν, wavelength λ entering the interferometer (Figure 49). The ray divides into two identical rays at the semi-reflecting beam splitter. Each ray reflects from a mirror and returns to the beam splitter, through which 50% of the energy is transmitted to the detector. The incident and reflected rays are shown at an angle to each other for the sake of clarity. Actually the rays are incident normally on the two mirrors and are reflected along the same path. As one of the mirrors moves to and fro with a constant velocity V, the two rays interfere with each other constructively or destructively according as the relative path difference is an even or odd multiple of $\lambda/2$. Thus the energy incident on the detector varies periodically. The time interval τ between successive maxima of the detector signal is time required for the path difference to change by λ, that is, for the oscillating mirror to move through the distance $\lambda/2$. Thus $\tau = \lambda/2V$.

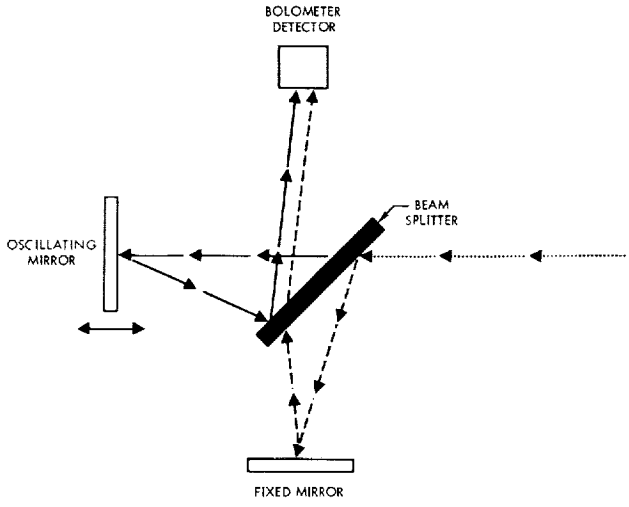

Figure 49—Optical schematic of the Michaelson interferometer.

The modulation frequency of the detector signal is $f_\nu = 1/\tau = 2V/\lambda = 2V\nu$. Thus the output frequency of the interferometer is proportional to the wave-number of the incident light.

If "white light" radiation falls on the entrance aperture, the output signal will consist of a large central peak at the point of zero retardation when all wave components are in phase plus smaller intensity peaks due to reinforcement of frequency components, ν_i, at mirror displacements that are integral multiples of $\lambda/2$. This output signal, called an interferogram, consists of a linear superposition of cosine waves of the form

$$I(x) = \int_{-\infty}^{\infty} G(\nu) \cos(2\pi\nu x)\, d\nu . \tag{15}$$

We use Fourier's integral theorem to transform the above expression, thereby obtaining the intensity as a function of frequency:

$$G(\nu) = \int_{-\infty}^{\infty} I(x) \cos(2\pi\nu x)\, dx . \tag{16}$$

Equation (16) implies that the interferogram has perfect even symmetry about the zero point and that there is an infinitely large mirror displacement. Since neither statement is true, we must compute both sine and cosine components, and restrict the domain of integration. Let the displacement of the mirror be from $-B/2$ to $+B/2$. The spectrum then has terms

$$P(\nu) = \int_{-B}^{+B} I(x) \cos(2\pi\nu x)\, dx , \tag{17}$$

$$Q(\nu) = \int_{-B}^{+B} I(x) \sin(2\pi\nu x)\, dx . \tag{18}$$

In terms of these quantities the energy spectrum G is given by

$$G = \left(P^2 + Q^2\right)^{1/2} . \tag{19}$$

The phase relationship between frequency components is computed from

$$\phi = \arctan \frac{Q}{P} . \tag{20}$$

The phase at the point of zero retardation can be set equal to zero (or 360°), and a change in the direction of net energy flow will then produce a 180° phase shift.

2. Experimental Procedure

The I-4 interferometer was mounted on the same stand as the P-4 (Figure 45). The instrument is pointed directly towards the sun through an Irtran-4 window. The data were recorded on tape as analog signals almost continuously during the six flights. For low angles of elevation of the sun, the mount of the two interferometers was transferred to a lower stand to view the sun through the side window.

3. Data Processing and Analysis

The analog signals of the interferograms were sampled at constant intervals of path retardation, and digitized for computer analysis. One hundred interferograms in succession were co-added to improve the signal to noise ratio for each spectrum. The Fourier transform and phase relationship of each spectral component were then found. A typical amplitude spectrum with the associated phase plot is shown in Figure 50 in terms of output frequency and corresponding wavelength.

At long wavelengths the phase becomes important due to detector radiation. The field of view of the instrument covers an angle of 12 degrees while the sun subtends an angle of only one-half

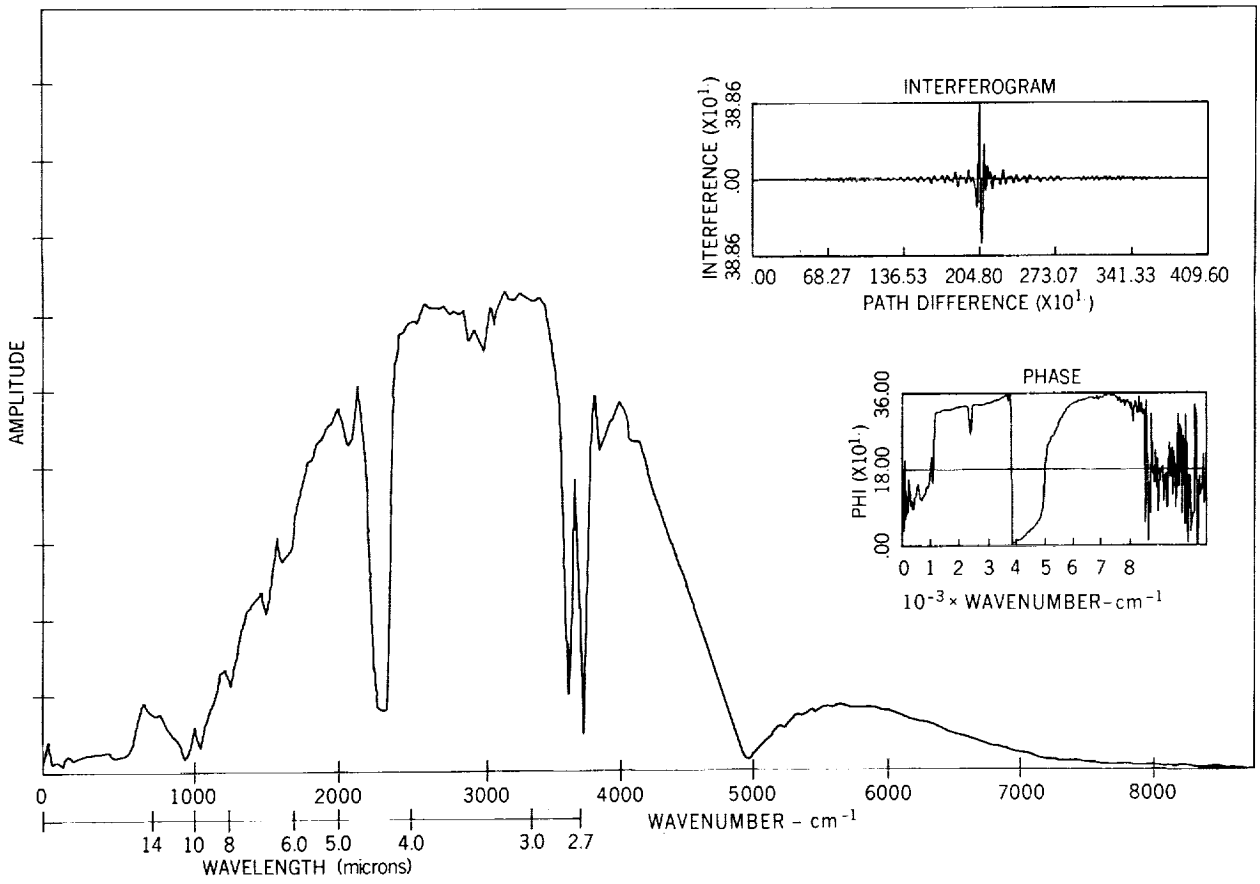

Figure 50—Data from the I-4 interferometer.

degree. The thermostatically controlled thermistor bolometer operates at 37°C and therefore radiates energy to the cold sky about the sun and the window frame. This detector radiation becomes an increasingly large fraction of the net energy interchange as we approach the longer wavelengths. At wavelengths greater than 10 μ the net energy is directed out, i.e., the detector radiates more energy than it receives from the sun.

To account for the detector radiation, a series of measurements was taken while the instrument was pointed away from the sun. Figure 51 is the reduced data from one such measurement. The energy calibration was obtained with a blackbody source manufactured by Infrared Industries, Santa Barbara, California. It was run at a temperature of 1200°K with a 1.53 cm diameter aperture, at a distance of 87 cm from the I-4 interferometer. The effect of detector radiation was negligible during the calibration runs since the front plate of the source had a temperature of 35°C.

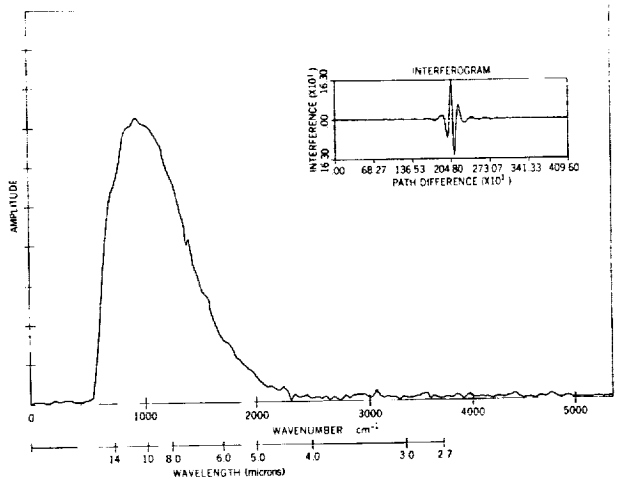

Figure 51—Data from the I-4 interferometer, pointed away from the sun.

The transmittance of the Irtran 4 window as a function of wavelength and angle of incidence was obtained by viewing the blackbody source with the I-4 interferometer through the window. The data were incorporated into a computer program that solved the equation

$$I_\lambda = \frac{\left[S_{(BKG)_\lambda} \pm S_{(meas)_\lambda}\right] \times I_{(BB)_\lambda}}{T_{\alpha\lambda} \times S_{(BB)_\lambda}}, \qquad (21)$$

where $S_{(BKG)_\lambda}$ is the signal obtained from the background run at wavelength λ; $S_{(meas)_\lambda}$, the signal while viewing the sun; $I_{(BB)}$, the irradiance on the aperture of the I-4 interferometer due to the calibration source; $S_{(BB)}$ the signal due to $I_{(BB)}$; and $T_{\alpha,\lambda}$ is the transmittance of the Irtran 4 window as a function of angle of incidence α, and wavelength λ.

The plus or minus sign is used according as the net energy transfer is directed into the instrument or out of it, as is shown by the phase. Ideally the phase should be constant except for the 180° phase reversals but noise in the signal, slight errors in locating the center of the interferogram, and dispersion in one of the optical paths, will produce departures from constancy. Since the data were automatically reduced, a phase-referencing system was adopted whereby the phase at 3.6 μ (in the short wavelength region and removed from major absorption bands) was used as a reference. If the phase at this point lay in the region 0°-90° or 270°-360°, the plus sign was used for all spectral elements that had a phase value in the same range, and the minus sign was used for all elements whose phase lay outside the region.

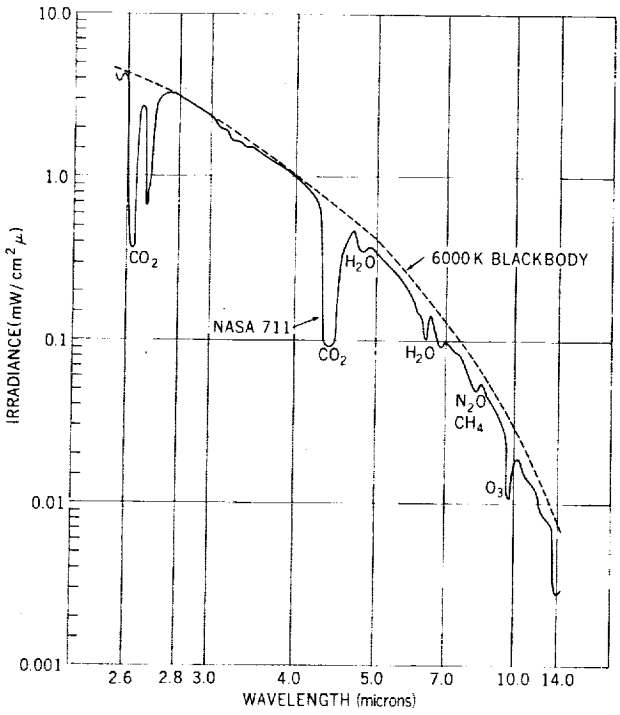

Figure 52—Solar spectrum from the I-4 interferometer at air mass 1.13.

4. Results of I-4 Interferometer Data

The reduced data for an air mass of 1.13 is presented in Figure 52 showing some of the major atmospheric absorption bands. The spectral irradiance of the sun, assuming it to be a 6000°K blackbody, is also plotted for comparison. It can be seen that at long wavelengths the solar spectral irradiance curve falls below the 6000°K curve. This is of interest because in estimating the solar constant, most earlier observers had assumed the solar spectral curve in the range beyond 0.6 μ to be that of a 6000°K blackbody.[5,7] It is unfortunate that data at large air masses are not available due to saturation of the instrument when operated with a lower attenuation. This problem illustrates the major drawback of Fourier spectroscopy—the results are not available in time to detect and correct such difficulties. However, in the infrared region of the spectrum, the transmittance of the atmospheric "windows" is nearly 100%, so an envelope of the reduced curve can be considered a zero air mass curve.

PART IV

CONCLUSION

M. P. Thekaekara

We give below the weighted average results of all the GSFC experiments on board NASA 711 Galileo. These values have been published earlier in a GSFC X-Document and in an article in *Applied Optics*.[18] Considerable work has since been done in critical evaluation of these results in comparison with data from other observers. The objective was to propose, for engineering use, standard values of the solar constant and solar spectral irradiance for zero air mass. For the sake of completeness we also give this proposed standard, which, as will be seen, is very close to the NASA 711 Galileo results.

A. GSFC, NASA 711 GALILEO RESULTS

The following values of the solar constant were measured on board NASA 711 Galileo at 38,000 ft in August 1967:

Cone radiometer	135.8 ± 2.4 mW cm^{-2},
Hy-Cal pyrheliometer	135.2 ± 2.2 mW cm^{-2},
Ångström pyrheliometer (6618)	134.3 ± 2.6 mW cm^{-2},
Ångström pyrheliometer (7635)	134.9 ± 4.0 mW cm^{-2}.

These values agree within the range of the estimated errors of the respective instruments. An arithmetical average yields 135.05 mW cm^{-2}. A weighted average, assuming for each instrument a weight inversely proportional to the estimated error, yields 135.08 mW cm^{-2}. A more rigorous statistical method,[47] identifying estimated error with standard deviation, would give the average 135.12 ± 1.3 mW cm^{-2}.

We accept 135.1 ± 1.3 mW cm^{-2} as the value of the solar constant. The estimated error, average of those of the four instruments, is ± 2.8 mW cm^{-2}. Assuming for the mechanical equivalent of heat 4.184 joules per cal,[6] the solar constant is 1.937 ± 0.040 cal min^{-1} cm^{-2}. This is 3.3% lower than Johnson's value of 2.00 cal min^{-1} cm^{-2}, but intermediate between two recently published higher altitude values—1.950 cal min^{-1} cm^{-2} by Drummond *et al.*,[15] and 1.919 cal min^{-1} cm^{-2} by Murcray.[16]

We give a table (Table 6) of values of spectral irradiance of the sun for zero air mass and for the average sun-earth distance, and solar spectral irradiance curves (Figures 53 and 54) which display the values of Table 6 graphically. The wavelength range covered by our measurements is 0.3 to 15 μ, but for the sake of completeness and for obtaining an integrated value of the solar constant, the table of values has been extended to 0.14 μ in the UV and to 20 μ in the IR. The F. S. Johnson curve is shown by dashed lines. The values given by a weighted average of our spectral

Table 6

Solar Spectral Irradiance (Based on Measurements on Board NASA-711 "Galileo" at 11.58 km) λ—wavelength in microns; P_λ—Solar Spectral Irradiance averaged over small bandwidth centered at λ, in W cm^{-2} $micron^{-1}$; D_λ—percentage of the Solar Constant associated with wavelengths shorter than wavelength λ. Solar Constant 0.13510 W cm^{-2}.

λ	P_λ	D_λ	λ	P_λ	D_λ	λ	P_λ	D_λ	λ	P_λ	D_λ
0.140	0.0000048	0.00050	0.395	0.1191	8.189	0.630	0.1542	39.26	3.8	0.00111	98.902
0.150	0.0000176	0.00059	0.400	0.1433	8.675	0.640	0.1517	40.39	3.9	0.00103	98.982
0.160	0.000059	0.00087	0.405	0.1651	9.245	0.650	0.1487	41.50	4.0	0.00095	99.055
0.170	0.00015	0.00164	0.410	0.1759	9.876	0.660	0.1468	42.00	4.1	0.00087	99.122
0.180	0.00035	0.00349	0.415	0.1783	10.53	0.670	0.1443	43.67	4.2	0.00078	99.182
0.190	0.00076	0.00760	0.420	0.1758	11.19	0.680	0.1418	44.73	4.3	0.00071	99.238
0.200	0.00130	0.0152	0.425	0.1705	11.83	0.690	0.1398	45.78	4.4	0.00065	99.289
0.205	0.00167	0.0207	0.430	0.1651	12.45	0.700	0.1369	46.80	4.5	0.00059	99.335
0.210	0.00269	0.0288	0.435	0.1675	13.06	0.710	0.1344	47.80	4.6	0.00053	99.376
0.215	0.00445	0.0420	0.440	0.1823	13.71	0.720	0.1314	48.79	4.7	0.00048	99.414
0.220	0.00575	0.0609	0.445	0.1936	14.41	0.730	0.1290	49.75	4.8	0.00045	99.448
0.225	0.00649	0.0835	0.450	0.2020	15.14	0.740	0.1260	50.69	4.9	0.00041	99.480
0.230	0.00667	0.1079	0.455	0.2070	15.90	0.750	0.1235	51.62	5.0	0.000383	99.509
0.235	0.00593	0.1312	0.460	0.2080	16.66	0.800	0.1107	55.95	6.0	0.000175	99.716
0.240	0.00630	0.1534	0.465	0.2060	17.43	0.850	0.0988	59.83	7.0	0.000099	99.817
0.245	0.00723	0.1788	0.470	0.2045	18.19	0.900	0.0889	63.30	8.0	0.000060	99.876
0.250	0.00704	0.2053	0.475	0.2055	18.95	0.950	0.0835	66.49	9.0	0.000038	99.912
0.255	0.0104	0.2375	0.480	0.2085	19.72	1.000	0.0746	69.42	10.0	0.000025	99.935
0.260	0.0130	0.2808	0.485	0.1986	20.47	1.1	0.0592	74.37	11.0	0.0000170	99.951
0.265	0.0185	0.3391	0.490	0.1959	21.20	1.2	0.0484	78.35	12.0	0.0000120	99.962
0.270	0.0232	0.4163	0.495	0.1966	21.92	1.3	0.0396	81.61	13.0	0.0000087	99.969
0.275	0.0204	0.4960	0.500	0.1946	22.65	1.4	0.0336	84.32	14.0	0.0000055	99.975
0.280	0.0222	0.5758	0.505	0.1922	23.36	1.5	0.0287	86.62	15.0	0.0000049	99.9785
0.285	0.0315	0.6752	0.510	0.1882	24.07	1.6	0.0244	88.59	16.0	0.0000038	99.9817
0.290	0.0482	0.8225	0.515	0.1833	24.76	1.7	0.0202	90.24	17.0	0.0000031	99.9843
0.295	0.0584	1.020	0.520	0.1833	25.43	1.8	0.0159	91.58	18.0	0.0000024	99.9863
0.300	0.0514	1.223	0.525	0.1852	26.12	1.9	0.0126	92.63	19.0	0.0000020	99.9879
0.305	0.0602	1.430	0.530	0.1842	26.80	2.0	0.0103	93.48	20.0	0.0000016	99.9893
0.310	0.0686	1.668	0.535	0.1818	27.48	2.1	0.0090	94.19	λ_∞		100.0
0.315	0.0757	1.935	0.540	0.1783	28.14	2.2	0.0079	94.82			
0.320	0.0819	2.227	0.545	0.1754	28.80	2.3	0.0068	95.36			
0.325	0.0958	2.555	0.550	0.1725	29.44	2.4	0.0064	95.85			
0.330	0.1037	2.925	0.555	0.1720	30.08	2.5	0.0054	96.287			
0.335	0.1057	3.312	0.560	0.1695	30.71	2.6	0.0048	96.664			
0.340	0.1050	3.702	0.565	0.1700	31.34	2.7	0.0043	97.001			
0.345	0.1047	4.090	0.570	0.1705	31.97	2.8	0.0039	97.305			
0.350	0.1074	4.483	0.575	0.1710	32.60	2.9	0.0035	97.579			
0.355	0.1067	4.879	0.580	0.1705	33.23	3.0	0.0031	97.823			
0.360	0.1055	5.271	0.585	0.1700	33.86	3.1	0.0026	98.034			
0.365	0.1122	5.674	0.590	0.1685	34.49	3.2	0.00226	98.214			
0.370	0.1173	6.099	0.595	0.1665	35.11	3.3	0.00192	98.368			
0.375	0.1152	6.529	0.600	0.1646	35.72	3.4	0.00166	98.501			
0.380	0.1117	6.949	0.605	0.1626	36.33	3.5	0.00146	98.616			
0.385	0.1097	7.359	0.610	0.1611	36.93	3.6	0.00135	98.720			
0.390	0.1099	7.765	0.620	0.1576	38.11	3.7	0.00123	98.816			

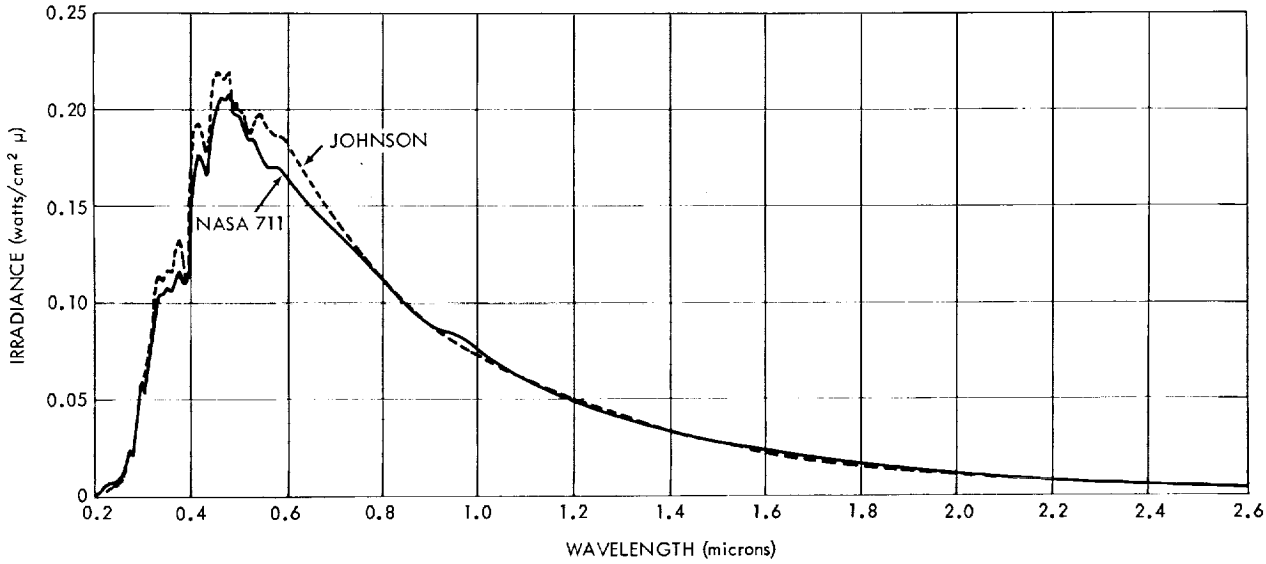

Figure 53—Solar spectrum for zero air mass from NASA 711 Galileo, 0.2-2.6 μ, compared with F. S. Johnson curve.

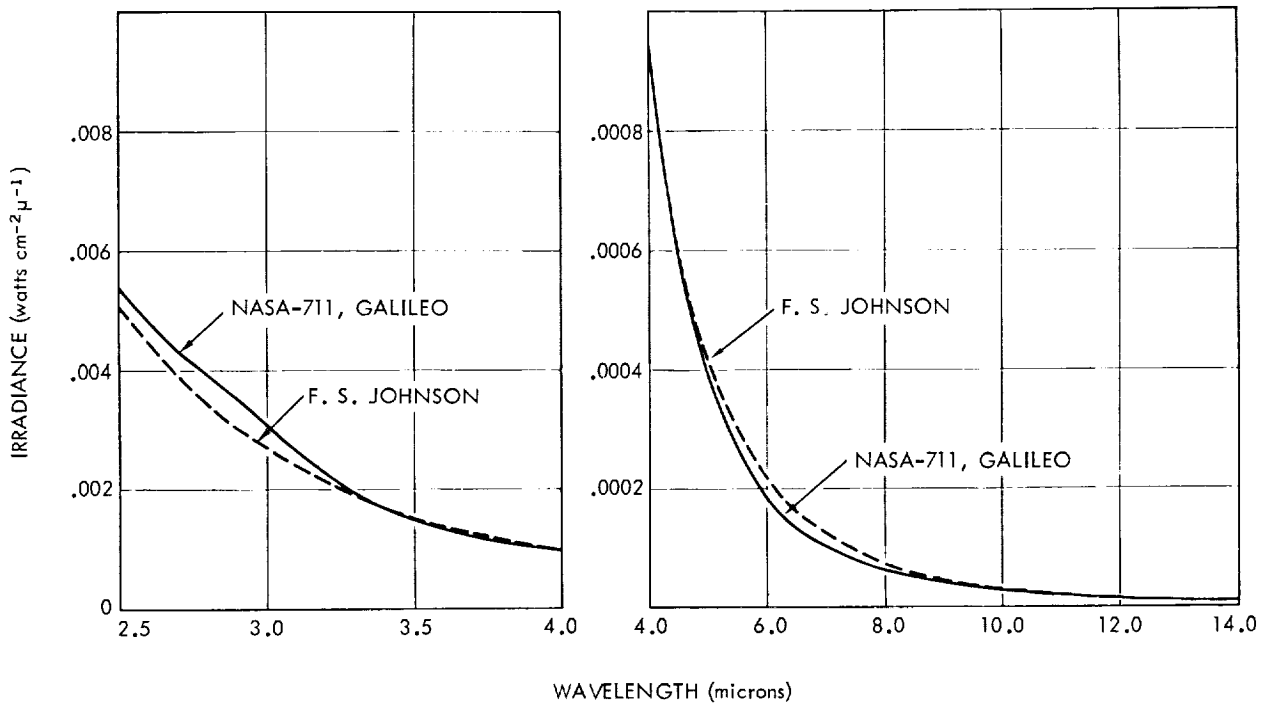

Figure 54—Solar spectrum for zero air mass from NASA 711 Galileo, 2.5-14 μ, compared with F. S. Johnson curve.

irradiance measurements were scaled down by about 0.1 percent, so that the integrated area under the curve is 135.1 mW cm^{-2} as given by our total irradiance instruments. We believe that the agreement within 0.1 percent between the total and spectral measurements was more fortuitous than warranted by the estimated errors of the nine experiments.

In the wavelength range 0.3 to 2.2 μ, which accounts for all but 6.4 percent of the energy of the sun, our values are based on the Perkin-Elmer and Leiss monochromators, the filter radiometer and the P-4 interferometer, though not all of these instruments cover the whole range. The agreement between the instruments is within the estimated errors of each. The differences are small except in the range 0.4 to 0.7 μ, where the ratio of the spectral irradiance of the sun to that of the standard lamp is very high. In this range the Perkin-Elmer monochromator values are higher than those of the filter radiometer. The normalized values of the Leiss monochromator are close to those of the latter, but the unnormalized values are close to those of the former. In the range 0.3 to 0.75 μ, the value given for each wavelength is the average irradiance for a 100 Å bandwidth centered at that wavelength. This gives a solar irradiance independent of the detailed Fraunhofer structure which each instrument displays in a different way according to its wavelength resolution. In the range beyond 0.7 μ, where the Fraunhofer structure is small and our wavelength resolution becomes less, wider bandwidths are used for the averaging. In the range 1.0 to 5.0 μ, each irradiance value is the average irradiance over 1000 Å. The wavelength range 2.2 to 15 μ is covered by the Perkin-Elmer monochromator up to 4 μ, and by the I-4 interferometer from 2.6 to 15 μ.

Table 6 and Figures 53 and 54 seem to present the first direct and detailed measurements of solar irradiance in the wavelength range longer than 0.7 μ. In this range the widely accepted Johnson curve, following that of P. Moon, is as stated earlier that of a 6000°K blackbody. Our data indicate an effective blackbody temperature which decreases as the wavelength increases. This is in agreement with measurements made at three wavelengths between 1.0 and 2.5 μ by Peyturaux,[22] at 11 μ by Saiedy and Goody,[48] and at 6 mm by Whitehurst *et al.*[49] Our extrapolation of the curve in the range 15 to 20 μ is based on this decrease of effective blackbody temperature. Representative values of the effective blackbody temperature of the sun are 5360°K at 5 μ, 5000°K at 15 μ and 4950°K at 20 μ. In the wavelength range below 0.3 μ, where the ozone above the aircraft is an almost complete absorber, we have used the rocket data of the Naval Research Laboratory as given by Detwiler, Garrett, Purcell and Tousey[50] for the range 0.14 to 0.26 μ and by Johnson[5] for the range 0.26 to 0.30 μ. Since our observed values in the range 0.3 to 0.4 μ are 0.927 times those of Johnson, and Detwiler *et al.* had adjusted their irradiance values for wavelengths less than 0.26 μ to Johnson's scale, we have scaled the NRL values down by 7.3%.

In column 3 of Table 6 we give D_λ, the percentage of the total solar energy associated with wavelengths from 0 to λ. The value for the first entry, 0.140 μ, is based on Detwiler *et al.* who give the irradiance down to 0.085 μ.

A point by point comparison of our spectral irradiance values with those of Johnson shows that our values are lower almost everywhere, especially in the UV and visible range. In two short wavelength ranges in the IR, 0.9 to 1.05 μ and 1.35 to 1.9 μ, our values are higher. The disagreement between our curve and that of Johnson is most pronounced in the range 0.52 to 0.70 μ, ours being lower by as much as 12% at 0.55 μ.

Our final table is based on a detailed analysis of many sets of data from a variety of instruments. Instrumental errors arise from different sources for each instrument, and intercomparison

of data permits to a great extent the minimizing of their effects on the final weighted average. Hence we estimate that our spectral irradiance values have an accuracy of ±5 percent.

B. Blackbody Temperature of the Sun

The solar spectral irradiance curve leads to a related question—the effective blackbody temperature of the sun. Text books of physics and astronomy often state that the sun's radiation is that of a blackbody at a temperature of about 6000°K.[51] Figure 9, which has been reproduced from the *Handbook of Geophysics,* shows the 6000°K blackbody curve among the four important curves related to solar energy. It had long been felt that the 6000°K blackbody curve has too high a value. The early Smithsonian data, from which this value was derived, were not of sufficient accuracy. The Johnson curve, following that of P. Moon, had assumed a 6000°K Planckian function for the infrared. Hence it would be begging the question to derive a blackbody temperature of the sun from the Johnson curve.

It should be noted that none of the solar irradiance curves which has been proposed over the years has exactly the same shape as a Planckian curve. However closely the photosphere of the sun may approximate a blackbody, the spectral distribution is affected by such factors as variation of optical thickness of the photosphere with wavelength, Fraunhofer absorption, limb darkening, surface irregularities, etc. But to a first approximation the assumption of a blackbody is valid and has practical usefulness.

The amount of energy absorbed by a surface, for example, that of a spacecraft, is given by an integral of the form

$$E^s = \int_0^\infty P_\lambda^S \alpha_\lambda \, d\lambda ,$$

where P_λ^s is the solar spectral irradiance and α_λ is the spectral absorbance of the surface. Although the absorbance changes with wavelength, this change is slow for most surfaces; absorbance remains nearly the same over large bandwidths. Hence if a blackbody spectral curve, P_λ^B, can be found which agrees closely with P_λ^s for all wavelengths, the integral

$$E^B = \int_0^\infty P_\lambda^B \alpha_\lambda \, d\lambda$$

would be very close to E^s.

Since the solar spectral irradiance curve we have derived in Section A is based on the first detailed, high altitude measurements over almost the entire wavelength range, it is meaningful to find the temperature of the blackbody curve which would best fit the solar spectral irradiance curve.

Best fit is defined by the equation

$$\int_0^\infty |P_\lambda^s - P_\lambda^B(T)|\, d\lambda = \Delta A(T) = \text{minimum}, \tag{22}$$

where P_λ^s is the solar spectral irradiance as given in Table 6, and $P_\lambda^B(T)$ is the normalized radiance of a blackbody at temperature T. The normalization of the blackbody function is such that the area under the curve is equal to the solar constant. The two curves cross each other at several wavelengths, enclosing small elements of area between them; $\Delta A(T)$ is the sum of these elements. The blackbody function is defined by the equation

$$P_\lambda^B(T) = \frac{c_1}{\lambda^5 \left(e^{c_2/\lambda T} - 1\right)}. \tag{23}$$

Of the three parameters c_1, c_2 and T on the right hand side, only temperature T is of significance for the shape of the curve. c_2 varies reciprocally with T, and c_1 is adjusted by the normalization equation

$$S = \int_0^\infty P_\lambda^B(T)\, d\lambda = c_1 \int_0^\infty \lambda^{-5} \left(e^{c_2/\lambda T} - 1\right)^{-1} d\lambda, \tag{24}$$

where S is the solar constant.

A computer program was developed to evaluate the blackbody function for a given temperature at each wavelength of Table 6, to normalize the function, and to evaluate the sum $\Delta A(T)$ of area elements. The integral on the left hand side of Equation (22) was replaced by a series summation of the form

$$\Delta A(T) = \sum_{i=1}^{n} |P_{\lambda_i}^S - P_{\lambda_i}^B(T)| \left(\lambda_{i+1} - \lambda_{i-1}\right) \times 0.5. \tag{25}$$

The value of $\Delta A(T)$ was computed for different values of T, in order to find the effective blackbody temperature (that for which $\Delta A(T)$ is a minimum). The wavelength range for the computation was 0.007 to 38 μ, and P_λ^S was assumed to be zero at the two extremes.

The effective blackbody temperature of the sun as determined from the NASA 711 Galileo curve is 5622°K. This is 378°K less than the value commonly given in text books.

A similar computation using the Johnson curve instead of ours gives a value 5693°K; this is higher than ours mainly because of the relatively higher irradiance in the range below 0.5 μ.

Two simpler methods of defining the effective temperature of the sun may also be mentioned here. The spectral curve has a maximum near 0.47 μ, and from Wien's displacement law this corresponds to 6166°K. The solar constant is related to the temperature by the equation

$$S = \frac{\sigma T^4 r^2}{R^2}, \tag{26}$$

where σ is the Stefan-Boltzmann constant, T is the temperature, r is the radius of the solar disc and R is the mean sun-earth distance. Assuming 135.1 mW cm^{-2} for S, T is found to be 5760°K. The astrophysical constants for these computations have been taken from C. W. Allen.[52]

These two values are less significant from the theoretical and practical standpoint than is the first value 5622°K derived from closeness of fit. In fact it is possible to determine a blackbody brightness temperature at each wavelength, as has been done by Makarova and Kharitonov,[53] and others.

C. Proposed Standards for Solar Constant and Solar Spectrum

In this section we shall present the results of studies which have been made to compare the GSFC NASA 711 results with other recent high altitude data. These studies were made on behalf of an *ad hoc* Committee on "Solar Electromagnetic Radiation." The Committee had a two-fold independent sponsorship: the NASA Space Vehicles Design Criteria group, and the East Coast Group, Solar Simulation, Institute of Environmental Sciences. The members of the Committee are A. J. Drummond, P. R. Gast, D. G. Murcray, E. G. Laue, R. C. Willson and M. P. Thekaekara (Chairman).

In addition to the data on the solar constant from the four instruments on board NASA 711, listed in Section A, the following values from independent sources were considered as having a high degree of reliability. Earlier values which had been obtained by integrating the spectral curve were not included.

Balloon, U. of Denver (Murcray)[16]	133.8 ± 0.6 mW cm^{-2},
Mariner, JPL (Plamondon)[54]	135.3 ± 2.0 mW cm^{-2},
Balloon, U. of Leningrad (Kondratyev *et al.*)[55]	135.3 ± 1.4 mW cm^{-2},
X-15, B57B, NASA 711, Eppley-J.P.L. (Drummond *et al.*)[15]	136.0 ± 2.3 mW cm^{-2}.

Balloon data on the solar constant are available from two independent sources, i.e., Murcray, and Kondratyev *et al.* At the altitude of 31 km or above, water vapor in the atmosphere was no more a source of uncertainty then for the GSFC NASA 711 measurements. The instruments were above 99% of the permanent gases of the atmosphere. Murcray's three series of flights gave values fairly close to each other, though they are rather low compared to the data from other high altitude measurements. The correction factors for residual atmosphere have been suggested as a possible explanation for the low value.[56] The detectors were Eppley normal incidence pyrheliometers which had been calibrated with reference to standard Ångström pyrheliometers, and hence represent the

International Pyrheliometric Scale (IPS 56). The value proposed by Kondratyev *et al.* is based on balloon measurements made from 1961 to 1966. The detectors were two actinometers which had been calibrated with reference to IPS 56. The measurement technique has been discussed in literature.[57]

Two other highly significant sources of solar constant determination are the JPL Mariner data and the Eppley-JPL data. The JPL Mariner value published in May 1969 is based on telemetered results of two Mariner Space probes. Both instruments, though far apart in space, gave values which when reduced to one astronomical unit distance from the sun were in close agreement. A large mass of data was obtained for several weeks before the detectors began to show signs of degradation. The radiometric scale, like that of the GSFC NASA 711 cone, is referenced to absolute units. The Eppley-JPL value is also based on a large mass of data. The data were obtained from a flight on October 17, 1967 of an X-15 rocket aircraft, a series of flights on board a NASA B57B jet aircraft (converted Canberra) in July and August 1966 and March 1967, and one flight on board NASA 711 Galileo in October 1967. The flight altitudes of the jet aircrafts ranged between 9.3 and 15 km. The X-15 rocket aircraft was at an altitude of 82 km when the data were taken; this constituted the first direct measurement of the solar constant totally free of the ozonosphere. The radiometer which has been described in detail in literature[58] was a twelve-channel model incorporating fast response, high sensitivity, wire-wound plated thermopiles, with associated quartz lenses and optical bandpass filters. The results of the filter channels are discussed later. The radiometric calibration was made before and after each flight. The reference standards were a primary group of Eppley-Ångström pyrheliometers which are maintained at Newport, Rhode Island, and are compared frequently in Davos, Switzerland with World Meteorological Organization standards. Thus the reference scale of the Eppley-JPL value is the IPS 56, and the agreement with the reference may claim a higher confidence level than for the other high altitude values.

Of the eight values given above, five are on the IPS 56, and three—those from the JPL Mariner Cavity radiometer, GSFC cone radiometer and GSFC Hy-Cal pyrheliometer—are on independent scales, which within the limits of accuracy of these measurements cannot be distinguished from IPS 56.

Based on the criticisms and evaluations of the members of the Committee, a weighted average of the eight values was taken. Maximum weight (weighting factor f = 10) was given to the values from the JPL Mariner, Leningrad balloon and Eppley-JPL aircraft, since the final values in each case are based on a large mass of data. A high degree of reliability (f = 8) was assigned to the values from the GSFC cone radiometer and GSFC Hy-Cal pyrheliometer. A large number of data points was considered; a careful technique of extrapolation to zero air mass was utilized. The U. of Denver balloon value (f = 4) is also worth serious consideration. That it is so low points to some of the basic problems of radiometry in general and solar radiometry in particular. The two GSFC Ångströms yielded relatively fewer points and hence are given less weight (f = 3).

The proposed value of the solar constant, which is the weighted average of these eight values, is 135.3 mW cm^{-2}, or 1.940 cal min^{-1} cm^{-2}.

The estimated error is ±2.1 mW cm^{-2} or ±0.03 cal min^{-1} cm^{-2}. We believe that this estimate of error, 1.5%, is quite conservative, considering the large mass of high altitude measurements on which it is based. The proposed standard value is almost identical with that obtained from the GSFC NASA 711 spectral irradiance instruments, 0.15% higher than the average of the GSFC NASA 711 total irradiance instruments, and 3% lower than the NRL Johnson value.

For zero air mass solar spectral irradiance, practically all the available data, apart from those given in this report, were deduced from ground-based measurements. Because of the large uncertainties in extrapolating to zero air mass, these data were not considered sufficiently significant to modify the GSFC NASA 711 curve. One notable exception was a complete set of high altitude filter data recently made available from the Eppley-JPL measurements. The consensus of the Committee was to modify the GSFC NASA 711 curve where needed in the light of the filter results.

Preliminary results of the Eppley-JPL program have been published in literature;[58] more complete data have recently become available.[59] Values of the integrated solar irradiance over narrow wavelength bands are computed from the readings of the multichannel filter radiometer. There are 19 readings from narrow band pass filters and 9 from differences in readings of short wavelength cutoff, broad band pass filters. The widths of the bands in the visible and UV ranges are between 500 and 1000 Å. Assuming the spectral distribution within each of the bands to be that given by the GSFC NASA 711 curve, it is possible to make a point by point comparison of the Eppley-JPL data with the GSFC NASA 711 data. It was found that the two sets of data are in very close agreement. The differences are well within the experimental uncertainties of the two sets of measurements. The Eppley-JPL values are referenced to the IPS 56, and the GSFC values to the NBS standard lamp and hence to a blackbody source.

The proposed standard curve was derived from the GSFC NASA 711 curve with modifications based on the Eppley-JPL results. In the wavelength range where several of the filters are in agreement in showing a value slightly different from that of GSFC, a weighted average of the two sets of data was taken. This produces a small revision of the GSFC curve in the wavelength range 0.3 to 0.7 μ and increases the integrated value under the curve, the solar constant, from 135.1 mW cm^{-2} given in Section 1 to the new proposed standard 135.3 mW cm^{-2}.

The proposed zero air mass solar spectral irradiance standard is given in Figure 55 and Table 7. Figure 55 covers the range 0.2 to 2.6 μ; Table 7 covers the wider range 0.12 to 1000 μ. Except for a few minor changes it is the same as Table 6. An extra column A_λ, the irradiance for all wavelengths below λ, has been added. The tabular columns have been reproduced photographically from the computer printout. For A_λ and D_λ, several of the final digits in the printout which did not seem significant have been deleted, without rounding off to the nearest integer the last digit which has been retained.

The energy in the range 0 to 0.12 μ is 0.6 μW cm^{-2}; it is based on the extensive measurements of Hinteregger *et al.*[60] The value of P_λ at 0.12 μ is high compared to those at 0.14 and 0.15 μ; this is due to Lyman α emission line. In the range 0.12 to 2.0 μ, Table 6 has been based

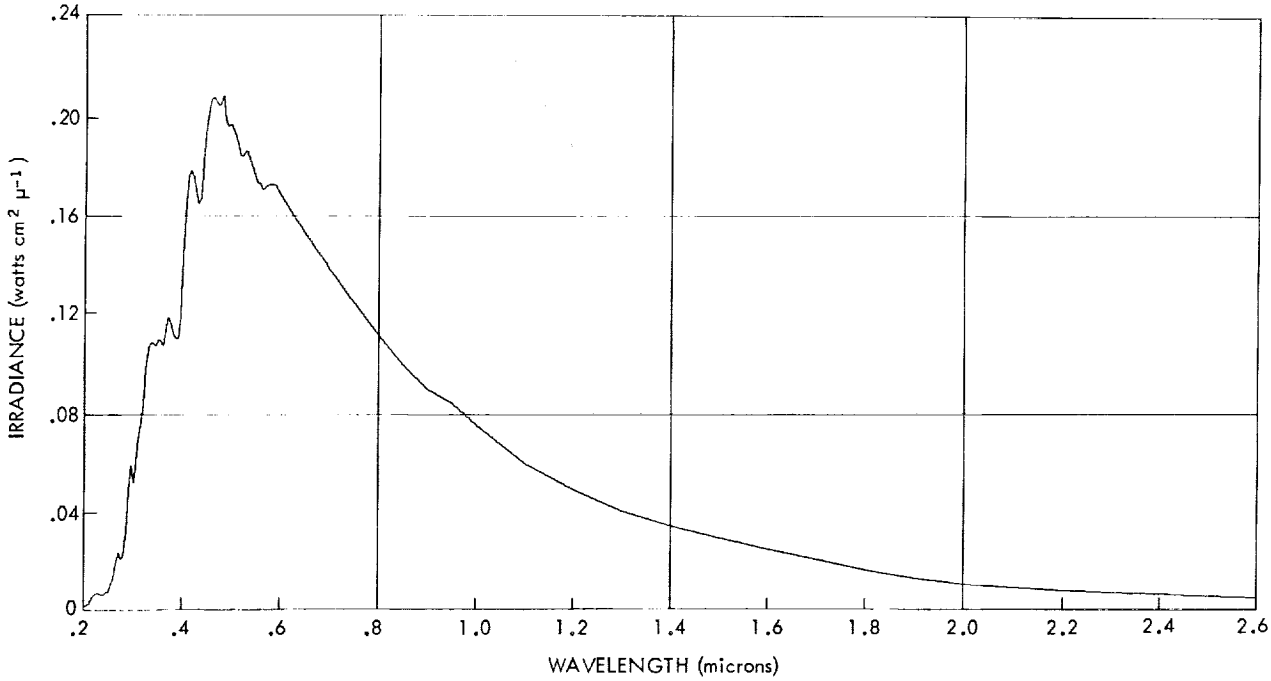

Figure 55—Proposed standard curve of solar spectral irradiance for zero air mass—revision of GSFC NASA 711 data using Eppley-JPL data.

on NRL data, which both Heath[61] and Parkinson and Reeves[62] have found to be about 2.5 times too high. The values have hence been adjusted downwards. In the range 0.22 to 0.30 μ, the correction of 7.3% to the NRL data which had been assumed for Table 6 has been confirmed by Heath, and hence no changes were made. The Eppley-JPL data were used, as stated earlier, for revisions in the range 0.3 to 0.7 μ. The maximum changes are +2.3% at 0.34 μ, -0.7% at 0.45 μ, +1.6% at 0.63 μ and percentages varying between zero and these maxima at intermediate wavelengths. Table 6 has been retained for the range 0.7 to 20 μ. A few entries have been added in the range 20 to 1000 μ. Irradiance values at these wavelengths have been computed from the combined data on brightness temperature of the sun from many different authors as quoted by Shimabukuro and Stacey.[63]

It is instructive to inquire how far and at which wavelengths the proposed standard curve differs from other zero air mass solar spectral curves which have been proposed earlier. A comparison between the GSFC NASA 711 curve and the NRL Johnson curve was shown in Figure 53. This mode of comparison fails to bring out the difference in spectral distribution as distinct from that in the solar constant.

A slightly different method of presentation has been employed for a comparative study of the proposed standard and other earlier curves. Figure 56 shows a comparison between the Johnson curve and the proposed standard. The X-axis is wavelength in microns and the Y-axis is the ratio

$$R = k \frac{P_\lambda'}{P_\lambda},$$

TABLE 7

Solar Spectral Irradiance - Proposed Standard Curve

λ - Wavelength in microns

P_λ - Solar spectral irradiance averaged over small bandwidth centered at λ, in Watts $cm^{-2}\mu^{-1}$

A_λ - Area under the solar spectral irradiance curve in the wavelength range 0 to λ, mW cm^{-2}

D_λ - Percentage of the solar constant associated with wavelengths shorter than λ

Solar Constant - 135.30 mW cm^{-2}

λ	P_λ	A_λ	D_λ	λ	P_λ	A_λ	D_λ	λ	P_λ	A_λ	D_λ
.120	.000010	.00059992	.00044	.475	.2044	25.6001	18.921	2.4	.0064	129.695	95.858
.140	.000003	.00072999	.00053	.480	.2074	26.6296	19.681	2.5	.0054	130.285	96.294
.150	.000007	.00077999	.00057	.485	.1976	27.6421	20.430	2.6	.0048	130.795	96.671
.160	.000023	.00092999	.00068	.490	.1950	28.6236	21.155	2.7	.0043	131.250	97.007
.170	.000063	.00135999	.00100	.495	.1960	29.6011	21.878	2.8	.00390	131.660	97.3107
.180	.000125	.00229999	.00169	.500	.1942	30.5766	22.599	2.9	.00350	132.030	97.5838
.190	.000271	.00427999	.00316	.505	.1920	31.5421	23.312	3.0	.00310	132.360	97.8277
.200	.00107	.010984	.0081	.510	.1882	32.4926	24.015	3.1	.00260	132.645	98.0387
.210	.00229	.027784	.0205	.515	.1833	33.4214	24.701	3.2	.00226	132.898	98.2179
.220	.00575	.067984	.0502	.520	.1833	34.3379	25.379	3.3	.00192	133.097	98.3724
.225	.00849	.098584	.0728	.525	.1852	35.2591	26.059	3.4	.00166	133.276	98.5047
.230	.00967	.113484	.0871	.530	.1842	36.1826	26.742	3.5	.00146	133.432	98.6200
.235	.00993	.116984	.1204	.535	.1818	37.0976	27.418	3.6	.00135	133.573	98.7238
.240	.00830	.193559	.1430	.540	.1783	37.9979	28.084	3.7	.00123	133.702	98.8192
.245	.00723	.227384	.1680	.545	.1754	38.8821	28.737	3.8	.00111	133.819	98.9056
.250	.00704	.263059	.1944	.550	.1725	39.7519	29.380	3.9	.00103	133.926	98.9847
.255	.0104	.306659	.226	.555	.1720	40.6131	30.017	4.0	.00095	134.025	99.0579
.260	.0130	.365159	.269	.560	.1695	41.4669	30.648	4.1	.00087	134.116	99.1252
.265	.0185	.443909	.328	.565	.1705	42.3169	31.276	4.2	.00078	134.198	99.1861
.270	.0232	.548159	.405	.570	.1712	43.1711	31.907	4.3	.00071	134.273	99.2412
.275	.0204	.657159	.485	.575	.1719	44.0289	32.541	4.4	.00065	134.341	99.2915
.280	.0222	.763659	.564	.580	.1715	44.8874	33.176	4.5	.00059	134.403	99.3373
.285	.0315	.897909	.663	.585	.1712	45.7441	33.809	4.6	.00053	134.459	99.3787
.290	.0482	1.09715	.810	.590	.1700	46.5971	34.439	4.7	.00048	134.509	99.4160
.295	.0584	1.36365	1.007	.595	.1682	47.4426	35.064	4.8	.00045	134.556	99.4504
.300	.0514	1.63815	1.210	.600	.1666	48.2796	35.683	4.9	.00041	134.599	99.482195
.305	.0603	1.91740	1.417	.605	.1647	49.1079	36.295	5.0	.0003830	134.63905	99.511500
.310	.0689	2.24040	1.655	.610	.1635	49.9284	36.902	6.0	.0001750	134.91805	99.717708
.315	.0764	2.60365	1.924	.620	.1602	51.5469	38.098	7.0	.0000990	135.05505	99.818965
.320	.0830	3.00215	2.218	.630	.1570	53.1329	39.270	8.0	.0000600	135.13455	99.877723
.325	.0975	3.45340	2.552	.640	.1544	54.6899	40.421	9.0	.0000380	135.18355	99.913939
.330	.1059	3.96190	2.928	.650	.1511	56.2174	41.550	10.0	.0000250	135.21505	99.937220
.335	.1081	4.49690	3.323	.660	.1486	57.7159	42.657	11.0	.0000170	135.23605	99.952742
.340	.1074	5.03565	3.721	.670	.1456	59.1869	43.744	12.0	.0000120	135.25055	99.963458
.345	.1069	5.57140	4.117	.680	.1427	60.6284	44.810	13.0	.0000087	135.26090	99.971109
.350	.1093	6.11190	4.517	.690	.1402	62.0429	45.855	14.0	.0000055	135.26800	99.976356
.355	.1083	6.65590	4.919	.700	.1369	63.4284	46.879	15.0	.0000049	135.27320	99.980199
.360	.1068	7.19365	5.316	.710	.1344	64.7849	47.882	16.0	.0000038	135.27755	99.983414
.365	.1132	7.74365	5.723	.720	.1314	66.1139	48.864	17.0	.0000031	135.28100	99.985964
.370	.1181	8.32190	6.150	.730	.1290	67.4159	49.826	18.0	.0000024	135.28375	99.987997
.375	.1157	8.90640	6.582	.740	.1260	68.6909	50.769	19.0	.0000020	135.28595	99.989627
.380	.1120	9.47565	7.003	.750	.1235	69.9384	51.691	20.0	.0000016	135.28775	99.990953
.385	.1098	10.0301	7.413	.800	.1107	75.7934	56.018	25.0	.000000610	135.29328	99.995036
.390	.1098	10.5791	7.819	.850	.0988	81.0309	59.889	30.0	.000000300	135.29555	99.996718
.395	.1189	11.1509	8.241	.900	.0889	85.7234	63.358	35.0	.000000160	135.29670	99.997568
.400	.1429	11.8054	8.725	.950	.0835	90.0334	66.543	40.0	.000000094	135.29734	99.998037
.405	.1644	12.5736	9.293	1.000	.0746	93.9859	69.464	50.0	.000000038	135.29800	99.998525
.410	.1751	13.4224	9.920	1.100	.0592	100.675	74.409	60.0	.000000019	135.29828	99.998736
.415	.1774	14.3036	10.571	1.200	.0484	106.055	78.385	80.0	.000000007	135.29854	99.998928
.420	.1747	15.1839	11.222	1.300	.0396	110.455	81.637	100.0	.000000003	135.29864	99.999002
.425	.1693	16.0439	11.858	1.400	.0338	114.115	84.342	1000.0	0	135.30000	100.000000
.430	.1639	16.8769	12.473	1.500	.0287	117.230	86.645				
.435	.1663	17.7024	13.083	1.600	.0244	119.885	88.607				
.440	.1810	18.5706	13.725	1.700	.0202	122.115	90.255				
.445	.1922	19.5036	14.415	1.800	.0159	123.920	91.589				
.450	.2006	20.4856	15.140	1.900	.0126	125.345	92.642				
.455	.2057	21.5014	15.891	2.000	.0103	126.490	93.489				
.460	.2066	22.5321	16.653	2.100	.0090	127.455	94.202				
.465	.2048	23.5606	17.413	2.200	.0079	128.300	94.826				
.470	.2033	24.5809	18.167	2.300	.0068	129.035	95.370				

where P_λ is the spectral irradiance at wavelength λ for the standard curve (Table 7), P_λ' is the corresponding quantity for the Johnson curve (obtained by linear interpolation for wavelengths not on the Johnson table), and k is a normalizing constant which makes the area under the Johnson curve equal to that under the standard over the wavelength range 0.25 to 2.5 μ.

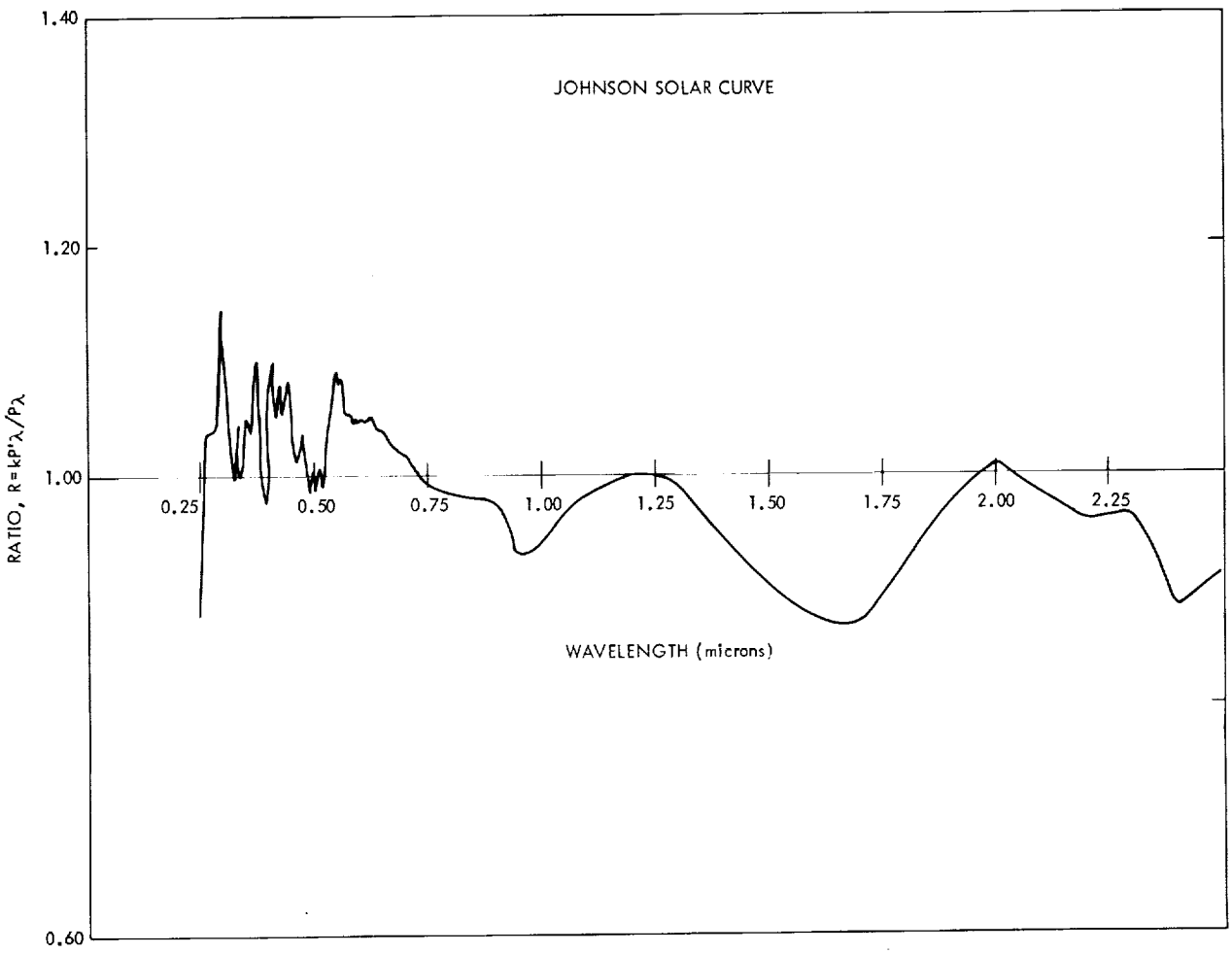

Figure 56—Comparison of the proposed standard and the Johnson data.
Curve shows the ratio of normalized values of Johnson to the standard values.

Figures 57, 58, 59 and 60 show similar comparisons of four other curves to the same standard: Figure 57, Nicolet[64] in the range 0.3 to 2.2 μ; Figure 58, Labs and Neckel[17] in the range 0.25 to 2.5 μ; Figure 59, Stair and Ellis,[44] in the range 0.3 to 0.53 μ, and Figure 60, GSFC NASA 711 (Table 6) in the range 0.25 to 2.5 μ. No normalization factor was used for Figure 60, so the ordinate gives the ratio by which values in Table 6 were divided to give Table 7. A comparison of Figures 56 and 58 shows that in the range 0.25 to 0.45 μ, the Johnson values are high and the Labs and Neckel values are low compared to the proposed standard. It will be recalled that Johnson had scaled Dunkelman and Scolnik's value upward by 8.8%. Labs and Neckel's values are low, probably because of the difficulty of estimating the true solar continuum in a wavelength range which is so rich in Fraunhofer lines. Both Nicolet and Labs and Neckel show a sharp change in the ratio near the Balmer discontinuity, which is not seen in Figures 56 and 59 where the data are based on the irradiance of the whole disc rather than radiance of the center of the disc. The spectral radiance curve obtained by Stair and Ellis has a special significance. Two instruments were used—a Leiss monochromator and a filter radiometer. The excursions of the curve above

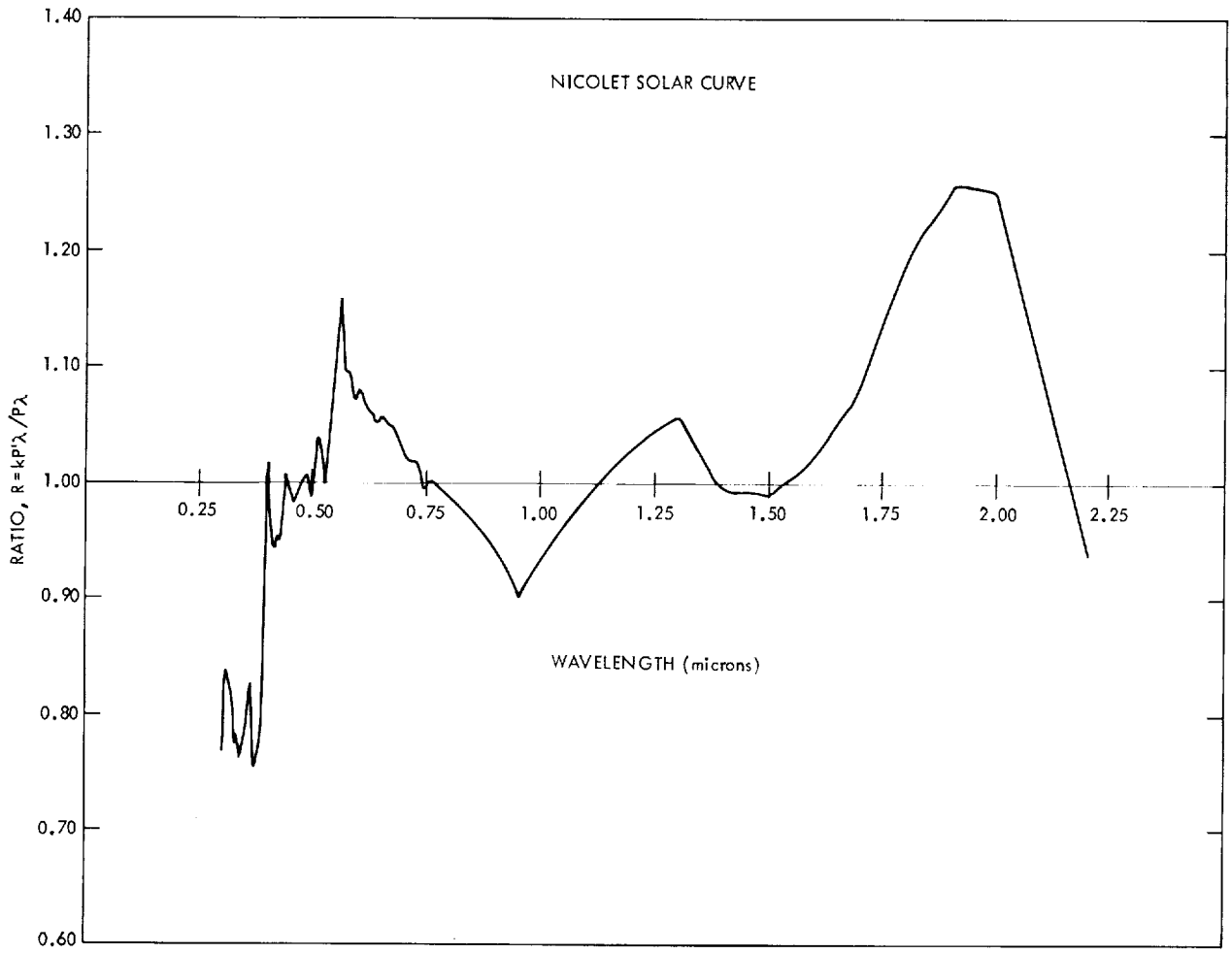

Figure 57—Comparison of the proposed standard and the Nicolet data.
Curve shows the ratio of normalized values of Nicolet to the standard values.

and below the 1.00 ratio line are more or less evenly balanced. In the wavelength range 0.5 to 0.7 μ, where Figures 56, 57 and 58 show $R > 1.0$, the agreement between the GSFC NASA 711 results and the Eppley-JPL results was so close that revision of Table 6 did not seem justified beyond what is shown in Figure 60.

In conclusion, we give some of the astrophysical quantities which can be derived from the solar constant and solar spectrum, and are of great usefulness in science and industry. The effective blackbody temperature of the sun derived from the solar spectral curve of Table 7 is 5631°K. This is the temperature at which the area enclosed between the solar spectral curve and the normalized blackbody curve is a minimum. The temperature derived from Wien's displacement law is the same as for the GSFC NASA 711 curve, 6166°K. From the Stefan-Boltzmann law, the solar constant of 135.3 mW cm^{-2} corresponds to a temperature of 5762°K. Brightness temperature of the sun has been computed at each of the wavelengths listed in Table 7, using Equation (23). The constants c_1 and c_2, with suitable scaling for P_λ in W cm^{-2} μ^{-1}, and λ in μ, are

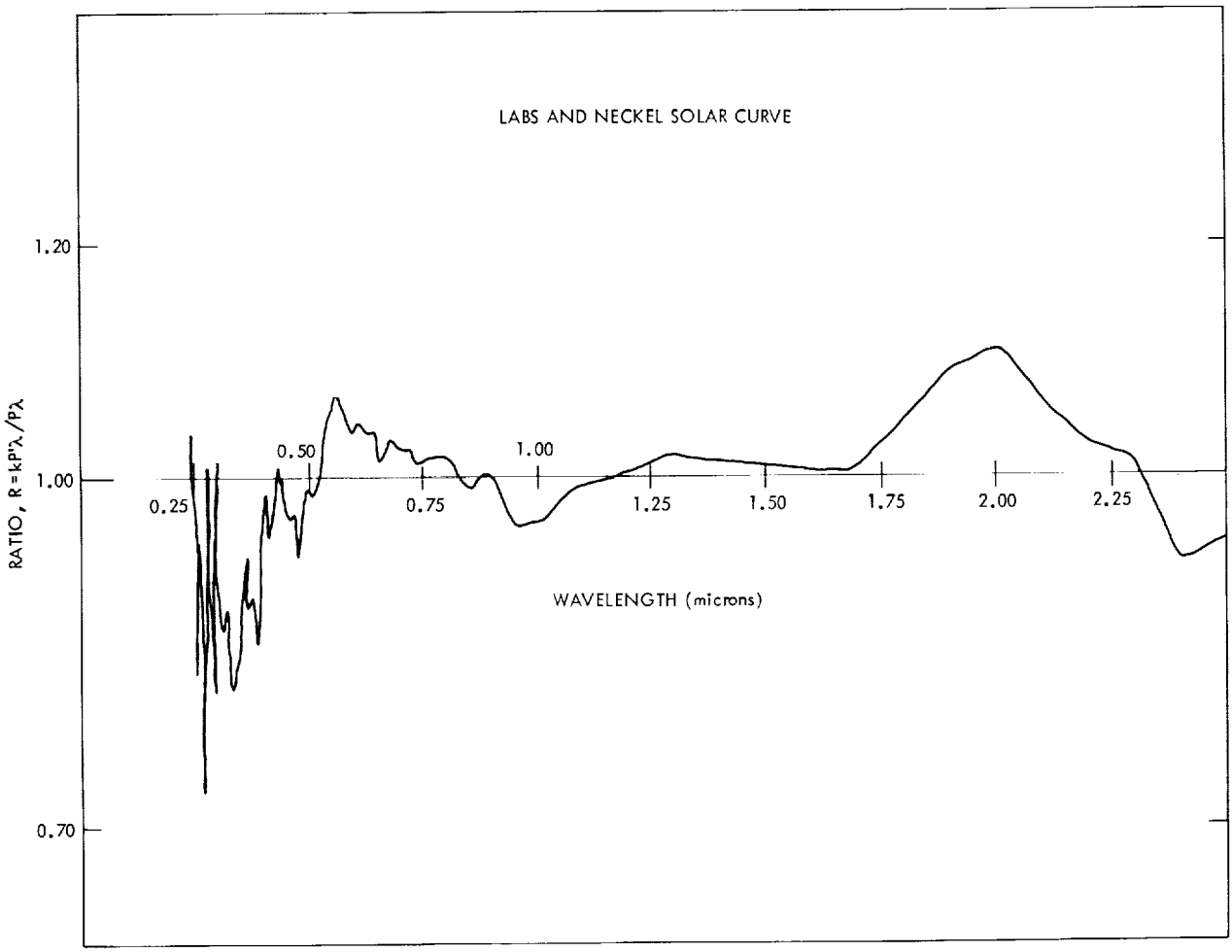

Figure 58—Comparison of the proposed standard and the Labs and Neckel data. Curve shows the ratio of normalized values of Labs and Neckel to standard values.

c_1 = 0.809748 and c_2 = 14387.9. The brightness temperature, which is relatively high in the X-ray range, drops to a minimum of about 4540°K at 0.15 μ; it rises to a high value near 6000°K in the visible and near infrared. In the infrared the temperature falls slowly, reaching a minimum of about 4360°K at about 50 μ, and then rises to relatively higher values in the microwave range.

The irradiance at the distance of one astronomical unit leads to an evaluation of the total energy radiated by the sun. The sun radiates energy at the rate of 3.805×10^{26} watts. From the relativistic equivalence of mass and energy, the rate of diminution of the mass of the sun is 4.234×10^{12} gm per second. A question might be raised how far this loss of mass in conversion of hydrogen to helium would cause a diminution in solar radiance. The loss is very small compared to the mass of the sun, 1.989×10^{33} gm. If the exponential decay of hydrogen were the only factor, assuming that three fourths of the sun's mass is hydrogen, it can be shown that the solar radiance would decrease by 0.1 percent in 8×10^5 years. But other factors such as increased

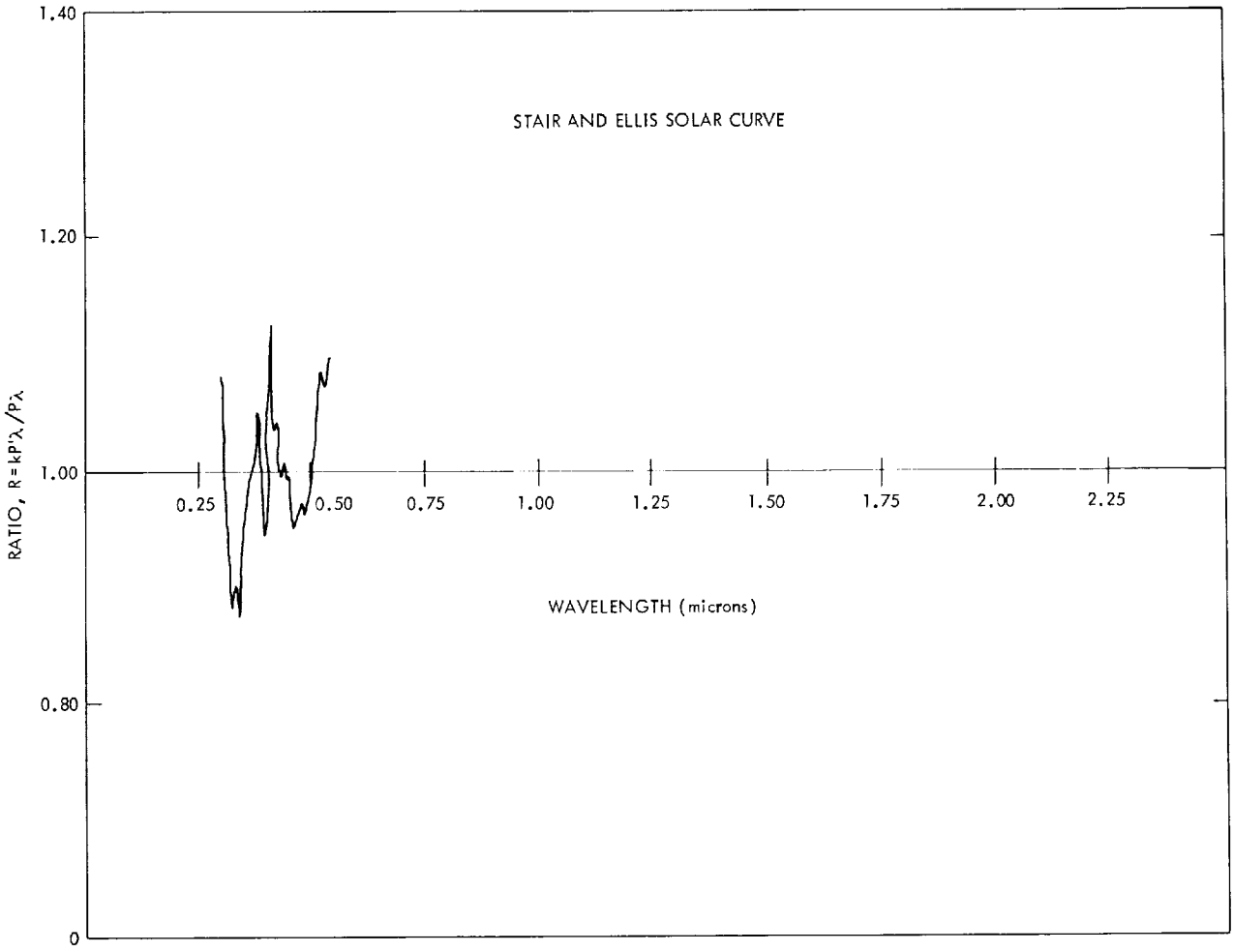

Figure 59—Comparison of the proposed standard and the Stair and Ellis data. Curve shows the ratio of normalized values of Stair and Ellis to standard values.

reaction rate due to helium accumulation are involved, and astrophysical theory postulates a secular increase rather than decrease in solar radiance.

As stated earlier, the solar constant is defined for one astronomical unit, 1.496×10^{13} cm. The following are the values of solar irradiance in mW cm^{-2} at the sun-earth distance in the absence of the atmosphere on the first day of each month, January (in parentheses, 1) through December (in parentheses, 12): (1) 139.9; (2) 139.3; (3) 137.8; (4) 135.5; (5) 133.2; (6) 131.6; (7) 130.9; (8) 131.3; (9) 132.9; (10) 135.0; (11) 137.4; (12) 139.2. The maximum and minimum values are respectively, at perihelion (about Jan. 3), 139.9, and at aphelion (about July 4), 130.9. The changes in sun-earth distance from year to year are such that these values may change by ±1 microwatt cm^{-2}. For purposes of precise comparison the American Ephemeris[31] should be

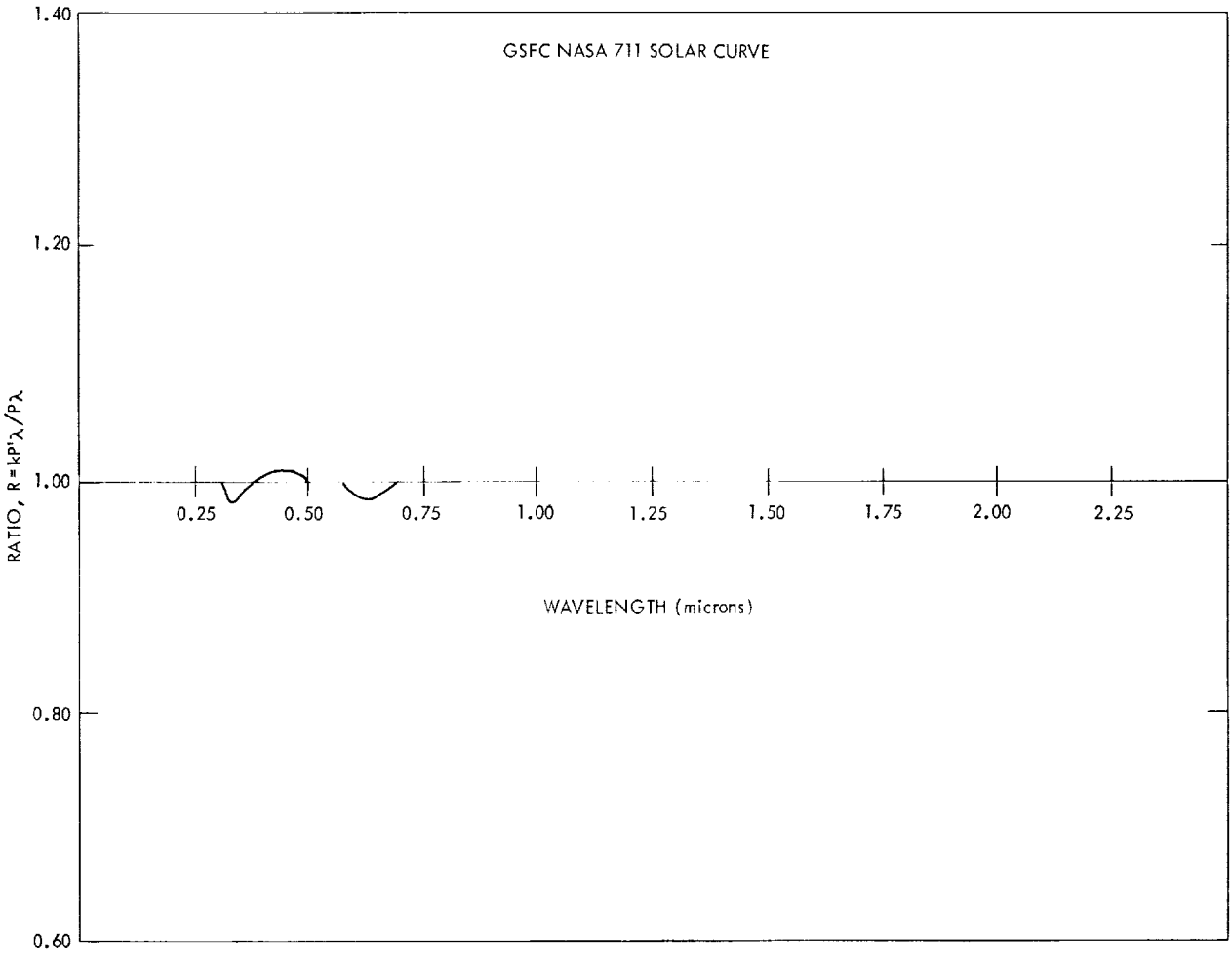

Figure 60—Comparison of the proposed standard and the GSFC NASA 711 data. Curve shows the ratio of the GSFC NASA 711 data (unnormalized) to the standard values.

consulted. Two other values, also important in space simulation, are the solar irradiance at the distances of Venus and Mars, which are 258.6 and 58.3 mW cm^{-2}, respectively.

Goddard Space Flight Center
National Aeronautics and Space Administration
Greenbelt, Maryland, May 4, 1970
124-09-27-01-51

REFERENCES

1. Stair, R., Johnston, R. G. and Bagg, R. C., "Spectral Distribution of Energy from the Sun," *J. Res. National Bureau Standards* 53:113-119, 1954.

2. Thekaekara, M. P., "Solar Irradiance Curves and Absorbance of Satellite Coatings," *Solar Energy* 12(2):205-215, December 1968.

3. Minnaert, M., "The Photosphere," in *The Sun,* ed. by Kuiper, G. P., p. 90, University of Chicago Press, 1952; Aller, L. H., *Astrophysics,* Chapters 7, 8, and 9, New York: Ronald Press Company, 1953.

4. Abbot, C. G., "Solar Radiation and Weather," *Smithsonian Miscellaneous Collections* Vol. 146, No. 3, October 1963.

5. Johnson, F. S., "The Solar Constant," *J. Meteor.* 11(6):431-439, December 1954.

6. Condon, E. U., "Principles of Thermodynamics," in *Handbook of Physics,* ed. by Condon, E. U., and Odenshaw, H, p. 5-3, New York: McGraw-Hill Book Co., 1958; Zimmerman, O. T. and Lavine, I., *Conversion Factors and Tables,* Dover, New Hampshire: Industrial Research Service, Inc., 1961.

7. Moon, P., "Proposed Standard Solar-Radiation Curves for Engineering Use," *J. Franklin Institute* 230:583-617, November 1940.

8. Aldrich, L. B. and Abbott, C. G., "Smithsonian Pyrheliometry and the Standard Scale of Solar Radiation,"*Smithsonian Misc. Coll.* 110(5); Publ. No. 3920, Washington: Smithsonian Institution, April 15, 1948.

9. Schuepp, W., "Die Bestimmung der Komponenten der Atmosphärischen Trübung aus Aktinometermessungen," *Arch. Met. Geoph. Biokl.* serie B, 1, 257, 1949 (in German), Dissertation, Basel, 1949.

10. Allen, C. W.,*Observatory* 70, 154, 1950.

11. Aldrich, L. B. and Hoover, W. H., "The Solar Constant," *Science* 116(3024):3, December 12, 1952.

12. Allen, C. W., *Astrophysical Quantities,* p. 168, London, England: University of London, 1955.

13. Stair, R. and Johnston, R. G., "Preliminary Spectroradiometric Measurements of the Solar Constant," *J. Res. National Bureau Standards* 57(4):205-211, October 1956.

14. Allen, C. W., "Solar Radiation," *Quarterly J. Roy. Meteor. Soc.* 84(362):307-318, October 1958.

15. Drummond, A. J., Hickey, J. R., Scholes, W. J. and Laue, E. G., "Multi-Channel Radiometer Measurement of Solar Irradiance," *J. of Spacecraft and Rockets* 4(9):1200-1206; September 1967; Laue, E. G. and Drummond, A. J., "Solar Constant: First Direct Measurements," *Science* 161, 888-891, 30 August 1961; Drummond, A. J. and Hickey, J. R., "The Eppley-JPL Solar Constant Measurement Program," *Solar Energy* 12(2):217-232, December 1968.

16. Murcray, D. G., "Balloon-Borne Measurements of the Solar Constant," Report AFCRL-69-0070, Denver, Colorado: University of Denver, January 1969; Murcray, D. G., Kyle, T. G., Kosters, J. J. and Gast, P. R., "The Measurements of the Solar Constant from High Altitude Balloons," Report AFCRL-68-0452, Denver, Colorado: University of Denver, August 1968.

17. Labs, D., and Neckel, H., "The Radiation of the Solar Photosphere from 2000 Å to 100 μ," *Z. Astrophys.* 69:1-73, 1968.

18. Thekaekara, M. P., Kruger, R. and Duncan, C. H., "Solar Irradiance Measurements from a Research Aircraft," *App. Optics* 8(8);1713-1723, August 1968; Thekaekara, M. P. *et al.*, GSFC Document X-322-68-304, Goddard Space Flight Center, Greenbelt, Maryland, August 1968.

19. Deirmedjian, D. and Sekera, Z., "Atmospheric Turbidity and the Transmission of Ultraviolet Sunlight," *J. Opt. Soc. Am.* 46(8):565-571, August 1956.

20. Johnson, F. S., Purcell, J. D., Tousey, R. and Wilson, N., *Rocket Exploration of the Upper Atmosphere,* p. 279, ed. by Boyd and Seaton, London, England: Pergamon Press, 1954.

21. Makarova, E. A., "A Photometric Investigation of the Energy Distribution in the Continuous Solar Spectrum in Absolute Units," *Soviet Astronomy-AJ* 1(4):531-546, April 1957.

22. Peyturaux, R., "Contribution a l'Etude du Fond Continu du Spectre Solaire dans le Proche Infra-Rouge," *Annales d'Astrophysique* 15(3):302-351, July-September 1952 (in French).

23. Labs, D., "The Intensity of the Continuum of the Center of the Solar Disk in the Wavelength Range 3300 to 6900 Å," *Zeitschrift für Astrophysik* 44(1):37-55, December 1957 (in German).

24. Gast, P. R., "Solar Radiation," in *Handbook of Geophysics,* ed. by Campen, C. F. et al., pp. 16-14 to 16-30, New York: McMillan Co., 1960.

25. Dunkelman, L. and Scolnik, R., "Solar Spectral Irradiance and Vertical Atmospheric Attenuation in the Visible and Ultraviolet," *Opt. Soc. Amer. J.* 49(4):356-367, April 1959.

26. Thekaekara, M. P., "Survey of the Literature on the Solar Constant and the Spectral Distribution of Solar Radiant Flux," NASA publication SP-74, Washington, D. C., 1965; Thekaekara, M. P., "The Solar Constant and Spectral Distribution of Solar Radiant Flux," *Solar Energy* 9(1):7-20, January 1965.

27. Arvesen, J. C., Griffin, R. N. and Pearson, B. D., Jr., "Determination of Extraterrestrial Solar Spectral Irradiance from a Research Aircraft," *App. Optics* 8(11):2215-2232, November 1969.

28. Elterman, L., and Toolin, R. B., "Atmospheric Optics," in *Handbook of Geophysics and Space Environments,* ed. by Valley, S. L., pp. 7-12 to 7-35, New York: McGraw-Hill Book Co., 1965.

29. "Solar Instrumentation Installation in Convair 990A Aircraft," Report. NASA Goddard Contract NAS-5-3744, Fairchild-Hiller Corp., Germantown, Maryland, 1967.

30. Gutnik, M., "Atmospheric Water Vapor," in *Handbook of Geophysics and Space Environments*, ed. by Valley, S. L., p. 3-37, New York: McGraw-Hill Book Co., 1965.

31. U. S. Nautical Almanac Office, *The American Ephemeris and Nautical Almanac for the Year* 1967, U. S. Government Printing Office, Washington, D. C., *passim.* 1965.

32. Bemporad, A., "Search for a New Empirical Formula to Represent the Variation of Solar Radiation with Zenith Distance," *Meteorologische Zeitschrift* 24(7):306-313, July 1907 (in German).

33. Kasten, F., "A New Table and Approximation Formula for the Relative Optical Air Mass," Tech. Report 136 (AD610554), Cold Regions Research and Engineering Laboratory, Hanover, New Hampshire, 1964.

34. Gouffé, A., "Corrections d'Ouverture des Corps-Noirs Artificiels Compte tenu des Diffusions Internes," *Revue d'Optique* 24(1-3):1-10, January-March 1945 (in French).

35. Campanaro, P. and Ricolfi, T., "New Determination of the Total Normal Emissivity of Cylindrical and Conical Cavities," *Opt. Soc. Am. J.* 57(1):48-50, January 1967.

36. Ångström, A., "Radiation to Actinometric Receivers and its Dependence on Aperture Conditions," *Tellus* 13(3):425-431, September 1961. Preprint Series No. F6, Eppley Foundation for Research, Newport, Rhode Island.

37. Stair, R., *et al.*, "Some Developments in Improved Methods for the Measurement of the Spectral Irradiances of Solar Simulators," NASA CR-201, pp. 1-51, National Aeronautics and Space Administration, Washington, D. C., April 1965.

38. Jenkins, F. A. and White, H. E., *Fundamentals of Optics*, p. 511, New York: McGraw-Hill Book Company, Inc., third edition, 1957.

39. Thekaekara, M. P. and Winker, A. R., "Transmittance Measurements on a Thick Plate of Optical Material," GSFC Document X-322-69-399, Goddard Space Flight Center, Greenbelt, Maryland, September 1969.

40. Hass, G. and Hadley, L., "Optical Constants of Metals," in *American Institute of Physics Handbook*, ed. by Gray, D. E., second edition, p. 6-107, New York: McGraw-Hill Book Co., Inc., 1963.

41. Moss, T. S., *Optical Properties of Semiconductors*, p. 7, London, England: Butterworth's Scientific Publications, 1959.

42. Minnaert, M., Mulders, G. F. W. and Houtgast, J., *Photometric Atlas of the Solar Spectrum*, Amsterdam: D. Schnabel, 1940.

43. Stair, R., Schneider, W. E. and Jackson, J. K., "A New Standard of Spectral Irradiance," *App. Optics* 2(11):1151-1154, November 1963.

44. Stair, R. and Ellis, H. T., "The Solar Constant Based on New Spectral Irradiance Data from 3100 to 5300 Ångströms," *J. App. Meteorology* 7(8):635, August 1968.

45. Stair, R., "Preliminary Report on the Measurement of Spectral Solar Radiation with a Photoelectric Filter Radiometer on Six CV-990 Flights During August 1967," NASA, Goddard Contract Report NAS 5-9488, 29 pp., NASA, Goddard Space Flight Center, Greenbelt, Md., August 1967.

46. Webb, J., "An Electronic Scanning Spectrometer for UV Measurements," 15 pp., paper presented at the Conference of Analytical Chemistry and Applied Spectroscopy, Pittsburgh, Pa., February 1966; GSFC Document X-713-67-108, August 1967.

47. Young, H. D., *Statistical Treatment of Experimental Data,* New York: McGraw-Hill Book Co., Inc., 1962, p. 108.

48. Saiedy, F. and Goody, R. M., "The Solar Emission Intensity at 11 μ," *Monthly Notices Roy. Astron. Soc.* 119(3):213-222, March 1959.

49. Whitehurst, R. N., Copland, J. and Mitchell, F. H., "Solar Radiation and Atmospheric Attenuation at 6-Millimeter Wavelength," *J. App. Physics* 28(3):295-298, March 1957.

50. Detwiler, C. R., Garrett, D. L., Purcell, J. D. and Tousey, R., "The Intensity Distribution in the Ultraviolet Solar Spectrum," *Ann. de Geophysique* 17(3):9-18, July-September 1961.

51. Roberts, J. K. and Miller, A. R., *Heat and Thermodynamics,* New York: Interscience Publishers, Inc., 1960, p. 523; Abetti, G., *The Sun,* London, England: Faber and Faber, 1955, p. 279.

52. Allen, C. W., *Astrophysical Quantities,* second edition. University of London: The Athlone Press, 1962, pp. 16, 17.

53. Makarova, E. A. and Kharitonov, A. V., "Mean Absolute Energy Distribution in the Solar Spectrum from 1800 Å to 4 mm, and the Solar Constant," *Soviet Astronomy-AJ* 12(4):599-609, January-February 1969.

54. Plamondon, J. A., "The Mariner Mars 1969 Temperature Control Flux Monitor," JPL Space Program Summary, 37-59, Vol. III, pp. 162-168.

55. Kondratiev, K. Ya and Nikolsky, G. A., "Solar Radiation and Solar Activity." Preprint of a paper to be published in *Quart. J. Roy. Meteorol. Soc.,* 1970.

56. Ångström, A., private communication, February 1970.

57. Kondratiev, K. Ya, Nikolsky, G. A., Badinov, T. Ya and Andreyev, S. D., "Direct Solar Radiation up to 30 km and Stratification of Attenuation Components in the Stratosphere," *App. Optics* 6(2):197-207, February 1967.

58. Drummond, A. J., Hickey, J. R., Scholes, W. J. and Laue, E. G., Proc. Intern. Astronautical Fed. Eighteenth Congress, Belgrade, 1967.

59. Drummond, A. J., private communication, February 1970.

60. Hinteregger, H. E., private communication, to be published in *Ann. de Geophysique,* 1970; Hinteregger, H. E. and Hall, L. A., *Solar Physics* 6, 175-182, 1969.

61. Heath, D. F., "Observations on the Intensity and Variability of the Near Ultraviolet Solar Flux from the Nimbus III Satellite, *J. Atmospheric Sciences* 26(5), p. 2: 1157-1160, September 1969.

62. Parkinson, W. H. and Reeves, E. M., private communication, to be published in *Solar Physics,* 1970.

63. Shimabukuro, F. J. and Stacey, J. M., "Brightness Temperature of the Quiet Sun at Centimeter and Millimeter Wavelengths," *Astrophys. J.* 152(6):777-782, June 1968.

64. Nicolet, M., "Sur le Problème de la Constante Solaire," Ann. d' Astrophysique, 14(3):249-265, July-September 1951 (in French).

NASA-Langley, 1970 —— 30